Advanced Low Order Orthotropic Finite Element Formulations

by

Susanna Elizabeth Geyer

A dissertation submitted in partial fulfillment
of the requirements for the degree of

Master of Engineering

in the Department of Mechanical and Aeronautical Engineering,
University of Pretoria

December 2000

Supervisor:
Prof. Albert A. Groenwold

Abstract

Title: Advanced Low Order Orthotropic Finite Element Formulations

Author: Susanna Elizabeth Geyer

Degree: M.Eng (Mechanical)

Department: Mechanical Engineering

Supervisor: Prof. Albert A. Groenwold

Keywords: Drilling d.o.f., Assumed stress, Membrane, Flat shell, Finite element, Orthotropy

In this study advanced low order finite elements for the linear analysis and ultimately, the global optimization of orthotropic shells structures, are presented. Low order quadrilaterals are attractive in optimization, since they result in low connectively of the structural stiffness matrix, and hence, reduced computational effort. However, standard 4-node quadrilaterals are notorious for their low accuracy.

Both drilling degrees of freedom and assumed stress interpolations have the potential to improve the modeling capabilities of low order quadrilateral finite elements. Therefore, it seems desirable to formulate low order elements with both an assumed stress interpolation field and drilling degrees of freedom, on condition that the elements are rank sufficient and invariant.

Firstly, a variational basis for the formulation of two families of assumed stress membrane finite elements with drilling degrees of freedom, is presented. This formulation depends on the formulation of Hughes and Brezzi, and is derived using the unified formulation presented by Di and Ramm. The recent stress mode classification method presented by Feng *et al.* is used to derive the stress interpolation matrices. The families, denoted 8β(M) and 8β(D), are rank sufficient, invariant, and free of locking. The membrane locking correction suggested by Taylor ensures that the consistent nodal loads of both families are identical to those of a quadrilateral 4-node membrane finite element with two translational degrees of freedom per node.

Secondly, the rectangular assumed strain plate element presented by Bathe and Dvorkin

is combined with the above mentioned membrane families to form flat shell finite elements. The strain-displacement measures of these elements are modified on the element level to incorporate the effect of element warp.

Thirdly, the constitutive relationship of the flat shell elements is extended to include symmetric orthotropy. In opposition to the general trend to employ quadratic or even cubic elements for orthotropic analyses, it is shown that the simpler 4-node assumed stress families with drilling degrees of freedom presented herein are highly accurate and effective.

Finally, the influence of the stability parameter γ, the integration scheme order and the effect of the membrane locking correction are evaluated. The numerical value of the parameter γ is shown to be irrelevant in the patch test. The effect of the previously proposed membrane-bending locking correction when included in in-plane analysis is demonstrated.

The elements have been incorporated in the EDSAP/CALSAP finite element infrastructure.

Opsomming

Titel: Gevorderde Lae-Orde Ortotropiese Eindige Element Formulerings

Outeur: Susanna Elizabeth Geyer

Graad: M.Ing (Meganies)

Departement: Meganiese Ingenieurswese

Sudieleier: Prof. Albert A. Groenwold

Sleutelwoorde: Boor-vryheidsgraad, Aangenome-spanning, Membraan, Plat dop, Eindige-element, Ortotropie

In hierdie studie word gevorderde lae-orde eindige-elemente vir die lineêre analise van ortotropiese dop-strukture ontwikkel. Die uiteindelike doel van hierdie elemente is die globale optimering van ortotropiese dop-strukture. Lae-orde vierhoekige elemente is aantreklik in optimering, omdat dit lei tot lae koppeling in die styfheidsmatriks. Dit lei weer tot verminderde berekeningstyd. Vier-node vierhoekige elemente is egter berug vanweë hulle lae akkuraatheid.

Beide boor-vryheidsgrade ('drilling degrees of freedom') en aangenome-spanningsinterpolasies ('assumed stress interpolations') het die potensiaal om die modelleringseienskappe van lae-orde vierhoekige elemente te verbeter. Daarom is dit wenslik om lae-orde elemente te formuleer met beide 'n aangenome-spanningsinterpolasieveld en boor-vryheidsgrade, op voorwaarde dat die elemente se rang voldoende is en dat die elemente invariant is.

Eerstens word 'n variasionele basis vir die formulering van twee aangenome-spanning membraan eindige-element families met boor-vryheidsgrade aangebied. Dit is gebaseer op die formulasie van Hughes en Brezzi en is afgelei deur gebruik te maak van die genormaliseerde formulasie van Di en Ramm. Die spanningsmode klassifikasie van Feng *et al.* is gebruik vir die afleiding van die spanningsinterpolasie-matrikse. Die families, genoem 8β(M) en 8β(D), se rang is voldoende en is invariant. Hierdie families toon ook geen sluitingsgedrag nie. Die membraan-sluitingskorreksie wat voorgestel is deur Taylor verseker dat die nodale kragte in dié families ooreenstem met 'n vier-node vierhoekige membraan eindige-element wat twee verplasings-vryheidsgrade per node besit.

Tweedens word die reghoekige aangenome-vervorming plaat element van Bathe en Dvorkin gekombineer met bogenoemde membraan element families om plat dop eindige-elemente te vorm. Die vervorming-verplasing verwantskap van hierdie elemente word op die element vlak gemanipuleer om die effek van element uit-vlak distorsie te akkomodeer.

Derdens word die materiaalverwantskap van die plat dop elemente uitgebrei om simmetriese ortotropie in te sluit. In teenstelling met die algemene gebruik om kwadratiese of kubiese elemente vir ortotropiese analises te gebruik, word die eenvoudiger vier-node aangenome-spanning families met boor-vryheidsgrade hier voorgestel. Hierdie elemente lewer baie goeie resultate en is effektief.

Laastens word die invloed van die stabiliteitsparameter γ, die integrasieskema-orde en die effek van die membraan-sluitingskorreksie geëvalueer. Daar word getoon dat die numeriese waarde van die parameter γ irrelevant is in die laptoets ('patch test'). Die effek van die voorheen voorgestelde membraan-sluitingskorreksie wanneer dit ingesluit word in in-vlak analises word gedemonstreer.

Die elemente is geakkomodeer in die EDSAP/CALSAP eindige-element infrastruktuur.

Acknowledgments

I would like to express my sincere gratitude towards the following persons:

- Dr. Albert Groenwold, for his support throughout this study. It was an honor to work with him. His availability and willingness to assist made this work a pleasure. Sincere thanks to his wife for always being friendly.
- Prof E.E. Rosinger of the Department of Mathematics at the University of Pretoria, for the opportunity for discussions.
- Willy Calder, for the time and effort he put into this work, in his holidays, to ensure that the language is acceptable.
- Detlef Grygier and Justin Mann of KENTRON, for financial support, information on composite materials and the interest they took in this study.
- SASOL, for the opportunity to complete this study.
- My family, for their support, encouragement and prayers that helped me through this study.
- Jana van Graan, my cousin, and her mother, for knowing that the only way they would be able to see me was by offering a free meal.
- Gerrie van der Westhuizen, for understanding even if he did not understand what I was talking about.
- Last but not least, our study group and in particular Michael Hindley (our social organizer), for 'Let's go and play pool' when the office got to small.

Contents

List of Figures

List of Tables

Chapter 1

Introduction

1.1 Motivation

Composite materials are quite different from metals. Composites are combinations of materials differing in composition or form where the individual constituents retain their separate identities and do not dissolve or merge together. These separate constituents act together to give the necessary mechanical strength or stiffness to the composite part.

Composites in structural applications have the following characteristics [2]:

- They generally consist of two or more physically distinct and mechanically separable materials.
- They are made by mixing the separate materials in such a way as to achieve controlled and uniform dispersion of the constituents.
- Mechanical properties of composites are superior to, and in some cases uniquely different from, the properties of their constituents. This is clearly seen with glass-reinforced plastics. In the case of glass-reinforced plastics, the epoxy resin is a relatively weak, flexible, and brittle material, and although the glass fibers are strong and stiff, they can be loaded in tension only as a bare fiber. When combined, the resin and fiber give a strong, stiff composite with excellent toughness characteristics.

In recent years, composite materials have been used increasingly in various engineering disciplines because of their versatility. For example, composites are used in the space, aircraft, automotive, boat and locomotive industries [2].

However, there is also a great number of difficulties associated with composites materials, one of which is their increased complexity. Because of this complexity, the design process of composites is ideally performed using optimization methods. Unfortunately, determination of the optimum parameters is not simple and can be expensive since a large number of locally optimal stacking sequences typically appear, which implies that this problem is a global optimization problem [3].

Usually, composite structures are geometrically quite complex, both in-plane and trough the thickness, and they cannot be solved by analytical methods. This implies that numerical methods have to be used for the analysis and design of these structures, of which the finite element method seems to be the most suitable. Because the finite elements method is an approximate method, convergence is only obtainable in the limit of mesh refinement and, since, in optimization, a complete finite element analysis yields only a single design iteration, it is desirable to perform the finite element analysis with minimal computational effort.

Hence, it is desirable to keep the cost of forming the element stiffness matrices and the cost of solving the equilibrium equations as low a possible. Elements that are 'inexpensive' are normally inaccurate, implying that highly refined meshes may be required to obtain convergence, with implied high assembly and solution costs. 'Visa versa', higher order elements typically require less elements on the structural level, but are associated with expensive evaluations of the element stiffness matrix, as well as increased connectivity on the structural level.

Therefore, advanced low order formulations are a natural candidate for the analysis of orthotropic shell structures. This is in particular true when these elements are included in a computationally expensive optimization infrastructure. However, there is a surprisingly small literature base devoted to the behavior of simple composite shell elements. This is possibly a result of earlier convictions that high order elements were a requirement when analyzing composites [4].

Flat orthotropic shell elements are not a popular choice for the analysis of orthotropic structures. Typically, doubly curved quadratic or even cubic elements are formulated. However, orthotropy is independent of shell curvature, and the results will mainly depend on the kinematic ability and accuracy of the flat shell element.

Both drilling degrees of freedom and assumed stress interpolations have the potential to improve the modeling capabilities of, in particular, low order quadrilateral finite elements. Therefore, it seems desirable to formulate low order elements with both an assumed stress interpolation field and drilling degrees of freedom, on condition that the elements are rank sufficient and invariant. These elements can truly be called advanced, state-of-the-art finite elements for the analysis of orthotropic structures.

1.2 Objectives

This study has the ultimate objective of suggesting advanced low order finite elements for the linear analysis, and ultimately the global optimization, of orthotropic shell structures.

The main requirement is the formulation of a suitable shell finite element for symmetric orthotropy. The element must have an acceptable balance between

- element cost and
- numerical accuracy.

Further requirements for the element are:

- The final formulation must be rank sufficient, invariant and robust.
- None (or as few as possible) adjustable numerical parameters should be present.
- The ability to model general warped geometries should be included.

1.3 Approach

Firstly, suitable isotropic assumed stress membrane elements with in-plane drilling degrees of freedom are formulated.

Secondly, the selected membrane elements are combined with a suitable plate element to form flat shell finite elements.

Finally, the constitutive relationship of the flat shell elements is extended to provide for symmetric orthotropy.

Extensive numerical evaluation is performed in order to obtain information on element performance, convergence rates, sensitivity to distortion, etc.

1.4 Thesis overview

In Chapter 2 assumed stress membrane finite elements with drilling degrees of freedom are discussed. This chapter starts with the variational formulation of these elements, as formulated by Hughes and Brezzi [5]. The membrane locking correction proposed by Taylor [6] is also introduced in this chapter. Chapter 3 presents numerical results for the membrane elements formulated in Chapter 2.

Chapter 4 starts with the formulation of the plate element proposed by Bathe and Dvorkin [7]. This plate element is then combined with the above mentioned membrane elements to form flat shell elements. Numerical results are presented in Chapter 5.

The constitutive relationship of the flat shell elements is extended in Chapter 6 to accommodate layered symmetric orthotropy. Numerical results for these elements are presented in Chapter 7.

The capabilities of the proposed elements are summarized in Chapter 8.

The operators arising from the finite element interpolation are summarized in Appendix A.

The stress mode classification after Feng *et al.* [8] is presented in Appendix B.

The transformation operators for the constrained stress fields are presented in Appendix C.

The different integration schemes used in this study are presented in Appendix D.

In Appendix E fragments of the source code developed during this study are presented.

In Appendix F a list of some of the terms used in this study are given.

Chapter 2

Assumed stress membranes with drilling d.o.f.

2.1 Introduction

2.1.1 Summary of recent research

Both finite elements with drilling degrees of freedom and mixed/hybrid assumed stress formulations are currently research topics of note. Drilling degrees of freedom are for obvious reasons highly desirable when modeling, for instance, folded plates and beam-shell (or membrane) intersections [9].

Classical attempts to develop membrane elements with rotational degrees of freedom were unsuccessful [5]. Compilations of these early efforts are presented by Frey [10] and Bergan and Felippa [11]. The papers of Bergan and Felippa and Allman [12] presented fresh approaches to the formulation of membrane elements with rotational degrees of freedom [13]. The key to their success was the use of a quadratic displacement function for the normal component of displacement rather than the cubic functions employed in earlier works.

Allman with his simple, but powerful formulation, introduced the term 'vertex rotation' [12]. In this formulation, the vertex rotations are related to the derivatives computed at the element nodes. The vertex rotations introduced by Allman in the constant strain triangle dramatically improved the in-plane behavior of his element. Cook presented a quadrilateral element with drilling degrees of freedom, derived from the Allman triangle [14]. A similar formulation was presented by Allman [15].

Since these attempts, many papers on the subject have appeared, notably those by Jetteur, Jaamei and Frey [10, 16, 17, 18] and by Taylor and Simo *et al.* [6, 19, 20]. However, these elements all suffered from the serious drawback that they are rank deficient. To address this deficiency, Hughes and Brezzi [5] presented a rigorous framework wherein elements with independently interpolated rotation fields could be formulated. Utilizing the formulation of Reissner [21], they argue that formulations employing 'convenient' displacement, rotation and stress interpolations are doomed to failure. Instead, they propose a modified variational

principle based on the Euler-Lagrange equations presented by Reissner. However, they improved the stability properties in the discrete approximations.

Finite element interpolations employing the formulation of Hughes and Brezzi were finally presented by Hughes *et al.* [22] and Ibrahimbegovic *et al.* [23, 24]. Since then, the developments in membrane finite elements with drilling degrees of freedom has been numerous.

Previously, Groenwold and Stander applied the 5-point quadrature presented by Dovey [1] to drilling degree of freedom membranes, which improved the element behavior through the introduction of a 'soft' higher order deformation mode [3, 25].

The developments in mixed/hybrid membrane finite elements has been equally important during recent years. Since the assumed stress hybrid finite element presented by Pian [26], numerous formulations have been proposed. A compilation is presented by Pian [27]. The biggest difficulty in deriving hybrid finite elements seems to be the lack of a rational methodology for deriving stress terms [8]. Many approaches were made to address this deficiency, e.g. see [28, 29].

It is recognized that the number of stress modes m in the assumed stress field should satisfy

$$m \geq n - r \tag{2.1}$$

with n the total number of nodal displacements, and r the number of rigid body modes in an element. If (2.1) is not satisfied, rank deficiencies arise, viz. the element stiffness matrix rank is less than the total degree of deformation modes. Furthermore, the equality represented by (2.1) is optimal, since $m > n-r$ increases the element stiffness [30]. Therefore, assumed stress formulations should not only satisfy the requirements of rank sufficiency and invariance, but preferably also the equality condition represented by (2.1). Feng *et al.* [8] present a brief compilation of studies dealing with criteria for stability and convergence. Amongst others, notable contributions are those by Brezzi [31] and Babuska [32], who present necessary and sufficient conditions. Feng *et al.* propose a classification method which also proves that kinematic modes can exist even if $m > n - r$, and show that the m modes are to be chosen from m different stress groups.

The limiting principle of Fraeijs de Veubeke [33] states that a complete but unconstrained assumed stress field becomes identical to the corresponding assumed displacement element. This has lead to the introduction of additional incompatible displacements in numerous formulations. Di and Ramm [34] have chosen not to introduce incompatible modes, but present a rigorous unified formulation to propose stress interpolations.

Previously, a mixed/hybrid assumed stress membrane finite element with drilling degrees of freedom has been presented by Aminpour [35, 36]. However, this element is rank deficient (by one). The framework presented by Hughes and Brezzi [5] can however be used to overcome this drawback.

Sze and Ghali [37] presented a rank sufficient formulation using only 8 interpolating stress modes, denoted HQ8*, which is one less than the equality expressed in (2.1). They used four zero energy modes. One is the equal-rotations mode and the other three are the rigid-body modes. The equal-rotations mode, known as an hourglass mode, is stabilized by a quadratic stress mode. This important contribution probably represents the first ranks sufficient assumed stress membrane finite element with drilling degrees of freedom.

The element presented by Sze and Ghali does not include a locking correction to overcome membrane locking when the element is used as the membrane component of a flat shell finite element. In addition, the interpolation field in the element is not necessarily optimally constrained.

2.1.2 This study

In this study, a variational basis for the formulation of two families of assumed stress membrane finite elements with drilling degrees of freedom is presented, depending on the formulation of Hughes and Brezzi. The families are derived using the unified formulation presented by Di and Ramm [34]. The recent stress mode classification method presented by Feng *et al.* [8] is used to derive the stress interpolation matrices. Both families, denoted 8β(M) and 8β(D), are rank sufficient, invariant, and free of locking. The membrane locking correction suggested by Taylor [6] is used to ensure that the consistent nodal loads in both families are identical to those of a quadrilateral 4-node membrane finite element with two translational degrees of freedom per node.

2.2 A framework for independently interpolated rotation fields

In this section, a rigorous framework for the formulation of independently interpolated rotation fields is presented. The formulation of Hughes and Brezzi [5] is closely followed. The interpolation fields proposed by Ibrahimbegovic *et al.* are presented in Section 2.2.2.

2.2.1 Variational formulation

Let $\Omega \subset \mathbb{R}^d$ be an open set with a piecewise smooth boundary. $d \geq 2$ denotes the number of spatial dimensions. The stress tensor, $\boldsymbol{\sigma}$ (do not assume symmetry), the displacement vector, $\boldsymbol{u}$, and the skew-symmetric rotational tensor, $\boldsymbol{\psi}$, are taken as dependent variables.

The Dirichlet boundary value problem is the focus for this framework. More complicated boundary conditions provide no essential difficulties and may be handled by standard means (see, e.g., [38]). The Euclidean decomposition of a second-rank tensor is used, e.g.,

$$\boldsymbol{\sigma} = \text{symm}\ \boldsymbol{\sigma} + \text{skew}\ \boldsymbol{\sigma} \tag{2.2}$$

where

$$\text{symm}\ \boldsymbol{\sigma} = \frac{1}{2}(\boldsymbol{\sigma} + \boldsymbol{\sigma}^T) \tag{2.3}$$

$$\text{skew}\ \boldsymbol{\sigma} = \frac{1}{2}(\boldsymbol{\sigma} - \boldsymbol{\sigma}^T) \tag{2.4}$$

The boundary value problem

Given $\boldsymbol{f}$, the body force vector, find $\boldsymbol{u}$, $\boldsymbol{\psi}$ and $\boldsymbol{\sigma}$, such that:
For all $\boldsymbol{x} \in \Omega$

$$\begin{aligned} \text{div}\,\boldsymbol{\sigma} + \boldsymbol{f} &= \boldsymbol{0} && (2.5)\\ \text{skew}\,\boldsymbol{\sigma} &= \boldsymbol{0} && (2.6)\\ \boldsymbol{\psi} &= \text{skew}\boldsymbol{\nabla u} && (2.7)\\ \text{symm}\,\boldsymbol{\sigma} &= \boldsymbol{C} \cdot \text{symm}\boldsymbol{\nabla u} && (2.8) \end{aligned}$$

and on the boundary $\Gamma = \partial\Omega$

$$\boldsymbol{u} = \boldsymbol{0} \qquad (2.9)$$

where (2.5) through (2.9) are, respectively, the equilibrium equations, the symmetry conditions for stress, the definition of rotation in terms of displacement gradients, the constitutive equations and the displacement boundary condition.

The elastic moduli, $\boldsymbol{C} = \{C_{ijkl}\}$, $1 \leq i,j,k,l \leq d$, are assumed to satisfy the following conditions:

$$\begin{aligned} C_{ijkl} &= C_{klij} && (2.10)\\ C_{ijkl} &= C_{jikl} = C_{ijlk} && (2.11)\\ C_{ijkl}\epsilon_{ij}\epsilon_{kl} &> 0 \;\; \forall\; \epsilon_{ij} = \epsilon_{ji} \neq 0 && (2.12) \end{aligned}$$

where (2.10) through (2.12) are referred to as, respectively, the major symmetry, the minor symmetries, and positive-definiteness.

For an isotropic material and plane stress, the constitutive modulus tensor $\boldsymbol{C} = \{C_{ijkl}\}$ has the form

$$C_{ijkl} = \lambda\delta_{ij}\delta_{kl} + \mu\left(\delta_{ik}\delta_{jl} + \delta_{il}\delta_{jk}\right) \qquad i,j,k,l \in \{1,2\} \qquad (2.13)$$

where

$$\begin{aligned} \lambda &= \frac{\nu E}{(1-\nu^2)} && (2.14)\\ \mu &= \frac{E}{2\,(1+\nu)} && (2.15) \end{aligned}$$

where E and ν are Young's modulus and Poisson's ratio, respectively. λ and μ are the Lamé parameters and δ_{ij} is the Kronecker delta.

Variational form of the boundary value problem

Let $L_2(\Omega)$ denote the space of square-integrable functions on Ω, and let $H^1(\Omega)$ denote the space of functions in $L_2(\Omega)$ with generalized derivatives also in $L_2(\Omega)$. $H^1_0(\Omega)$ is the subset

of $H^1(\Omega)$ whose members satisfy zero boundary conditions. The spaces relevant to the boundary value problem are:

$$V = \left\{\boldsymbol{v} | \boldsymbol{v} \in \left(H_0^1(\Omega)\right)^d\right\} \tag{2.16}$$

$$W = \left\{\boldsymbol{\omega} | \boldsymbol{\omega} \in (L_2(\Omega))^d, \text{symm } \boldsymbol{\omega} = \mathbf{0}\right\} \tag{2.17}$$

$$T = \left\{\boldsymbol{\tau} | \boldsymbol{\tau} \in (L_2(\Omega))^d\right\} \tag{2.18}$$

where V is the space of trail displacements, W of trail rotations, and T of trail stresses. Consider the following functional [21]:

$$\Pi = V \times W \times T \to \mathbb{R} \tag{2.19}$$

$$\Pi(\boldsymbol{v}, \boldsymbol{\omega}, \boldsymbol{\tau}) = -\frac{1}{2}\int_\Omega \text{symm } \boldsymbol{\tau} \cdot \boldsymbol{C}^{-1} \cdot \text{symm } \boldsymbol{\tau} \, \mathrm{d}\Omega + \int_\Omega \boldsymbol{\tau}^T \cdot (\nabla \boldsymbol{v} - \boldsymbol{\omega}) \, \mathrm{d}\Omega - \int_\Omega \boldsymbol{v} \cdot \boldsymbol{f} \, \mathrm{d}\Omega \tag{2.20}$$

The stationary condition and integration-by-parts reveals that the Euler-Lagrange equations emanating from Π correspond to the equations of the boundary value problem (i.e. (2.5)-(2.8)), viz.

$$\begin{aligned} 0 &= \delta\Pi(\boldsymbol{u}, \boldsymbol{\psi}, \boldsymbol{\sigma})(\boldsymbol{v}, \boldsymbol{\omega}, \boldsymbol{\tau}) \\ &= -\int_\Omega \text{symm } \boldsymbol{\tau} \cdot \boldsymbol{C}^{-1} \cdot \text{symm } \boldsymbol{\sigma} \, \mathrm{d}\Omega + \int_\Omega \boldsymbol{\tau}^T \cdot (\nabla \boldsymbol{u} - \boldsymbol{\psi}) \, \mathrm{d}\Omega \\ &\quad + \int_\Omega \boldsymbol{\sigma}^T \cdot (\nabla \boldsymbol{v} - \boldsymbol{\omega}) \, \mathrm{d}\Omega - \int_\Omega \boldsymbol{v} \cdot \boldsymbol{f} \, \mathrm{d}\Omega \qquad (2.21) \\ &= -\int_\Omega \text{symm } \boldsymbol{\tau} \cdot (\boldsymbol{C}^{-1} \cdot \text{symm } \boldsymbol{\sigma} - \text{symm} \nabla \boldsymbol{u}) \, \mathrm{d}\Omega \\ &\quad - \int_\Omega \text{skew } \boldsymbol{\tau} \cdot (\text{skew} \nabla \boldsymbol{u} - \boldsymbol{\psi}) \, \mathrm{d}\Omega - \int_\Omega \boldsymbol{v} \cdot (\text{div } \boldsymbol{\sigma} + \boldsymbol{f}) \, \mathrm{d}\Omega \\ &\quad + \int_\Omega \boldsymbol{\omega} \cdot \text{skew } \boldsymbol{\sigma} \, \mathrm{d}\Omega \quad \forall \, \{\boldsymbol{v}, \boldsymbol{\omega}, \boldsymbol{\tau}\} \in V \times W \times T \qquad (2.22) \end{aligned}$$

So that there is no confusion with the index-free notation, note that:

$$\boldsymbol{\sigma}^T \cdot (\nabla \boldsymbol{v} - \boldsymbol{\omega}) \equiv \sigma_{ij}(v_{i,j} - \omega_{ij}) \tag{2.23}$$

where

$$\nabla \boldsymbol{v} = [v_{i,j}] \tag{2.24}$$

From (2.22) observe that $\boldsymbol{\omega}$ plays the role of a Lagrange multiplier that enforces the symmetry of the stress.

Mathematical theory of the continuous case

Let $U \equiv V \times W$. The following mapping needs to be introduced:

$$
\begin{aligned}
a &: T \times T \to \mathbb{R} && (2.25)\\
b &: T \times U \to \mathbb{R} && (2.26)\\
f &: U \to \mathbb{R} && (2.27)\\
a(\boldsymbol{\sigma}, \boldsymbol{\tau}) &= -\int_\Omega \text{symm } \boldsymbol{\sigma} \cdot \boldsymbol{C}^{-1} \cdot \text{symm } \boldsymbol{\tau} \, \mathrm{d}\Omega && (2.28)\\
b(\boldsymbol{\tau}, \{\boldsymbol{v}, \boldsymbol{\omega}\}) &= (\boldsymbol{\tau}^T, \nabla \boldsymbol{v} - \boldsymbol{\omega}) \equiv \int_\Omega \boldsymbol{\tau}^T \cdot (\nabla \boldsymbol{v} - \boldsymbol{\omega}) \, \mathrm{d}\Omega && (2.29)\\
f(\{\boldsymbol{v}, \boldsymbol{\omega}\}) &= \int_\Omega \boldsymbol{v} \cdot \boldsymbol{f} \, \mathrm{d}\Omega && (2.30)
\end{aligned}
$$

Note that (2.28) and (2.29) are bilinear forms. (2.28) is symmetric, and $\boldsymbol{f}$ is continuous.
The variational form of the boundary value problem,(2.22), can now be rewritten as follows:

Problem (M)
Find $\{\boldsymbol{u}, \boldsymbol{\psi}\} \in U$ and $\boldsymbol{\sigma} \in T$ such that

$$
\begin{aligned}
a(\boldsymbol{\sigma}, \boldsymbol{\tau}) + b(\boldsymbol{\tau}, \{\boldsymbol{u}, \boldsymbol{\psi}\}) = 0 \quad \forall \quad \boldsymbol{\tau} \in T && (2.31)\\
b(\boldsymbol{\sigma}, \{\boldsymbol{v}, \boldsymbol{\omega}\}) = f(\{\boldsymbol{v}, \boldsymbol{\omega}\}) \quad \forall \quad \{\boldsymbol{v}, \boldsymbol{\omega}\} \in U && (2.32)
\end{aligned}
$$

The discrete problem

Let V^h, W^h and T^h be finite dimensional subspaces of V, W and T, respectively. The superscript 'h' denotes dependence upon a mesh parameter. V^h, W^h and T^h are typical finite element spaces involving piecewise polynomial interpolations. The standard way of developing a discrete approximation is to pose (2.31) and (2.32) in terms of the finite dimensional subspaces.

Problem (M^h)
Find $\{\boldsymbol{u}^h, \boldsymbol{\psi}^h\} \in U^h \equiv V^h \times W^h$ and $\boldsymbol{\sigma}^h \in T^h$ such that

$$
\begin{aligned}
a(\boldsymbol{\sigma}^h, \boldsymbol{\tau}^h) + b(\boldsymbol{\tau}^h, \{\boldsymbol{u}^h, \boldsymbol{\psi}^h\}) = 0 \quad \forall \quad \boldsymbol{\tau}^h \in T^h && (2.33)\\
b(\boldsymbol{\sigma}^h, \{\boldsymbol{v}^h, \boldsymbol{\omega}^h\}) = f(\{\boldsymbol{v}^h, \boldsymbol{\omega}^h\}) \quad \forall \quad \{\boldsymbol{v}^h, \boldsymbol{\omega}^h\} \in U^h && (2.34)
\end{aligned}
$$

Problem (M^h) has a unique solution $\{\boldsymbol{u}^h, \boldsymbol{\psi}^h\} \in U^h$, $\boldsymbol{\sigma}^h \in T^h$. A proof is presented by Hughes and Brezzi [5].

A modified variational formulation

The ellipticity of the continuous problem is not inherited by the discrete problem for convenient finite element spaces. In order to improve upon the ellipticity of the standard mixed formulation, consider the following functional:

$$\Pi_\gamma : V \times W \times T \to \mathbb{R} \tag{2.35}$$

$$\begin{aligned} \Pi_\gamma(\boldsymbol{v}, \boldsymbol{\omega}, \boldsymbol{\tau}) &= \Sigma_\gamma \left(\Pi(\boldsymbol{v}, \boldsymbol{\omega}, \boldsymbol{\tau})\right) \\ &\equiv \Pi(\boldsymbol{v}, \boldsymbol{\omega}, \boldsymbol{\tau}) - \frac{1}{2}\gamma^{-1} \int_\Omega |\text{skew } \boldsymbol{\tau}|^2 \, \mathrm{d}\Omega \end{aligned} \tag{2.36}$$

This functional gives rise to a system of variational equations formally equivalent to those of Π. This may be seen as follows:

$$\begin{aligned} 0 &= \delta\Pi(\boldsymbol{u}, \boldsymbol{\psi}, \boldsymbol{\sigma})(\boldsymbol{v}, \boldsymbol{\omega}, \boldsymbol{\tau}) \\ &= -\int_\Omega \text{symm } \boldsymbol{\tau} \cdot (\boldsymbol{C}^{-1} \cdot \text{symm } \boldsymbol{\sigma} - \text{symm}\nabla\boldsymbol{u}) \, \mathrm{d}\Omega \\ &\quad - \int_\Omega \text{skew } \boldsymbol{\tau} \cdot (\text{skew}\nabla\boldsymbol{u} - \boldsymbol{\psi} - \gamma^{-1}\text{skew } \boldsymbol{\sigma}) \, \mathrm{d}\Omega - \int_\Omega \boldsymbol{v} \cdot (\text{div } \boldsymbol{\sigma} + \boldsymbol{f}) \, \mathrm{d}\Omega \\ &\quad + \int_\Omega \boldsymbol{\omega} \cdot \text{skew } \boldsymbol{\sigma} \, \mathrm{d}\Omega \quad \forall \, \{\boldsymbol{v}, \boldsymbol{\omega}, \boldsymbol{\tau}\} \in V \times W \times T \end{aligned} \tag{2.37}$$

Observe that skew $\boldsymbol{\tau} = \boldsymbol{0}$. Thus the Euler-Lagrange equations of the continuous problem are unchanged. Nevertheless, the consequences of the additional term are significant in the context of approximate solutions. This may be seen more clearly by writing (2.37) in the standard format of a mixed problem.

Problem (M_γ)
Find $\{\boldsymbol{u}, \boldsymbol{\psi}\} \in U$ and $\boldsymbol{\sigma} \in T$ such that

$$a_\gamma(\boldsymbol{\sigma}, \boldsymbol{\tau}) + b(\boldsymbol{\tau}, \{\boldsymbol{u}, \boldsymbol{\psi}\}) = 0 \quad \forall \quad \boldsymbol{\tau} \in T \tag{2.38}$$

$$b(\boldsymbol{\sigma}, \{\boldsymbol{v}, \boldsymbol{\omega}\}) = f(\{\boldsymbol{v}, \boldsymbol{\omega}\}) \quad \forall \quad \{\boldsymbol{v}, \boldsymbol{\omega}\} \in U \tag{2.39}$$

where

$$a_\gamma(\boldsymbol{\sigma}, \boldsymbol{\tau}) = a(\boldsymbol{\sigma}, \boldsymbol{\tau}) - \gamma^{-1}(\text{skew } \boldsymbol{\sigma}, \text{skew } \boldsymbol{\tau}) \tag{2.40}$$

The finite dimensional counterpart of *Problem (M_γ)* is given by:

Problem (M_γ^h)
Find $\{\boldsymbol{u}^h, \boldsymbol{\psi}^h\} \in U^h$ and $\boldsymbol{\sigma}^h \in T^h$ such that

$$a_\gamma(\boldsymbol{\sigma}^h, \boldsymbol{\tau}^h) + b(\boldsymbol{\tau}^h, \{\boldsymbol{u}^h, \boldsymbol{\psi}^h\}) = 0 \quad \forall \quad \boldsymbol{\tau}^h \in T^h \tag{2.41}$$

$$b(\boldsymbol{\sigma}^h, \{\boldsymbol{v}^h, \boldsymbol{\omega}^h\}) = f(\{\boldsymbol{v}^h, \boldsymbol{\omega}^h\}) \quad \forall \quad \{\boldsymbol{v}^h, \boldsymbol{\omega}^h\} \in U^h \tag{2.42}$$

Various special cases of the previous variational formulation can be developed by eliminating fields through the use of Euler-Lagrange equations. The symmetrical components of stress can be eliminated by way of the constitutive equation. Define the functional π_γ by

$$\begin{aligned} \pi_\gamma(\boldsymbol{v}, \boldsymbol{\omega}, \text{skew } \boldsymbol{\tau}) &= \Pi_\gamma(\boldsymbol{v}, \boldsymbol{\omega}, \boldsymbol{C} \cdot \text{symm}\nabla\boldsymbol{v} + \text{skew } \boldsymbol{\tau}) \\ &= \frac{1}{2}\int_\Omega \text{symm}\nabla\boldsymbol{v} \cdot \boldsymbol{C} \cdot \text{symm}\nabla\boldsymbol{v} \, \mathrm{d}\Omega \\ &\quad + \int_\Omega \text{skew } \boldsymbol{\tau}^T \cdot (\text{skew}\nabla\boldsymbol{v} - \boldsymbol{\omega}) \, \mathrm{d}\Omega \\ &\quad - \frac{1}{2}\gamma^{-1}\int_\Omega |\text{skew } \boldsymbol{\tau}|^2 \, \mathrm{d}\Omega - \int_\Omega \boldsymbol{v} \cdot \boldsymbol{f} \, \mathrm{d}\Omega \end{aligned} \tag{2.43}$$

Displacement-type modified variational formulations

From the practical point of view, the most interesting formulation is one based entirely on kinematic variables, namely, displacement and rotation. To this end, the modified variational formulations permit the elimination of skew $\boldsymbol{\sigma}$ by way of the following Euler-Lagrange equation

$$\gamma^{-1}\text{skew } \boldsymbol{\sigma} = \text{skew}\nabla\boldsymbol{u} - \boldsymbol{\psi} \tag{2.44}$$

The following functional is derived by employing (2.44) in (2.43)

$$\tilde{\pi}_\gamma : V \times W \to \mathbb{R} \tag{2.45}$$

$$\begin{aligned} \tilde{\pi}_\gamma(\boldsymbol{v}, \boldsymbol{\omega}) &= \pi_\gamma(\boldsymbol{v}, \boldsymbol{\omega}, \gamma(\text{skew}\nabla\boldsymbol{v} - \boldsymbol{\omega})) \\ &= \frac{1}{2}\int_\Omega \text{symm}\nabla\boldsymbol{v} \cdot \boldsymbol{C} \cdot \text{symm}\nabla\boldsymbol{v} \, \mathrm{d}\Omega \\ &\quad + \frac{1}{2}\gamma\int_\Omega |\text{skew}\nabla\boldsymbol{v} - \boldsymbol{\omega}|^2 \, \mathrm{d}\Omega - \int_\Omega \boldsymbol{v} \cdot \boldsymbol{f} \, \mathrm{d}\Omega \end{aligned} \tag{2.46}$$

Since this is the simplest formulation within this framework, it is the one most likely to be used by program developers [5]. Indeed, this formulation was used by Ibrahimbegovic *et al.* in 1990 [23].

The variational equation emanating from (2.46) is

$$
\begin{aligned}
0 &= \delta\tilde{\pi}(\boldsymbol{u},\boldsymbol{\psi})\cdot(\boldsymbol{v},\boldsymbol{\omega}) \\
&= \int_\Omega \text{symm}\nabla\boldsymbol{v}\cdot\boldsymbol{C}\cdot\text{symm}\nabla\boldsymbol{u}\ \mathrm{d}\Omega \\
&\quad + \int_\Omega (\text{skew}\nabla\boldsymbol{v}-\boldsymbol{\omega})^T\cdot(\gamma(\text{skew}\nabla\boldsymbol{u}-\boldsymbol{\psi}))\ \mathrm{d}\Omega - \int_\Omega \boldsymbol{v}\cdot\boldsymbol{f}\ \mathrm{d}\Omega \qquad (2.47)\\
&= -\int_\Omega \boldsymbol{v}\cdot\text{div}\ [\boldsymbol{C}\cdot\text{symm}\nabla\boldsymbol{u}+\gamma(\text{skew}\nabla\boldsymbol{u}-\boldsymbol{\psi})+\boldsymbol{f}]\ \mathrm{d}\Omega \\
&\quad - \int_\Omega \boldsymbol{\omega}^T\cdot(\gamma(\text{skew}\nabla\boldsymbol{u}-\boldsymbol{\psi}))\ \mathrm{d}\Omega \qquad (2.48)
\end{aligned}
$$

The last term in (2.48) asserts that the skew-symmetric stresses are zero, and the first term express equilibrium in terms of the symmetric stresses. In the corresponding discrete case, the skew-symmetric stresses will not be in general identically zero and thus will play a role in the equilibrium conditions. The mathematical formulation of the variational problem is

Problem (D_γ)
Find $\{\boldsymbol{u},\boldsymbol{\psi}\}\in U$ such that

$$B_\gamma(\boldsymbol{u},\boldsymbol{\psi};\boldsymbol{v},\boldsymbol{\omega}\}) = f(\{\boldsymbol{v},\boldsymbol{\omega}\}) \quad \forall \quad \{\boldsymbol{v},\boldsymbol{\omega}\}\in U \qquad (2.49)$$

where

$$
\begin{aligned}
B_\gamma(\boldsymbol{u},\boldsymbol{\psi};\boldsymbol{v},\boldsymbol{\omega}\}) &= \int_\Omega \text{symm}\nabla\boldsymbol{v}\cdot\boldsymbol{C}\cdot\text{symm}\nabla\boldsymbol{u}\ \mathrm{d}\Omega \\
&\quad + \int_\Omega (\text{skew}\nabla\boldsymbol{v}-\boldsymbol{\omega})^T\cdot(\gamma(\text{skew}\nabla\boldsymbol{u}-\boldsymbol{\psi}))\ \mathrm{d}\Omega \qquad (2.50)
\end{aligned}
$$

is a symmetrical bilinear form. The corresponding discrete problem is:

Problem (D_γ^h)
Find $\{\boldsymbol{u}^h,\boldsymbol{\psi}^h\}\in U^h$ such that

$$B_\gamma(\boldsymbol{u}^h,\boldsymbol{\psi}^h;\boldsymbol{v}^h,\boldsymbol{\omega}^h\}) = f(\{\boldsymbol{v}^h,\boldsymbol{\omega}^h\}) \quad \forall \quad \{\boldsymbol{v}^h,\boldsymbol{\omega}^h\}\in U^h \qquad (2.51)$$

Generalization

Hu-Washizu variational formulations are frequently used as a basis for finite element discretizations. A Hu-Washizu-type variational formulation accounting for rotations and non-symmetric stress tensors derives from the following functional:

$$
\begin{aligned}
H(\boldsymbol{v},\boldsymbol{\omega},\text{skew}\boldsymbol{\tau},\text{symm}\boldsymbol{\tau},\epsilon) &= \frac{1}{2}\int_\Omega \epsilon\cdot\boldsymbol{C}\cdot\epsilon\ \mathrm{d}\Omega + \int_\Omega \text{symm}\boldsymbol{\tau}\cdot(\text{symm}\nabla\boldsymbol{v}-\epsilon)\ \mathrm{d}\Omega \\
&\quad + \frac{1}{2}\int_\Omega \text{skew}\boldsymbol{\tau}^T\cdot(\text{skew}\nabla\boldsymbol{v}-\boldsymbol{\omega})\ \mathrm{d}\Omega - \int_\Omega \boldsymbol{v}\cdot\boldsymbol{f}\ \mathrm{d}\Omega \qquad (2.52)
\end{aligned}
$$

where $\epsilon=\epsilon^T$.

2.2.2 Finite element interpolations by Ibrahimbegovic *et al.*

The rotational and translational interpolations of the formulation of Hughes and Brezzi [5] are addressed in detail in the papers of Hughes *et al.* [22] and Ibrahimbegovic *et al.* [23]. Here, the formulation of Ibrahimbegovic *et al.* [23] is followed closely.

The independent rotation field is interpolated as a standard bilinear field over each element. Accordingly

$$\psi^h = \sum_e \sum_{i=1}^{4} N_i^e(\xi,\eta)\psi_i \tag{2.53}$$

where (e.g., see [39])

$$N_i^e(\xi,\eta) = \frac{1}{4}(1+\xi_i\xi)(1+\eta_i\eta) \quad i = 1,2,3,4 \tag{2.54}$$

The in-plane displacement approximation is taken as an Allman-type interpolation field

$$\begin{aligned}\begin{pmatrix} u_1 \\ u_2 \end{pmatrix} &= \boldsymbol{u}^h \\ &= \sum_e \sum_{i=1}^{4} N_i^e(\xi,\eta)\boldsymbol{u}_i + \frac{l_{jk}}{8}\sum_e \sum_{i=5}^{8} NS_i^e(\xi,\eta)(\psi_k - \psi_j)\boldsymbol{n}_{jk} \\ &\quad + \sum_e NB_9^e(\xi,\eta)\Delta\boldsymbol{u}_9\end{aligned} \tag{2.55}$$

l_{jk} and $\boldsymbol{n}_{jk}$ denote the length and the outward unit normal vector on the element side associated with the corner nodes j and k.

$$\boldsymbol{n}_{jk} = \begin{Bmatrix} n_1 \\ n_2 \end{Bmatrix} = \begin{Bmatrix} \cos\alpha_{jk} \\ \sin\alpha_{jk} \end{Bmatrix} \tag{2.56}$$

and

$$l_{jk} = ((x_{k1} - x_{j1})^2 + (x_{k2} - x_{j2})^2)^{1/2} \tag{2.57}$$

The indices in the above are explicitly given in Appendix A.

In (2.55) the following Serendipity shape functions defined by Zienkiewicz and Taylor [39] are used.

$$NS_i^e(\xi,\eta) = \frac{1}{2}(1-\xi^2)(1+\eta_i\eta); \quad i = 5,7 \tag{2.58}$$

$$NS_i^e(\xi,\eta) = \frac{1}{2}(1+\xi_i\xi)(1-\eta^2); \quad i = 6,8 \tag{2.59}$$

To reflect the superior performance of the 9-node Lagrangian element over that of the 8-node Serendipity element, a hierarchical bubble function interpolation is added in (2.55) where

$$NB_9^e(\xi,\eta) = (1-\xi^2)(1-\eta^2) \tag{2.60}$$

The terms in the element stiffness matrix arising from this interpolation may be eliminated at the element level by static condensation [40].

2.2.3 On the numerical value of γ

For isotropic elasticity and Dirichlet boundary value problems, Ibrahimbegovic *et al.* take γ equal to the value of the shear modulus [23]. The choice of $\gamma = G$ was suggested by Hughes *et al.* [22]. Numerical studies by Ibrahimbegovic *et al.* [23] show that their element formulation is insensitive to the value of γ used, at least for several orders of magnitude which bound the shear modulus. This was however shown for one particular problem only. Results by Groenwold and Stander [25] indicated that there may be a more pronounced sensitivity to the value of γ for certain examples. For some problems, therefore, enforcement of the rotational field by sufficiently large values of γ is crucial [25].

Notwithstanding the undesirability of having a problem dependent parameter in the formulation, both the shear and extension patch tests (Figure 3.3) are passed for any positive value of γ. As the patch test is a necessary and sufficient condition for convergence (see [41]), the numerical value of γ becomes irrelevant in the limit of mesh refinement[1].

2.3 Assumed stress membrane element with drilling degrees of freedom formulation

2.3.1 Variational formulation

In this study, the formulation presented by Hughes and Brezzi (see (2.43)) is extended through the addition of the term

$$\int_\Omega \text{symm } \boldsymbol{\tau}^T \cdot (\text{symm}\boldsymbol{\nabla v} - \boldsymbol{\epsilon}) \, \mathrm{d}\Omega \tag{2.61}$$

where $\boldsymbol{\tau}^T$ represents a Lagrangian multiplier. The following Hu-Washizu like functional is obtained

Problem (M_c)

$$\begin{aligned} \boldsymbol{\Pi}_\gamma(\boldsymbol{v}, \boldsymbol{\omega}, \boldsymbol{\tau}) \;=\; & \frac{1}{2}\int_\Omega (\text{symm}\boldsymbol{\nabla v})^T \cdot \boldsymbol{C} \cdot \text{symm}\boldsymbol{\nabla v} \, \mathrm{d}\Omega + \int_\Omega \text{symm } \boldsymbol{\tau}^T \cdot (\text{symm}\boldsymbol{\nabla v} - \boldsymbol{\epsilon}) \, \mathrm{d}\Omega \\ & + \int_\Omega \text{skew } \boldsymbol{\tau}^T \cdot (\text{skew}\boldsymbol{\nabla v} - \boldsymbol{\omega}) \, \mathrm{d}\Omega - \frac{1}{2}\gamma^{-1}\int_\Omega [\text{skew } \boldsymbol{\tau}]^2 \, \mathrm{d}\Omega \\ & - \int_\Omega \boldsymbol{v}^T \cdot \boldsymbol{f} \, \mathrm{d}\Omega \end{aligned} \tag{2.62}$$

Substituting the constitutive relationship $\boldsymbol{\epsilon} = \boldsymbol{C}^{-1} \cdot \text{symm } \boldsymbol{\tau}$, *Problem ($M_c$)* can be rewritten to obtain

$$\begin{aligned} \boldsymbol{\Pi}_\gamma(\boldsymbol{v}, \boldsymbol{\omega}, \boldsymbol{\tau}) \;=\; & \int_\Omega \text{symm } \boldsymbol{\tau}^T \cdot \text{symm}\boldsymbol{\nabla v} \, \mathrm{d}\Omega - \frac{1}{2}\int_\Omega \text{symm } \boldsymbol{\tau}^T \cdot \boldsymbol{C}^{-1} \cdot \text{symm } \boldsymbol{\tau} \, \mathrm{d}\Omega \\ & + \int_\Omega \text{skew } \boldsymbol{\tau}^T \cdot (\text{skew}\boldsymbol{\nabla v} - \boldsymbol{\omega}) \, \mathrm{d}\Omega - \frac{1}{2}\gamma^{-1}\int_\Omega [\text{skew } \boldsymbol{\tau}]^2 \, \mathrm{d}\Omega \end{aligned}$$

[1] The effect of γ is extensively demonstrated in Chapters 3, 5, and 7

$$-\int_\Omega \boldsymbol{v}^T \cdot \boldsymbol{f}\ \mathrm{d}\Omega \tag{2.63}$$

The variational equation which results from variations on (2.63) is

$$\begin{aligned} 0 \;=\; \delta\boldsymbol{\Pi}_\gamma(\boldsymbol{v},\boldsymbol{\omega},\boldsymbol{\tau}) \;=\; & \int_\Omega \mathrm{symm}\ \boldsymbol{\sigma}^T \cdot \mathrm{symm}\boldsymbol{\nabla}\boldsymbol{v}\ \mathrm{d}\Omega + \int_\Omega \mathrm{symm}\ \boldsymbol{\tau}^T \cdot \mathrm{symm}\boldsymbol{\nabla}\boldsymbol{u}\ \mathrm{d}\Omega \\ & - \int_\Omega \mathrm{symm}\ \boldsymbol{\tau}^T \cdot \boldsymbol{C}^{-1} \cdot \mathrm{symm}\ \boldsymbol{\sigma}\ \mathrm{d}\Omega + \int_\Omega \mathrm{skew}\ \boldsymbol{\tau}^T \cdot (\mathrm{skew}\boldsymbol{\nabla}\boldsymbol{u} - \boldsymbol{\psi})\ \mathrm{d}\Omega \\ & + \int_\Omega (\mathrm{skew}\boldsymbol{\nabla}\boldsymbol{v}^T \cdot \mathrm{skew}\ \boldsymbol{\sigma} - \boldsymbol{\omega}^T \cdot \mathrm{skew}\ \boldsymbol{\sigma})\ \mathrm{d}\Omega - \gamma^{-1} \int_\Omega \mathrm{skew}\ \boldsymbol{\tau}^T \cdot \mathrm{skew}\ \boldsymbol{\sigma}\ \mathrm{d}\Omega \\ & - \int_\Omega \boldsymbol{u}^T \cdot \boldsymbol{f}\ \mathrm{d}\Omega \end{aligned} \tag{2.64}$$

Furthermore, it is possible to eliminate the skew-symmetric part of the stress tensor by substituting

$$\gamma^{-1}\mathrm{skew}\ \boldsymbol{\sigma} \;=\; \mathrm{skew}\boldsymbol{\nabla}\boldsymbol{u} - \boldsymbol{\psi} \tag{2.65}$$

into *Problem (M_c)* to obtain

Problem (D_c)

$$\begin{aligned} \boldsymbol{\Pi}_\gamma(\boldsymbol{v},\boldsymbol{\omega},\boldsymbol{\tau}) \;=\; & \int_\Omega \mathrm{symm}\ \boldsymbol{\tau}^T \cdot \mathrm{symm}\boldsymbol{\nabla}\boldsymbol{v}\ \mathrm{d}\Omega - \frac{1}{2}\int_\Omega \mathrm{symm}\ \boldsymbol{\tau}^T \cdot \boldsymbol{C}^{-1} \cdot \mathrm{symm}\ \boldsymbol{\tau}\ \mathrm{d}\Omega \\ & + \frac{1}{2}\gamma \int_\Omega [\mathrm{skew}\boldsymbol{\nabla}\boldsymbol{v} - \boldsymbol{\omega}]^2\ \mathrm{d}\Omega - \int_\Omega \boldsymbol{v}^T \cdot \boldsymbol{f}\ \mathrm{d}\Omega \end{aligned} \tag{2.66}$$

which is now similar to the generalization presented by Hughes and Brezzi (see [5]). The corresponding variational equation becomes

$$\begin{aligned} 0 \;=\; \delta\boldsymbol{\Pi}_\gamma(\boldsymbol{v},\boldsymbol{\omega},\boldsymbol{\tau}) \;=\; & \int_\Omega \mathrm{symm}\ \boldsymbol{\sigma}^T \cdot \mathrm{symm}\boldsymbol{\nabla}\boldsymbol{v}\ \mathrm{d}\Omega \\ & + \int_\Omega \mathrm{symm}\ \boldsymbol{\tau}^T \cdot \mathrm{symm}\boldsymbol{\nabla}\boldsymbol{u}\ \mathrm{d}\Omega - \int_\Omega \mathrm{symm}\ \boldsymbol{\tau}^T \cdot \boldsymbol{C}^{-1} \cdot \mathrm{symm}\ \boldsymbol{\sigma}\ \mathrm{d}\Omega \\ & + \gamma \int_\Omega (\mathrm{skew}\boldsymbol{\nabla}\boldsymbol{v} - \boldsymbol{\omega})^T \cdot (\mathrm{skew}\boldsymbol{\nabla}\boldsymbol{u} - \boldsymbol{\psi})\ \mathrm{d}\Omega - \int_\Omega \boldsymbol{u}^T \cdot \boldsymbol{f}\ \mathrm{d}\Omega \end{aligned} \tag{2.67}$$

2.3.2 Finite element interpolation

The discrete version of *Problem (M_c)* is obtained as

Problem (M_c^h)

$$\begin{aligned} 0 \;=\; & \int_{\Omega^h} (\mathrm{symm}\ \boldsymbol{\sigma}^h)^T \cdot \mathrm{symm}\boldsymbol{\nabla}\boldsymbol{v}^h\ \mathrm{d}\Omega + \int_{\Omega^h} (\mathrm{symm}\ \boldsymbol{\tau}^h)^T \cdot \mathrm{symm}\boldsymbol{\nabla}\boldsymbol{u}^h\ \mathrm{d}\Omega \\ & - \int_{\Omega^h} (\mathrm{symm}\ \boldsymbol{\tau}^h)^T \cdot \boldsymbol{C}^{-1} \cdot \mathrm{symm}\ \boldsymbol{\sigma}^h\ \mathrm{d}\Omega + \int_{\Omega^h} (\mathrm{skew}\ \boldsymbol{\tau}^h)^T \cdot (\mathrm{skew}\boldsymbol{\nabla}\boldsymbol{u}^h - \boldsymbol{\psi}^h)\ \mathrm{d}\Omega \\ & + \int_{\Omega^h} \left((\mathrm{skew}\boldsymbol{\nabla}\boldsymbol{v}^h)^T \cdot \mathrm{skew}\ \boldsymbol{\sigma}^h - (\boldsymbol{\omega}^h)^T \cdot \mathrm{skew}\ \boldsymbol{\sigma}^h \right)\ \mathrm{d}\Omega \\ & - \gamma^{-1} \int_{\Omega^h} (\mathrm{skew}\ \boldsymbol{\tau}^h)^T \cdot \mathrm{skew}\ \boldsymbol{\sigma}^h\ \mathrm{d}\Omega - \int_{\Omega^h} (\boldsymbol{u}^h)^T \cdot \boldsymbol{f}\ \mathrm{d}\Omega \end{aligned} \tag{2.68}$$

It is required that the three distinct independent interpolation fields arising from the translations, rotations, and the enhanced stresses are interpolated. The rotational and translational interpolations were addressed in detail in the paper of Ibrahimbegovic *et al.* [23] (see Section 2.2.2). However, the newly introduced assumed stress field is presented in more detail in the following.

The independent rotation field is interpolated as in Section 2.2.2. The in-plane displacement approximation is taken as an Allman-type interpolation field

$$\begin{pmatrix} u_1 \\ u_2 \end{pmatrix} = \boldsymbol{u}^h = \sum_e \sum_{i=1}^{4} N_i^e(\xi,\eta)\boldsymbol{u}_i + \frac{l_{jk}}{8} \sum_e \sum_{i=5}^{8} NS_i^e(\xi,\eta)(\psi_k - \psi_j)\boldsymbol{n}_{jk} \tag{2.69}$$

with NS_i the Serendipity shape functions. In accordance with the limiting principle of Fraeijs de Veubeke [33], the hierarchical bubble shape function is not included. l_{jk} and $\boldsymbol{n}_{jk}$ denote the length and the outward unit normal vector on the element side associated with the corner nodes j and k (Figure 2.1).

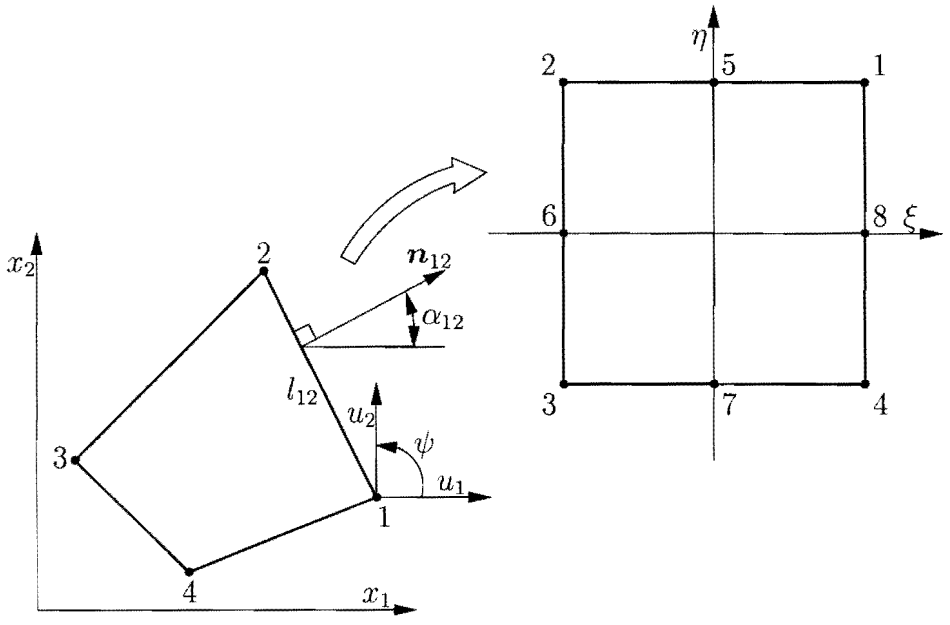

Figure 2.1: Membrane finite element

The skew-symmetric stress field is chosen constant over the element, i.e.

$$\text{skew } \boldsymbol{\tau}^h = \sum_e \boldsymbol{\tau}_0^e \tag{2.70}$$

Using matrix notation, $\text{symm}\nabla\boldsymbol{u}^e$ and $\text{skew}\nabla\boldsymbol{u}^e$ are respectively given by

$$\text{symm}\nabla\boldsymbol{u}^e = \boldsymbol{B}_i^e\boldsymbol{u}_i + \boldsymbol{G}_{\psi i}^e\boldsymbol{\psi}_i \tag{2.71}$$

and

$$\text{skew}\nabla\boldsymbol{u}^e = \boldsymbol{b}_i^e\boldsymbol{u}_i + \boldsymbol{g}_i^e\boldsymbol{\psi}_i \tag{2.72}$$

The operators arising from this interpolation are summarized in Appendix A.

For the assumed stress field, the global stresses are directly interpolated by the stress parameters β_i, i.e.

$$\text{symm } \boldsymbol{\sigma}^h = \sum_e \boldsymbol{P}^e \boldsymbol{\beta}^e \tag{2.73}$$

where $\boldsymbol{P}^e$ is the interpolation matrix in terms of the local coordinates and $\boldsymbol{\beta}^e$ is the stress parameter vector. Equations (2.73) represent an unconstrained interpolation field, which is not necessarily optimal. Constraints may be enforced by a suitable transformation matrix $\boldsymbol{A}^e$, such that

$$\text{symm } \boldsymbol{\sigma}^h = \sum_e \boldsymbol{A}^e \boldsymbol{P}^e \boldsymbol{\beta}^e \tag{2.74}$$

Various forms for $\boldsymbol{A}^e$ were presented by Di and Ramm [34], and are applied to the new families of elements in sections to follow.

The body force vector is given by

$$\boldsymbol{r} = \int_\Omega \boldsymbol{N}^T \boldsymbol{f} \, \mathrm{d}\Omega \tag{2.75}$$

In matrix notation, the stationary conditions result in

$$\begin{bmatrix} 0 & \boldsymbol{G}^{eT} & \boldsymbol{h}^e \\ \boldsymbol{h}^{eT} & 0 & -\gamma^{-1}\Omega^e \\ \boldsymbol{G}^e & -\boldsymbol{H}^e & 0 \end{bmatrix} \cdot \begin{bmatrix} \boldsymbol{q} \\ \boldsymbol{\beta} \\ \boldsymbol{\tau}_0 \end{bmatrix} = \begin{bmatrix} \boldsymbol{r} \\ 0 \\ 0 \end{bmatrix} \tag{2.76}$$

with

$$\boldsymbol{G}^e = \int_\Omega \boldsymbol{P}^{eT} \cdot [\boldsymbol{B}^e \; \boldsymbol{G}^e] \, \mathrm{d}\Omega \tag{2.77}$$

$$\boldsymbol{H}^e = \int_\Omega \boldsymbol{P}^{eT} \cdot \boldsymbol{C}^{-1} \cdot \boldsymbol{P}^e \, \mathrm{d}\Omega \tag{2.78}$$

$$\boldsymbol{h}^e = \int_\Omega [\boldsymbol{b}^e \; \boldsymbol{g}^e]^T \, \mathrm{d}\Omega \tag{2.79}$$

where $\boldsymbol{C}^{-1}$ denotes the elastic compliance matrix, and where $\boldsymbol{P}^e$ may be replaced by $\boldsymbol{A}^e \boldsymbol{P}^e$. The force-displacement relationship is defined by

$$\left[\boldsymbol{K}^e + \frac{\gamma}{\Omega^e} \boldsymbol{h}^e \boldsymbol{h}^{eT}\right] \boldsymbol{q} = \boldsymbol{r} \tag{2.80}$$

with

$$\boldsymbol{K}^e = \boldsymbol{G}^{eT} \boldsymbol{H}^{e-1} \boldsymbol{G}^e \tag{2.81}$$

Finally, stress recovery is obtained through

$$\boldsymbol{\beta} = \boldsymbol{H}^{e-1} \boldsymbol{G}^e \boldsymbol{q} \tag{2.82}$$

Similarly to the foregoing, the discrete version of *Problem* (D_c) yields

Problem (D_c^h)

$$\begin{aligned} 0 \;=\; & \int_{\Omega^h} (\text{symm}\ \boldsymbol{\sigma}^h)^T \cdot \text{symm}\boldsymbol{\nabla}\boldsymbol{v}^h \ \mathrm{d}\Omega + \int_{\Omega^h} (\text{symm}\ \boldsymbol{\tau}^h)^T \cdot \text{symm}\boldsymbol{\nabla}\boldsymbol{u}^h \ \mathrm{d}\Omega \\ & - \int_{\Omega^h} (\text{symm}\ \boldsymbol{\tau}^h)^T \cdot \boldsymbol{C}^{-1} \cdot \text{symm}\ \boldsymbol{\sigma}^h \ \mathrm{d}\Omega \\ & + \gamma \int_{\Omega^h} (\text{skew}\boldsymbol{\nabla}\boldsymbol{v}^h - \boldsymbol{\omega}^h)^T \cdot (\text{skew}\boldsymbol{\nabla}\boldsymbol{u}^h - \boldsymbol{\psi}^h) \ \mathrm{d}\Omega - \int_{\Omega^h} (\boldsymbol{u}^h)^T \cdot \boldsymbol{f} \ \mathrm{d}\Omega \end{aligned} \tag{2.83}$$

which directly results in

$$\left[\boldsymbol{K}^e + \boldsymbol{P}_\gamma^e\right] \boldsymbol{q} = \boldsymbol{r} \tag{2.84}$$

with

$$\boldsymbol{P}_\gamma^e \;=\; \gamma \int_\Omega \left\{ \begin{array}{c} \boldsymbol{b}^e \\ \boldsymbol{g}^e \end{array} \right\} \left[\boldsymbol{b}^e \ \ \boldsymbol{g}^e\right] \mathrm{d}\Omega \tag{2.85}$$

The parameter γ in the foregoing formulations is problem dependent, since it is part of a penalty term. The effect of γ is studied in Chapters 3, 5, and 7 to come.

2.3.3 Developing and constraining the assumed stress field

The stress field assumed in (2.73) may, without loss of generality, be expressed as

$$\text{symm}\ \boldsymbol{\sigma}^e = \boldsymbol{P}\boldsymbol{\beta} = \text{symm}\ \boldsymbol{\sigma}_c^e + \text{symm}\ \boldsymbol{\sigma}_h^e = \left[\boldsymbol{I}_c \ \boldsymbol{P}_h\right] \left\{ \begin{array}{c} \boldsymbol{\beta}_c \\ \boldsymbol{\beta}_h \end{array} \right\} \tag{2.86}$$

where the superscript e is dropped on $\boldsymbol{P}_\alpha$ for reasons of clarity. In (2.86), $\boldsymbol{I}_c$ allows for the accommodation of constant stress states. The higher order stress field is represented by

$$\text{symm}\ \boldsymbol{\sigma}_h^e = \boldsymbol{P}_h\boldsymbol{\beta}_h = \boldsymbol{P}_{h2}\boldsymbol{\beta}_{h2} + \boldsymbol{P}_{h3}\boldsymbol{\beta}_{h3} \tag{2.87}$$

where $\boldsymbol{P}_{h2}\boldsymbol{\beta}_{h2}$ and $\boldsymbol{P}_{h3}\boldsymbol{\beta}_{h3}$ are introduced for reasons of clarity. Therefore,

$$\text{symm}\ \boldsymbol{\sigma}^e = \boldsymbol{P}\boldsymbol{\beta} = \text{symm}\ \boldsymbol{\sigma}_c^e + \text{symm}\ \boldsymbol{\sigma}_h^e = \left[\boldsymbol{I}_c \ \boldsymbol{P}_{h2} \ \boldsymbol{P}_{h3}\right] \left\{ \begin{array}{c} \boldsymbol{\beta}_c \\ \boldsymbol{\beta}_{h2} \\ \boldsymbol{\beta}_{h3} \end{array} \right\} \tag{2.88}$$

Furthermore, the classification of Feng *et al.* [8] is now extended, and written as

$$\boldsymbol{I}_c\boldsymbol{\beta}_c \;=\; \left[\{\sigma_1\}\{\sigma_2\}\{\sigma_3\}\right] \left\{ \begin{array}{c} \beta_1 \\ \beta_2 \\ \beta_3 \end{array} \right\} \tag{2.89}$$

with $\{\sigma_1\}$ through $\{\sigma_3\}$ presented in Appendix B, and representing the constant stress capability of the formulation. Various possibilities exist for $\boldsymbol{P}_{h2}$ (e.g. see [8]), but the obvious choice is the linear capability, given for instance by

$$\boldsymbol{P}_{h2}\boldsymbol{\beta}_{h2} \;=\; \left[\{\sigma_5\}\{\sigma_6\}\right] \left\{ \begin{array}{c} \beta_4 \\ \beta_5 \end{array} \right\} \tag{2.90}$$

with $\{\sigma_5\}$ and $\{\sigma_6\}$ again given in Appendix B. (2.89) combined with (2.90) yields the usual formulation for a 5-parameter stress field, as is also for instance used by Di and Ramm [34], for their 5β elements. The additional terms required for the finite element with drilling degrees of freedom are chosen as

$$\boldsymbol{P}_{h3}\boldsymbol{\beta}_{h3} = [\{\sigma_{13}\}\{\sigma_{12}\}\{\sigma_{23}\}] \begin{Bmatrix} \beta_6 \\ \beta_7 \\ \beta_8 \end{Bmatrix} \tag{2.91}$$

viz.

$$\boldsymbol{P}_{h3} = \begin{bmatrix} -\xi & 0 & \eta^2 \\ 0 & -\eta & -\xi^2 \\ \eta & \xi & 0 \end{bmatrix} \tag{2.92}$$

This formulation is similar to the unconstrained field used by Sze and Ghali [37]. A different, invariant possibility is

$$\boldsymbol{P}^i_{h3} = [\{\sigma_9\}\{\sigma_8\}\{\sigma_{23}\}] \tag{2.93}$$

When using 9 interpolating stress modes, (i.e. $m = n - r = 12 - 3 = 9$), the stress modes may be selected as

$$\boldsymbol{P}_{h4}\boldsymbol{\beta}_{h4} = [\{\sigma_{13}\}\{\sigma_{12}\}\{\sigma_{17}\}\{\sigma_{15}\}] \begin{Bmatrix} \beta_6 \\ \beta_7 \\ \beta_8 \\ \beta_9 \end{Bmatrix} \tag{2.94}$$

viz.

$$\boldsymbol{P}_{h4} = \begin{bmatrix} -\xi & 0 & \eta^2 & 0 \\ 0 & -\eta & 0 & \xi^2 \\ \eta & \xi & 0 & 0 \end{bmatrix} \tag{2.95}$$

This formulation is similar to the formulation presented by Aminpour [35]. A different possibility is given by

$$\boldsymbol{P}^i_{h4} = [\{\sigma_9\}\{\sigma_8\}\{\sigma_{17}\}\{\sigma_{15}\}] \tag{2.96}$$

(Here, it is chosen to retain $\boldsymbol{P}_{h2}$ unmodified, which is not a requirement.) $\boldsymbol{P}_{h3}$ is then used instead of $\boldsymbol{P}_{h3}$. As stated previously, constraints may be enforced through a suitable transformation matrix $\boldsymbol{A}$, such that symm $\boldsymbol{\sigma}^e = \boldsymbol{A}^e\boldsymbol{P}^e\boldsymbol{\beta}$. Various forms for $\boldsymbol{A}^e$ were presented by Di and Ramm [34], and are applied in Table 2.1 to the 8β and 9β families, while the 5β family is also given for reasons of completeness. In the table, $|\boldsymbol{J}|$ indicates the determinant of the Jacobian $\boldsymbol{J}$, and g the determinant of the metric tensor. The transformation operators $\boldsymbol{T}_0$, $\boldsymbol{T}$ and $\boldsymbol{Q}$ are given in Appendix C.

The following notation is used:

- NC - The stresses are associated with the strain derived from the displacements and are not subjected to any constraint.
- EP - Pian and Sumihara [28] have developed a rational approach for the assumed stress element in which the equilibrium equations in a weak form related to the internal displacement field are used as a constraint condition; it serves as a pre-treatment for the initial assumed stress trial. With this method, an appropriate perturbation of element geometry is often needed to obtain sufficient constraints.

- OC - The higher order stress is selected to be orthogonal to the constant part in a weak sense [42].
- NT - The initial stress is decomposed into a constant and a higher order part, and then the higher order part is defined independently so that the constant part of the initial stress can be preserved. Following this approach the transformation for the higher order part of the initial stress defined in isoparametric space is normalized.
- PH - The physical components of the higher order stress part are first interpolated in isoparametric space and then converted to their contravariant components. Finally, the latter are transformed to the global system using the transformation matrix.

No	Element	Higher order stress
1	5β-NC	$\boldsymbol{P}_h = \boldsymbol{P}_{h2}$
2	5β-EP	$\boldsymbol{P}_h = \boldsymbol{T}_0\boldsymbol{P}_{h2}$
3	5β-OC	$\boldsymbol{P}_h = \frac{1}{\lvert\boldsymbol{J}\rvert}\boldsymbol{T}_0\boldsymbol{P}_{h2}$
4	5β-NT	$\boldsymbol{P}_h = g\boldsymbol{T}\boldsymbol{P}_{h2}$
5	5β-PH	$\boldsymbol{P}_h = \boldsymbol{T}\boldsymbol{Q}\boldsymbol{P}_{h2}$
6	8β(M)-NC and 8β(D)-NC	$\boldsymbol{P}_h = \boldsymbol{P}_{h2} + \boldsymbol{P}_{h3}$
7	8β(M)-EP and 8β(D)-EP	$\boldsymbol{P}_h = \boldsymbol{T}_0\boldsymbol{P}_{h2} + \boldsymbol{T}_0\boldsymbol{P}_{h3}$
8	8β(M)-OC and 8β(D)-OC	$\boldsymbol{P}_h = \frac{1}{\lvert\boldsymbol{J}\rvert}\boldsymbol{T}_0\boldsymbol{P}_{h2} + \frac{1}{\lvert\boldsymbol{J}\rvert}\boldsymbol{T}_0\boldsymbol{P}_{h3}$
9	8β(M)-NT and 8β(D)-NT	$\boldsymbol{P}_h = g\boldsymbol{T}\boldsymbol{P}_{h2} + g\boldsymbol{T}\boldsymbol{P}_{h3}$
10	8β(M)-PH and 8β(D)-PH	$\boldsymbol{P}_h = \boldsymbol{T}\boldsymbol{Q}\boldsymbol{P}_{h2} + \boldsymbol{T}\boldsymbol{Q}\boldsymbol{P}_{h3}$
11	9β(M)-NC and 9β(D)-NC	$\boldsymbol{P}_h = \boldsymbol{P}_{h2} + \boldsymbol{P}_{h4}$
12	9β(M)-EP and 9β(D)-EP	$\boldsymbol{P}_h = \boldsymbol{T}_0\boldsymbol{P}_{h2} + \boldsymbol{T}_0\boldsymbol{P}_{h4}$
13	9β(M)-OC and 9β(D)-OC	$\boldsymbol{P}_h = \frac{1}{\lvert\boldsymbol{J}\rvert}\boldsymbol{T}_0\boldsymbol{P}_{h2} + \frac{1}{\lvert\boldsymbol{J}\rvert}\boldsymbol{T}_0\boldsymbol{P}_{h4}$
14	9β(M)-NT and 9β(D)-NT	$\boldsymbol{P}_h = g\boldsymbol{T}\boldsymbol{P}_{h2} + g\boldsymbol{T}\boldsymbol{P}_{h4}$
15	9β(M)-PH and 9β(D)-PH	$\boldsymbol{P}_h = \boldsymbol{T}\boldsymbol{Q}\boldsymbol{P}_{h2} + \boldsymbol{T}\boldsymbol{Q}\boldsymbol{P}_{h4}$

Table 2.1: Unified formulation for the 5β, 8β and 9β families

2.4 Membrane locking correction

Flat shell elements assembled from membrane elements with in plane drilling degrees of freedom suffer undesirable membrane-bending interactions associated with the drilling degrees of freedom [6].

Mechanistically, the locking phenomena may be described as follows [6]: Flat quadrilateral shell elements approximate curved shell geometries with the possibilities of kinks between adjacent elements. In these situations the continuity of the three rotation parameters for the shell result in a situation where non-zero drilling degrees of freedom in one element leads to non-zero bending degrees of freedom in the adjacent element (and 'vice-versa'). Accordingly,

the elements will exhibit a membrane-bending locking performance, unless the drilling degree of freedom part of the membrane strains may assume a zero value over the element.

For the assumed displacement field of the 8β(M), 8β(D), 9β(M) and 9β(D) elements (see (2.69)) zero strains are not possible for non-zero rotations [6]. An exception is the special case of identical rotations at opposite nodes. One such case is for example, reflected in:

$$l_{ij}\cos\alpha_{ij}NS^e_{l,x_2} = l_{ik}\cos\alpha_{ik}NS^e_{m,x_2} \tag{2.97}$$

Taylor [6] presented a correction which alleviates the membrane-bending locking. The correction, which is based on a three field formulation (displacement, strain and stress), is repeated here, albeit with a slightly different notation.

Using matrix notation, symm$\boldsymbol{\nabla u}^e$ for the 8β(M), 8β(D), 9β(M) and 9β(D) elements is given by

$$\text{symm}\boldsymbol{\nabla u}^e = \boldsymbol{B}^e_i\boldsymbol{u}_i + \boldsymbol{G}^e_{\psi i}\boldsymbol{\psi}_i \quad i = 1,2,3,4 \tag{2.98}$$

where $\boldsymbol{u}_i$ and $\boldsymbol{\psi}_i$ are nodal values of displacement and rotation respectively and summation is implied.

In the following, the 8β(M), 8β(D), 9β(M) and 9β(D) elements with the interpolation given in (2.98) are now denoted 8β(M)$*$, 8β(D)$*$, 9β(M)$*$ and 9β(D)$*$. Here, the asterisk $(*)$ indicates that the membrane locking correction, (which is described in the following), is not performed. For the 8β(M), 8β(D), 9β(M) and 9β(D) elements, the modified strain relationship proposed by Taylor [6] is used. This relationship is given by

$$\text{symm}\boldsymbol{\nabla u}^e = \boldsymbol{B}^e_i\boldsymbol{u}_i + \boldsymbol{G}^e_{\psi i}\boldsymbol{\psi}_i + \text{symm}\boldsymbol{\nabla u}^e_0 \tag{2.99}$$

This modified strain relation is required to satisfy a requirement that the drilling parameter part can be inextensible. Accordingly, it is desired that

$$\boldsymbol{G}^e_{\psi i}\boldsymbol{\psi}_i + \text{symm}\boldsymbol{\nabla u}^e_0 = 0 \tag{2.100}$$

for rotational fields which are inextensible. Unless the drilling degrees of freedom are eliminated completely it is only possible to satisfy (2.100) in a weak sense. A suitable weak form may be constructed by augmenting the usual potential energy of each element for a shell by the term

$$\int_{\Omega^e} \bar{\boldsymbol{\sigma}}^T \left(\boldsymbol{G}^e_{\psi i}\boldsymbol{\psi}_i + \text{symm}\boldsymbol{\nabla u}^e_0\right)\, \mathrm{d}\Omega^e = 0 \tag{2.101}$$

where Ω^e is the surface region of the shell. Both $\bar{\boldsymbol{\sigma}}^T$ and symm$\boldsymbol{\nabla u}^e_0$ are assumed constant over each element. Performing the variation with respect to $\bar{\boldsymbol{\sigma}}^T$ leads to

$$\text{symm}\boldsymbol{\nabla u}^e_0 = -\frac{1}{\Omega^e}\int_{\Omega^e} \boldsymbol{G}^e_{\psi i}\boldsymbol{\psi}_i\, \mathrm{d}\Omega^e \tag{2.102}$$

and, therefore, the modified strain relationship

$$\text{symm}\boldsymbol{\nabla u}^e = \boldsymbol{B}_i^e \boldsymbol{u}_i + \left(\boldsymbol{G}_{\psi i}^e - \frac{1}{\Omega} \int_\Omega \boldsymbol{G}_{\psi i}^e \, \mathrm{d}\Omega \right) \boldsymbol{\psi}_i \tag{2.103}$$

which is the final result presented by Taylor [6].

Chapter 3

Numerical results: Isotropic membrane elements

In this chapter numerical results are presented for the isotropic membrane elements developed in Chapter 2.

In the following,

- Q4 denotes a standard 4-node bilinear membrane element with 8 degrees of freedom.
- QC9D refers to an implementation by Groenwold and Stander [25] of the Ibrahimbegovic *et al.* membrane finite element with drilling degrees of freedom [23]. The element is based on the variational formulation due to Hughes and Brezzi [5], and the formulation includes a hierarchical bubble shape function. This element has 12 degrees of freedom.
- 5β denotes an implementation of the 5β family due to Di and Ramm [34].
- 8β(M) and 8β(D) denote the two families proposed herein. An asterisk ($*$) indicates that the membrane locking correction is not included. (The formulation by Sze and Ghali [37] is similar to the 8β(D)$*$-EP element presented herein.)
- 9β(M) and 9β(D) denote the two families proposed herein with 9 interpolating parameters.

The penalty stiffness terms $(\gamma/\Omega^e)\boldsymbol{h}^e\boldsymbol{h}^{eT}$ and $\boldsymbol{P}^e_\gamma$ (in (2.80) and (2.84) respectively), which relate the in-plane rotations to the in-plane translations, respectively are integrated using a 2×2 Gaussian quadrature, and a 1 point quadrature. All other integrals are evaluated using 3×3 Gaussian quadrature.

Alternatively, $\boldsymbol{G}^{eT}\boldsymbol{H}^{e-1}\boldsymbol{G}^e$ in (2.81) may be integrated by the 5-point rule presented in [1, 25]. However, reduced integration in mixed/hybrid finite elements is in general not advantageous.

3.1 Element rank

Eigenvalue analyses of the different 8β(M)-NT and 9β(M)-NT formulations are presented in Table 3.1.

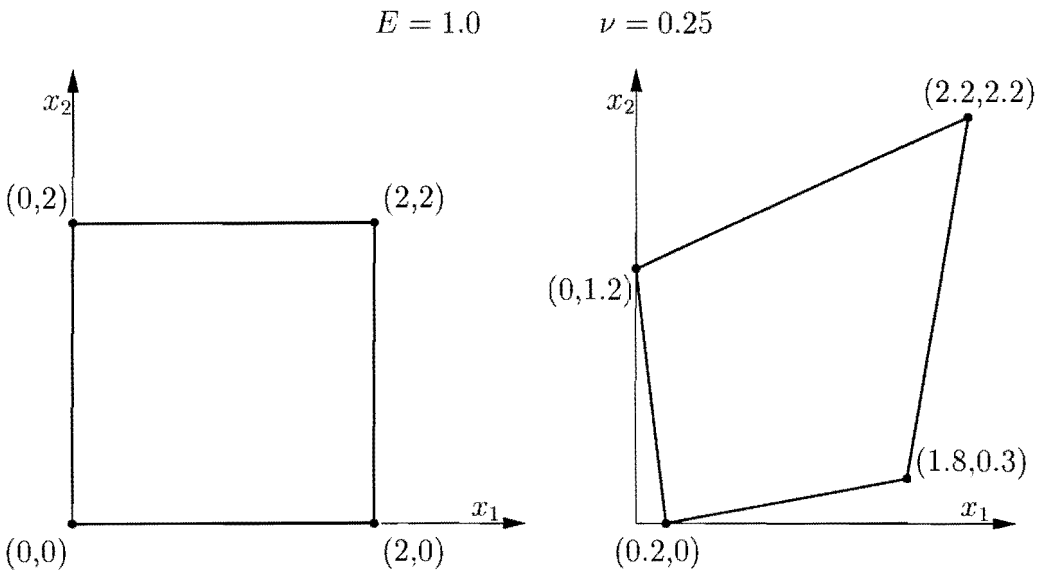

Figure 3.1: Regular and distorted element geometries for eigenvalue analysis

λ_i	P_{h3}	P^i_{h3}	P_{h4}	P^i_{h4}
1	0.14286E+01	0.14286E+01	0.14286E+01	0.14286E+01
2	0.76923E+00	0.76923E+00	0.76923E+00	0.76923E+00
3	0.76923E+00	0.76923E+00	0.76923E+00	0.76923E+00
4	0.57692E+00	0.57692E+00	0.57692E+00	0.57692E+00
5	0.39461E+00	0.50514E+00	0.39461E+00	0.50514E+00
6	0.39461E+00	0.50514E+00	0.39461E+00	0.50514E+00
7	0.80219E-01	0.84600E-01	0.80219E-01	0.84600E-01
8	0.80219E-01	0.84600E-01	0.80219E-01	0.84600E-01
9	0.44444E-01	0.44444E-01	0.44444E-01	0.44444E-01
10	0.63228E-16	0.42331E-16	0.41967E-16	0.37303E-16
11	0.95029E-17	0.13642E-17	0.35205E-16	-0.12714E-16
12	-0.37504E-16	-0.26489E-16	-0.14526E-16	-0.74542E-16

Table 3.1: Eigenvalues of square 8β(M)-NT and 9β(M)-NT elements (plane stress, $|\boldsymbol{J}| = 1$, $E = 1$, $\nu = 0.3$)

The different stress modes used in the elements are given in (2.93) through (2.96). The table reveals that all the formulations are of adequate rank, while rigid body modes are captured adequately. Using the distorted element geometry depicted in Figure 3.1 it is determined that the elements are invariant (not shown in tabulated form).

3.2 Membrane patch tests

A necessary and sufficient requirement for convergence of finite elements is that the patch tests suggested by Irons [43] is passed [41]. This also applies for mixed formulations [44], while a necessary condition for non-singularity is

$$m \geq n \tag{3.1}$$

where m is the number of degrees of freedom in the primary (displacement) variables, and n is the number of degrees of freedom in the constraint variables of the mixed formulation. The 8β(M) and 9β(M) families satisfy (3.1). For all the patch tests performed in this study, the mesh depicted in Figure 3.2 is used.

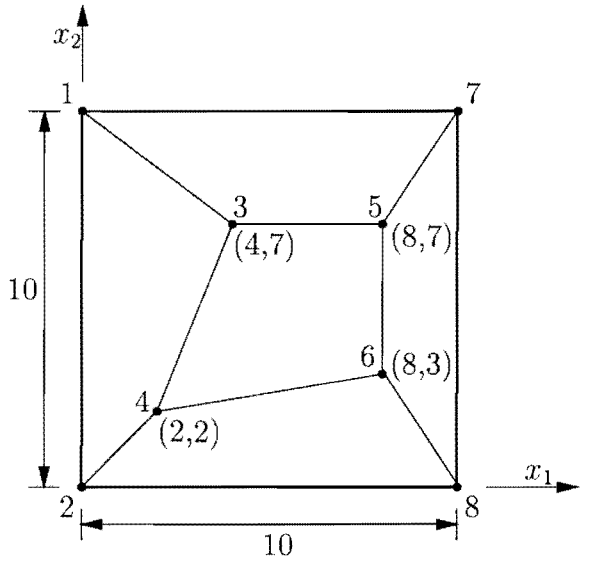

Figure 3.2: Mesh used in patch tests

3.2.1 Constant extension and constant shear patch tests

The 8β and 9β families pass these patch tests, with and without the membrane locking correction. When the membrane locking correction is excluded, constant nodal moments are required. The patch tests are passed for any $\gamma > 0$. See Figure 3.3 for boundary conditions.

3.2.2 Modified shear patch test

This new test illustrates the capabilities of membrane finite elements with drilling degrees of freedom (Figure 3.4).

For a square membrane subjected to complementary shear, the three degrees of freedom at a single node are constrained. The correct displacements and stresses are obtained, while no additional devices are required.

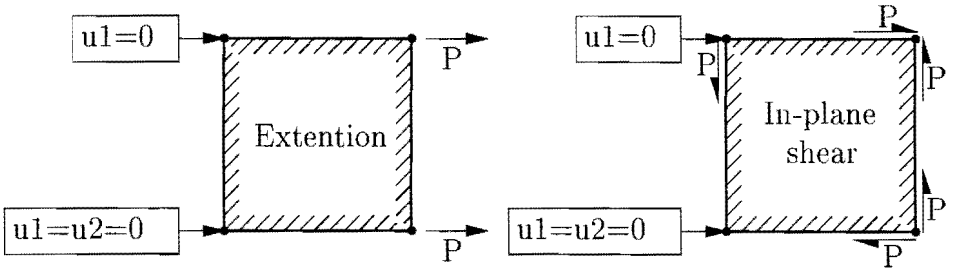

Figure 3.3: Constant extension patch test and constant shear patch test

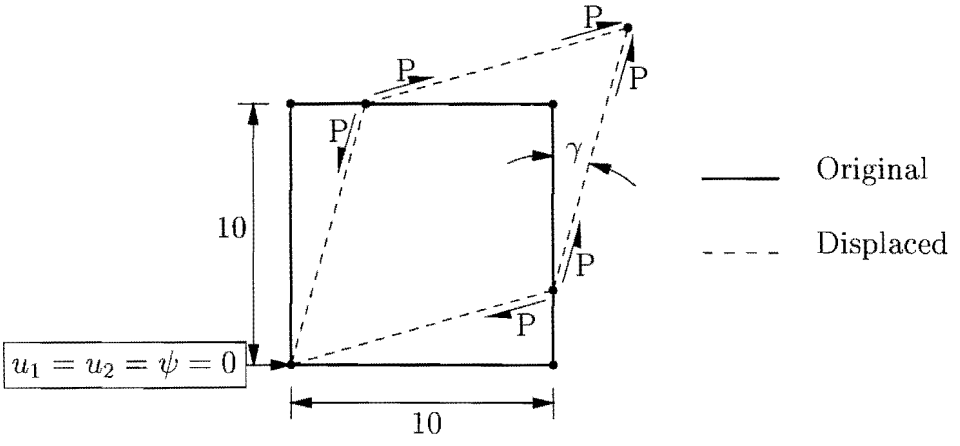

Figure 3.4: Modified constant shear patch test

3.3 Taylor's patch test and Ramm's cantilever beam

The geometry is depicted in Figure 3.5, and tabulated numerical results are presented in Table 3.2.

Load case 1 once again represents a patch test. Obviously, all the elements studied pass this test. Load case 2 represents bending behavior. In general, the NT-formulation in each family is the most accurate. When the locking correction is applied the error is smaller than without this correction.

In load cases 3 and 4 the effect of element distortion is examined. For both these load cases the error is smaller when the locking correction is not applied. For the displacements the $8\beta*$ formulation is by far the most accurate. For both load cases the 9β(M)*-NC formulation performs very good for the stress predictions.

The results obtained with the 8β and 9β families are almost identical. In general, the new families are more accurate than the QC9D element, but not quite as accurate as the 5β family.

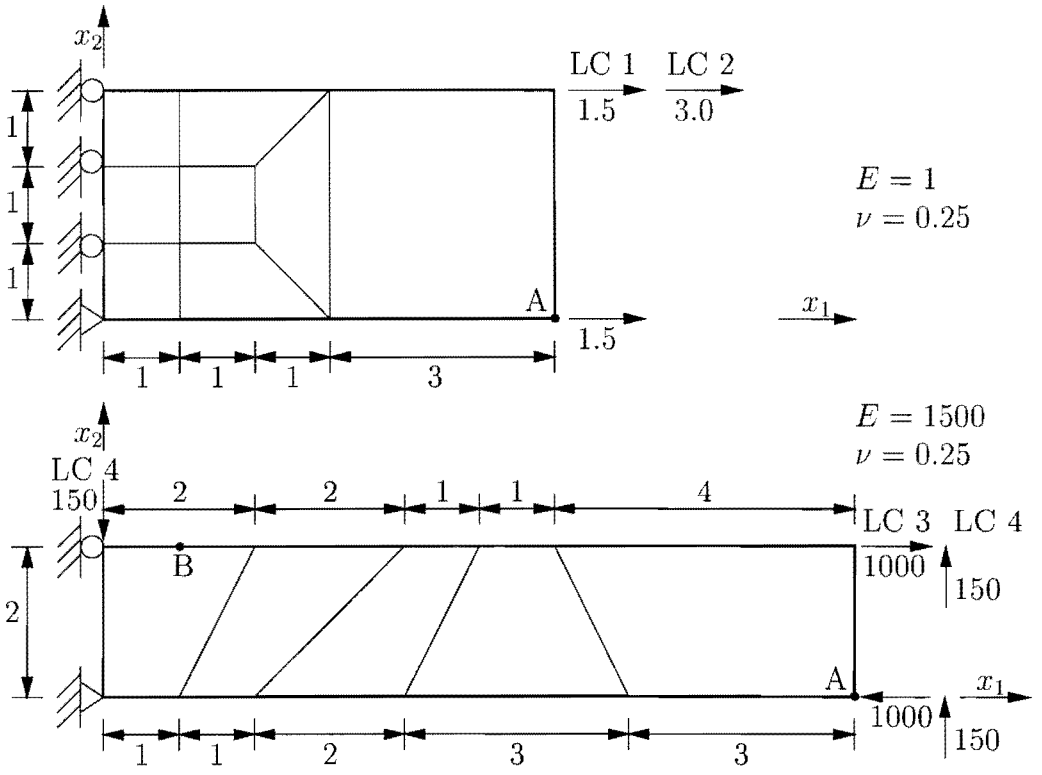

Figure 3.5: Taylor's patch test and Ramm's cantilever beam

3.4 Cook's membrane

This popular test problem (See Figure 3.6) has been used by many authors. The center displacement u_{2_C} for the various elements studied is tabulated in Table 3.3, while the stresses $(\sigma_{\min})_B$ and $(\sigma_{\max})_A$ are presented in Table 3.4.

From Table 3.3 it is clear that the NT-formulation outperforms all the other elements. The elements perform better without the locking correction.

Table 3.4 illustrates that the $8\beta*$ formulation performs better for the maximum stress, while the 9β families outperform the other elements for the minimum stress.

Once again, the displacement results obtained with the 8β and 9β families are almost identical, and in general more accurate than the QC9D results.

Table 3.5 shows that small values of γ lead to higher displacement accuracy, since the rotational field is only weakly enforced. However, the usual choice of $\gamma = G$ results in good accuracy. $\gamma = 0$ results in the most accurate formulation. Due to the redundant constraints in the problem no rank deficiencies arise. However, $\gamma = 0$ is not suitable for general problems.

Table 3.6 reveals that with the 5-point and 8-point integration schemes, the accuracy increases in general. Both the integration schemes improve the performance of the elements when the membrane locking correction is used, due to the introduction of a 'soft' higher order deformation mode.

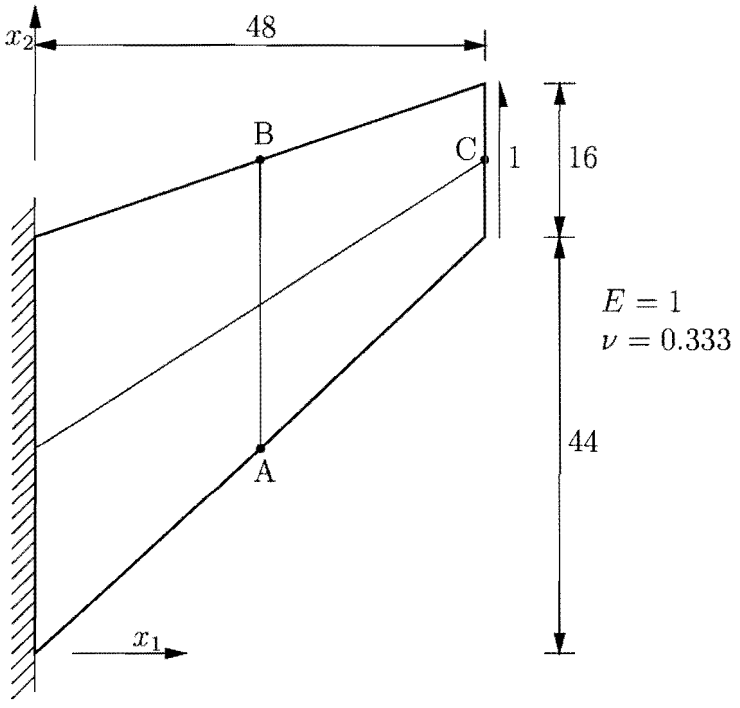

Figure 3.6: Cook's membrane

3.5 Thick walled cylinder

This problem is used to assess the performance of the elements studied for nearly incompressible materials. Depicted in Figure 3.7, numerical results for this problem are tabulated in Table 3.7.

The analytical solution is given by

$$u(r) = \frac{(1+\nu)pR_1^2}{E(R_2^2 - R_1^2)}\left[\frac{R_2^2}{r} + (1-2\nu)r\right] \tag{3.2}$$

where p represents the pressure on the inner surface, R_1 denotes the inner radius and R_2 the outer radius.

MacNeal and Harder [45] calculated the following values:

- $u_{1_A} = 5.0399 \times 10^{-3}$ for $\nu_1 = 0.49$,
- $u_{1_A} = 5.0602 \times 10^{-3}$ for $\nu_2 = 0.499$, and
- $u_{1_A} = 5.0623 \times 10^{-3}$ for $\nu_3 = 0.4999$.

Table 3.7 reveals that the QC9D element becomes over stiff as $\nu \to 0.5$, while the 5β, 8β and 9β families do not reveal this locking like behavior.

Note that the NC-formulations are the most accurate. In general, the 5β family slightly outperforms the other families.

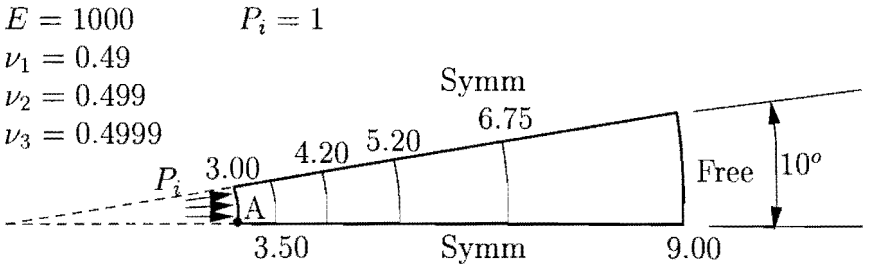

Figure 3.7: Thick walled cylinder

3.6 Cook's beam

The geometry is depicted in Figure 3.8. Numerical results for the displacements are given in Table 3.8, and the stress results are presented in Table 3.9.

For the displacements the $8\beta*$ and $9\beta*$ formulations outperform the other elements. For the stress evaluation the 5β family is by far the most accurate. For the irregular mesh the 8β-OC and $8\beta*$-OC formulations are very accurate. The 8β and 9β formulations are accurate for $-\sigma_{11}$. The results obtained with the 8β and 9β families are almost identical.

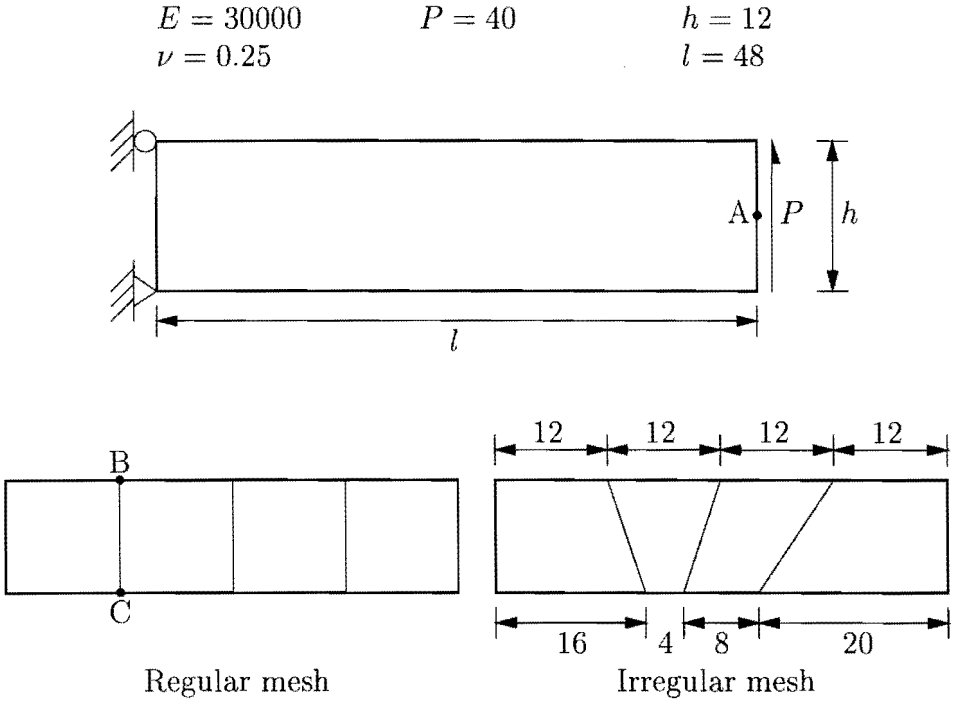

Figure 3.8: Cook's beam

3.7 Higher order patch test

Load case 1 (a unit couple applied at the free ends) represents a higher order patch test (Taylor *et al.* [41]). Load case 2 was presented by Ibrahimbegovic *et al.* [23] (See Figure 3.9). The center displacements and the tip rotations are given in Table 3.10.

For the center displacements of load case 1 with the regular mesh, the 5β family is very accurate. The EP-, OC- and NT-formulations for all the families are also accurate. Note that the 8β(M)-NC element and the OC-formulations for the irregular mesh are very accurate. For the tip rotations of Load case 1, the EP-, OC- and NT-formulations are very accurate for the regular mesh. The NT-formulation is also accurate for the irregular mesh.

The EP-, OC- and NT-formulations are also accurate for the center displacements of load case 2 for the regular mesh. For the irregular mesh the OC-formulations without the locking correction are the most accurate. For the tip rotations for load case 2 the NC- and PH-formulations outperform the other elements. QC9D is the most accurate for the irregular mesh.

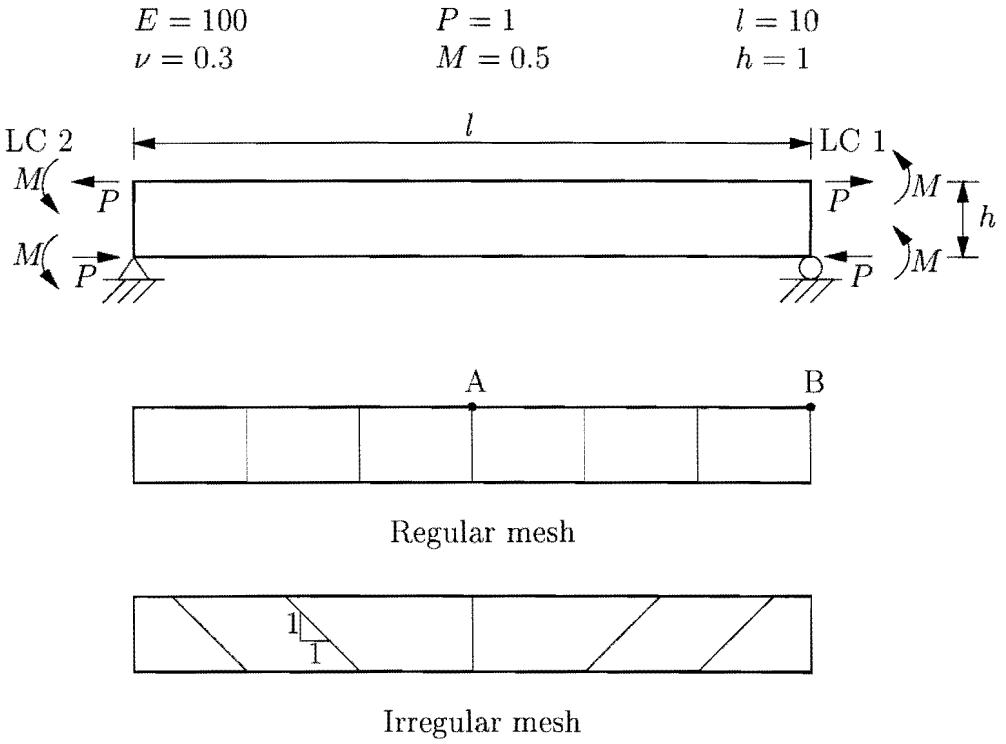

Figure 3.9: Higher order patch test

	Case 1	Case 2	Case 3		Case 4	
Element	u_{1_A}	$-u_{2_A}$	u_{2_A}	$-\sigma_{x_B}$	u_{2_A}	$-\sigma_{x_B}$
Q4	6.000	14.90	44.60	1724	49.54	2395
QC9D	6.000	16.78	81.86	2541	84.59	3453
5β-NC	6.000	17.50	77.54	2775	82.02	3829
5β-EP	6.000	17.28	96.18	3014	98.19	4137
5β-OC	6.000	17.18	93.13	2446	95.06	3349
5β-NT	6.000	18.33	97.33	3019	98.91	4148
5β-PH	6.000	17.86	96.33	2982	98.38	4095
8β(M)$*$-NC	6.000	16.60	98.34	3074	99.40	4151
8β(M)$*$-EP	6.000	16.41	98.97	3015	100.1	4148
8β(M)$*$-OC	6.000	16.63	101.0	2614	102.1	3609
8β(M)$*$-NT	6.000	17.60	99.28	3017	100.3	4141
8β(M)$*$-PH	6.000	17.20	97.37	2887	98.34	3990
8β(M)-NC	6.000	17.09	84.17	2732	87.26	3572
8β(M)-EP	6.000	16.86	84.82	2882	87.96	3824
8β(M)-OC	6.000	16.91	84.49	2456	87.23	3296
8β(M)-NT	6.000	17.73	85.71	2878	89.13	3844
8β(M)-PH	6.000	17.40	89.57	2409	92.30	3174
8β(D)$*$-NC	6.000	16.60	98.38	3055	99.45	4131
8β(D)$*$-EP	6.000	16.41	98.85	2998	99.96	4131
8β(D)$*$-OC	6.000	16.63	101.0	2598	102.0	3592
8β(D)$*$-NT	6.000	17.60	99.21	3004	100.2	4129
8β(D)$*$-PH	6.000	17.20	97.46	2873	98.43	3975
8β(D)-NC	6.000	17.10	84.22	2726	87.31	3565
8β(D)-EP	6.000	16.87	84.86	2881	88.00	3822
8β(D)-OC	6.000	16.92	84.50	2456	87.24	3295
8β(D)-NT	6.000	17.74	85.75	2878	89.18	3843
8β(D)-PH	6.000	17.41	89.67	2415	92.42	3178
9β(M)$*$-NC	6.000	16.60	98.27	3006	99.27	4030
9β(M)$*$-EP	6.000	16.41	98.88	2922	99.79	3960
9β(M)$*$-OC	6.000	16.62	98.95	2906	99.79	3948
9β(M)$*$-NT	6.000	17.60	99.06	2888	99.90	3907
9β(M)$*$-PH	6.000	17.19	97.03	2819	97.92	3863
9β(M)-NC	6.000	17.09	83.83	2551	86.77	3292
9β(M)-EP	6.000	16.86	83.75	2494	86.51	3234
9β(M)-OC	6.000	16.91	83.93	2518	86.80	3294
9β(M)-NT	6.000	17.73	84.23	2440	87.17	3169
9β(M)-PH	6.000	17.40	88.98	2194	91.61	2883
9β(D)$*$-NC	6.000	16.60	98.31	2985	99.32	4007
9β(D)$*$-EP	6.000	16.41	98.76	2899	99.67	3936
Analytical	6.000	18.00	100.0	3000	102.0	4050

Table 3.2: Taylor's patch test and Ramm's cantilever beam: Numerical results

	Case 1	2	Case 3		Case 4	
Element	u_{1_A}	$-u_{2_A}$	u_{2_A}	$-\sigma_{x_B}$	u_{2_A}	$-\sigma_{x_B}$
9β(D)$*$-OC	6.000	16.63	98.86	2887	99.69	3928
9β(D)$*$-NT	6.000	17.59	98.98	2868	99.82	3886
9β(D)$*$-PH	6.000	17.19	97.13	2804	98.02	3846
9β(D)-NC	6.000	17.10	83.87	2544	86.81	3284
9β(D)-EP	6.000	16.86	83.77	2492	86.53	3230
9β(D)-OC	6.000	16.91	83.95	2518	86.83	3292
9β(D)-NT	6.000	17.74	84.26	2439	87.19	3166
9β(D)-PH	6.000	17.40	89.08	2200	91.72	2887
Analytical	6.000	18.00	100.0	3000	102.0	4050

Table 3.2: Taylor's patch test and Ramm's cantilever beam: Numerical results (continued)

Element	2×2	4×4	8×8	16×16	32×32
Q4	11.80	18.29	22.08	23.43	23.82
QC9D	19.27	22.61	23.55	23.83	23.92
5β-NC	17.76	21.94	23.38	23.80	23.92
5β-EP	21.13	23.02	23.69	23.88	23.94
5β-OC	21.04	23.02	23.69	23.88	23.94
5β-NT	21.54	23.05	23.69	23.88	23.94
5β-PH	21.13	23.02	23.69	23.88	23.94
8β(M)$*$-NC	21.83	23.15	23.64	23.85	23.92
8β(M)$*$-EP	22.18	23.28	23.69	23.86	23.92
8β(M)$*$-OC	22.38	23.30	23.69	23.86	23.92
8β(M)$*$-NT	22.65	23.32	23.69	23.86	23.92
8β(M)$*$-PH	21.85	23.19	23.66	23.85	23.93
8β(M)-NC	19.60	22.63	23.56	23.83	23.92
8β(M)-EP	20.11	22.71	23.58	23.84	23.92
8β(M)-OC	20.18	22.73	23.58	23.84	23.92
8β(M)-NT	20.42	22.74	23.58	23.84	23.92
8β(M)-PH	19.59	22.65	23.57	23.84	23.92
8β(D)$*$-NC	21.81	23.15	23.64	23.85	23.92
8β(D)$*$-EP	22.21	23.29	23.69	23.86	23.92
8β(D)$*$-OC	22.41	23.30	23.69	23.86	23.92
8β(D)$*$-NT	22.67	23.32	23.69	23.86	23.92
8β(D)$*$-PH	21.84	23.19	23.66	23.85	23.93
8β(D)-NC	19.59	22.63	23.56	23.83	23.92
8β(D)-EP	20.12	22.72	23.58	23.84	23.92
Best known			23.90		

Table 3.3: Cook's membrane: Center displacement u_{2_C}

Element	2×2	4×4	8×8	16×16	32×32
8β(D)-OC	20.19	22.73	23.58	23.84	23.92
8β(D)-NT	20.42	22.74	23.58	23.84	23.92
8β(D)-PH	19.60	22.65	23.57	23.84	23.92
9β(M)$*$-NC	21.83	23.15	23.64	23.85	23.92
9β(M)$*$-EP	22.10	23.28	23.69	23.86	23.92
9β(M)$*$-OC	22.28	23.29	23.69	23.86	23.92
9β(M)$*$-NT	22.59	23.31	23.69	23.86	23.92
9β(M)$*$-PH	21.81	23.19	23.66	23.85	23.93
9β(M)-NC	19.51	22.63	23.56	23.83	23.92
9β(M)-EP	19.77	22.70	23.58	23.84	23.92
9β(M)-OC	19.86	22.71	23.58	23.84	23.92
9β(M)-NT	20.09	22.73	23.58	23.84	23.92
9β(M)-PH	19.52	22.65	23.57	23.84	23.92
9β(D)$*$-NC	21.81	23.15	23.64	23.85	23.92
9β(D)$*$-EP	22.13	23.28	23.69	23.86	23.92
9β(D)$*$-OC	22.30	23.29	23.69	23.86	23.92
9β(D)$*$-NT	22.61	23.31	23.69	23.86	23.92
9β(D)$*$-PH	21.81	23.19	23.66	23.85	23.93
9β(D)-NC	19.50	22.63	23.56	23.83	23.92
9β(D)-EP	19.78	22.71	23.58	23.84	23.92
9β(D)-OC	19.88	22.72	23.58	23.84	23.92
9β(D)-NT	20.11	22.73	23.58	23.84	23.92
9β(D)-PH	19.53	22.65	23.57	23.84	23.92
Best known			23.90		

Table 3.3: Cook's membrane: Center displacement u_{2_C} (continued)

	2×2 mesh		4×4 mesh		8×8 mesh	
Element	$(\sigma_{\max})_A$	$(\sigma_{\min})_B$	$(\sigma_{\max})_A$	$(\sigma_{\min})_B$	$(\sigma_{\max})_A$	$(\sigma_{\min})_B$
Q4	0.1278	-0.0908	0.1905	-0.1508	0.2251	-0.1866
QC9D	0.1839	-0.1616	0.2241	-0.1805	0.2323	-0.2013
5β-NC	0.1657	-0.1614	0.2201	-0.1832	0.2334	-0.1973
5β-EP	0.1855	-0.1564	0.2241	-0.1857	0.2345	-0.1986
5β-OC	0.1776	-0.1688	0.2225	-0.1855	0.2343	-0.1987
5β-NT	0.1721	-0.1775	0.2215	-0.1835	0.2344	-0.1982
5β-PH	0.1884	-0.1557	0.2250	-0.1851	0.2347	-0.1984
8β(M)$*$-NC	0.1675	-0.2042	0.2122	-0.1877	0.2266	-0.1981
8β(M)$*$-EP	0.2052	-0.2262	0.2340	-0.2025	0.2357	-0.2020
8β(M)$*$-OC	0.1927	-0.2261	0.2316	-0.2036	0.2355	-0.2020
Best known	0.2360	-0.2010	0.2360	-0.2010	0.2360	-0.2010

Table 3.4: Cook's membrane: Stress analysis

	2×2 mesh		4×4 mesh		8×8 mesh	
Element	$(\sigma_{\max})_A$	$(\sigma_{\min})_B$	$(\sigma_{\max})_A$	$(\sigma_{\min})_B$	$(\sigma_{\max})_A$	$(\sigma_{\min})_B$
8β(M)$*$-NT	0.1798	-0.2420	0.2293	-0.2043	0.2352	-0.2020
8β(M)$*$-PH	0.2147	-0.2315	0.2333	-0.1971	0.2357	-0.2021
8β(M)-NC	0.1564	-0.1569	0.2092	-0.1736	0.2269	-0.1955
8β(M)-EP	0.1813	-0.1645	0.2264	-0.1822	0.2355	-0.1989
8β(M)-OC	0.1765	-0.1842	0.2246	-0.1809	0.2352	-0.1989
8β(M)-NT	0.1601	-0.2066	0.2212	-0.1801	0.2345	-0.1990
8β(M)-PH	0.1856	-0.1777	0.2281	-0.1813	0.2358	-0.1996
8β(D)$*$-NC	0.1679	-0.2033	0.2122	-0.1877	0.2266	-0.1981
8β(D)$*$-EP	0.2058	-0.2257	0.2340	-0.2025	0.2357	-0.2020
8β(D)$*$-OC	0.1933	-0.2257	0.2316	-0.2037	0.2355	-0.2020
8β(D)$*$-NT	0.1804	-0.2417	0.2292	-0.2043	0.2352	-0.2020
8β(D)$*$-PH	0.2148	-0.2307	0.2332	-0.1971	0.2357	-0.2021
8β(D)-NC	0.1565	-0.1562	0.2092	-0.1736	0.2269	-0.1955
8β(D)-EP	0.1810	-0.1646	0.2264	-0.1822	0.2355	-0.1989
8β(D)-OC	0.1763	-0.1842	0.2245	-0.1809	0.2352	-0.1989
8β(D)-NT	0.1600	-0.2062	0.2212	-0.1801	0.2345	-0.1990
8β(D)-PH	0.1853	-0.1775	0.2280	-0.1812	0.2357	-0.1996
9β(M)$*$-NC	0.1639	-0.1991	0.2123	-0.1884	0.2266	-0.1981
9β(M)$*$-EP	0.1964	-0.2069	0.2317	-0.2014	0.2354	-0.2019
9β(M)$*$-OC	0.1876	-0.2121	0.2297	-0.2022	0.2351	-0.2019
9β(M)$*$-NT	0.1700	-0.2300	0.2263	-0.2030	0.2347	-0.2020
9β(M)$*$-PH	0.1946	-0.2261	0.2312	-0.1978	0.2350	-0.2021
9β(M)-NC	0.1606	-0.1685	0.2108	-0.1754	0.2270	-0.1960
9β(M)-EP	0.1850	-0.1795	0.2302	-0.1831	0.2352	-0.1995
9β(M)-OC	0.1766	-0.1886	0.2278	-0.1831	0.2349	-0.1996
9β(M)-NT	0.1629	-0.2089	0.2240	-0.1839	0.2342	-0.1999
9β(M)-PH	0.1868	-0.1928	0.2286	-0.1834	0.2352	-0.2001
9β(D)$*$-NC	0.1641	-0.1983	0.2124	-0.1884	0.2266	-0.1981
9β(D)$*$-EP	0.1967	-0.2066	0.2317	-0.2015	0.2354	-0.2019
9β(D)$*$-OC	0.1879	-0.2118	0.2296	-0.2022	0.2351	-0.2019
9β(D)$*$-NT	0.1703	-0.2297	0.2263	-0.2031	0.2347	-0.2020
9β(D)$*$-PH	0.1946	-0.2256	0.2312	-0.1978	0.2350	-0.2021
9β(D)-NC	0.1607	-0.1678	0.2108	-0.1754	0.2270	-0.1960
9β(D)-EP	0.1850	-0.1793	0.2302	-0.1831	0.2352	-0.1995
9β(D)-OC	0.1766	-0.1883	0.2277	-0.1831	0.2349	-0.1996
9β(D)-NT	0.1631	-0.2071	0.2240	-0.1839	0.2342	-0.1999
9β(D)-PH	0.1867	-0.1926	0.2285	-0.1834	0.2352	-0.2001
Best known	0.2360	-0.2010	0.2360	-0.2010	0.2360	-0.2010

Table 3.4: Cook's membrane: Stress analysis (continued)

γ	2×2
$G \times 0$	20.73
$G \times 10^{-3}$	20.73
$G \times 10^{-2}$	20.73
$G \times 10^{-2}$	20.67
$G \times 10^{0}$	20.42
$G \times 10^{1}$	20.05
$G \times 10^{2}$	19.94
$G \times 10^{3}$	19.93
Best known	23.90

Table 3.5: Cook's membrane: Influence of γ for the 2×2 mesh

Element	2×2	4×4	8×8	16×16	32×32
5 point integration					
8β(D)$*$-NC	21.93	23.15	23.64	23.85	23.92
8β(D)$*$-EP	22.28	23.29	23.69	23.86	23.92
8β(D)$*$-OC	22.02	23.23	23.68	23.86	23.92
8β(D)$*$-NT	22.31	23.25	23.68	23.86	23.92
8β(D)$*$-PH	21.68	23.16	23.66	23.85	23.93
8β(D)-NC	20.61	22.68	23.56	23.84	23.92
8β(D)-EP	20.47	22.73	23.58	23.84	23.92
8β(D)-OC	20.45	22.70	23.58	23.84	23.92
8β(D)-NT	20.68	22.72	23.58	23.84	23.92
8β(D)-PH	20.36	22.67	23.58	23.85	23.93
8 point integration					
8β(D)$*$-NC	21.93	23.15	23.64	23.85	23.92
8β(D)$*$-EP	22.28	23.29	23.69	23.86	23.92
8β(D)$*$-OC	22.10	23.26	23.68	23.86	23.92
8β(D)$*$-NT	22.40	23.28	23.69	23.86	23.92
8β(D)$*$-PH	21.76	23.17	23.66	23.85	23.93
8β(D)-NC	20.60	22.68	23.56	23.84	23.92
8β(D)-EP	20.47	22.73	23.58	23.84	23.92
8β(D)-OC	20.48	22.72	23.58	23.84	23.92
8β(D)-NT	20.72	22.74	23.58	23.84	23.92
8β(D)-PH	20.39	22.68	23.58	23.85	23.93
Full integration					
8β(D)$*$-NC	21.81	23.15	23.64	23.85	23.92
8β(D)$*$-EP	22.21	23.29	23.69	23.86	23.92
8β(D)$*$-OC	22.41	23.30	23.69	23.86	23.92
8β(D)$*$-NT	22.67	23.32	23.69	23.86	23.92
8β(D)$*$-PH	21.84	23.19	23.66	23.85	23.93
8β(D)-NC	19.59	22.63	23.56	23.83	23.92
8β(D)-EP	20.12	22.72	23.58	23.84	23.92
8β(D)-OC	20.19	22.73	23.58	23.84	23.92
8β(D)-NT	20.42	22.74	23.58	23.84	23.92
8β(D)-PH	19.60	22.65	23.57	23.84	23.92
Best known			23.90		

Table 3.6: Cook's membrane: Effect of integration scheme order

Element	$\nu_1 = .49$	$\nu_2 = .499$	$\nu_3 = .4999$
Q4	4.277E-03	1.821E-03	2.694E-04
QC9D	4.848E-03	3.832E-03	1.226E-03
5β-NC	5.035E-03	5.055E-03	5.057E-03
5β-EP	4.996E-03	5.015E-03	5.017E-03
5β-OC	4.996E-03	5.014E-03	5.016E-03
5β-NT	4.996E-03	5.015E-03	5.017E-03
5β-PH	4.996E-03	5.015E-03	5.017E-03
8β(M)*-NC	5.003E-03	5.022E-03	5.024E-03
8β(M)*-EP	4.990E-03	5.008E-03	5.010E-03
8β(M)*-OC	4.990E-03	5.007E-03	5.009E-03
8β(M)*-NT	4.990E-03	5.008E-03	5.010E-03
8β(M)*-PH	4.915E-03	4.866E-03	4.853E-03
8β(M)-NC	5.003E-03	5.022E-03	5.024E-03
8β(M)-EP	4.990E-03	5.008E-03	5.010E-03
8β(M)-OC	4.990E-03	5.007E-03	5.009E-03
8β(M)-NT	4.990E-03	5.008E-03	5.010E-03
8β(M)-PH	4.915E-03	4.865E-03	4.852E-03
8β(D)*-NC	5.003E-03	5.022E-03	5.024E-03
8β(D)*-EP	4.990E-03	5.008E-03	5.010E-03
8β(D)*-OC	4.990E-03	5.007E-03	5.009E-03
8β(D)*-NT	4.990E-03	5.008E-03	5.010E-03
8β(D)*-PH	4.915E-03	4.866E-03	4.853E-03
8β(D)-NC	5.003E-03	5.022E-03	5.024E-03
8β(D)-EP	4.990E-03	5.008E-03	5.010E-03
8β(D)-OC	4.990E-03	5.007E-03	5.009E-03
8β(D)-NT	4.990E-03	5.008E-03	5.010E-03
8β(D)-PH	4.915E-03	4.865E-03	4.852E-03
9β(M)*-NC	5.003E-03	5.022E-03	5.024E-03
9β(M)*-EP	4.990E-03	5.008E-03	5.009E-03
9β(M)*-OC	4.989E-03	5.007E-03	5.009E-03
9β(M)*-NT	4.990E-03	5.007E-03	5.009E-03
9β(M)*-PH	4.915E-03	4.865E-03	4.852E-03
9β(M)-NC	5.003E-03	5.022E-03	5.024E-03
9β(M)-EP	4.990E-03	5.008E-03	5.009E-03
9β(M)-OC	4.989E-03	5.007E-03	5.009E-03
9β(M)-NT	4.990E-03	5.007E-03	5.009E-03
9β(M)-PH	4.915E-03	4.865E-03	4.852E-03
9β(D)*-NC	5.003E-03	5.022E-03	5.024E-03
9β(D)*-EP	4.990E-03	5.008E-03	5.009E-03
9β(D)*-OC	4.989E-03	5.007E-03	5.009E-03
9β(D)*-NT	4.990E-03	5.007E-03	5.009E-03
Analytical	5.040E-03	5.060E-03	5.062E-03

Table 3.7: Thick-walled cylinder: Radial displacement

Element	$\nu_1 = .49$	$\nu_2 = .499$	$\nu_3 = .4999$
9β(D)$*$-PH	4.915E-03	4.865E-03	4.852E-03
9β(D)-NC	5.003E-03	5.022E-03	5.024E-03
9β(D)-EP	4.990E-03	5.008E-03	5.009E-03
9β(D)-OC	4.989E-03	5.007E-03	5.009E-03
9β(D)-NT	4.990E-03	5.007E-03	5.009E-03
9β(D)-PH	4.915E-03	4.865E-03	4.852E-03
Analytical	5.040E-03	5.060E-03	5.062E-03

Table 3.7: Thick-walled cylinder: Radial displacement (continued)

Element	1×4	2×8	4×16	Irregular mesh
Q4	0.2434	0.3161	0.3446	0.2108
QC9D	0.3426	0.3490	0.3536	0.3206
5β-NC	0.3505	0.3516	0.3544	0.3218
5β-EP	0.3505	0.3516	0.3544	0.3483
5β-OC	0.3505	0.3516	0.3544	0.3425
5β-NT	0.3505	0.3516	0.3544	0.3497
5β-PH	0.3505	0.3516	0.3544	0.3483
8β(M)$*$-NC	0.3465	0.3521	0.3548	0.3440
8β(M)$*$-EP	0.3465	0.3521	0.3548	0.3455
8β(M)$*$-OC	0.3465	0.3521	0.3548	0.3452
8β(M)$*$-NT	0.3465	0.3521	0.3548	0.3473
8β(M)$*$-PH	0.3465	0.3521	0.3548	0.3445
8β(M)-NC	0.3456	0.3497	0.3538	0.3264
8β(M)-EP	0.3456	0.3497	0.3538	0.3289
8β(M)-OC	0.3456	0.3497	0.3538	0.3298
8β(M)-NT	0.3456	0.3497	0.3538	0.3317
8β(M)-PH	0.3456	0.3497	0.3538	0.3308
8β(D)$*$-NC	0.3465	0.3521	0.3548	0.3440
8β(D)$*$-EP	0.3465	0.3521	0.3548	0.3456
8β(D)$*$-OC	0.3465	0.3521	0.3548	0.3492
8β(D)$*$-NT	0.3465	0.3521	0.3548	0.3474
8β(D)$*$-PH	0.3465	0.3521	0.3548	0.3445
8β(D)-NC	0.3456	0.3497	0.3538	0.3264
8β(D)-EP	0.3456	0.3497	0.3538	0.3289
8β(D)-OC	0.3456	0.3497	0.3538	0.3299
8β(D)-NT	0.3456	0.3497	0.3538	0.3318
8β(D)-PH	0.3456	0.3497	0.3538	0.3308
9β(M)$*$-NC	0.3465	0.3521	0.3548	0.3437
Analytical			0.3553	

Table 3.8: Cook's beam: Tip displacement u_{2_A}

Element	1×4	2×8	4×16	Irregular mesh
9β(M)$*$-EP	0.3465	0.3521	0.3548	0.3450
9β(M)$*$-OC	0.3465	0.3521	0.3548	0.3461
9β(M)$*$-NT	0.3465	0.3521	0.3548	0.3466
9β(M)$*$-PH	0.3465	0.3521	0.3548	0.3442
9β(M)-NC	0.3456	0.3497	0.3538	0.3257
9β(M)-EP	0.3456	0.3497	0.3538	0.3273
9β(M)-OC	0.3456	0.3497	0.3538	0.3291
9β(M)-NT	0.3456	0.3497	0.3538	0.3293
9β(M)-PH	0.3456	0.3497	0.3538	0.3304
9β(D)$*$-NC	0.3465	0.3521	0.3548	0.3437
9β(D)$*$-EP	0.3465	0.3521	0.3548	0.3450
9β(D)$*$-OC	0.3465	0.3521	0.3548	0.3461
9β(D)$*$-NT	0.3465	0.3521	0.3548	0.3466
9β(D)$*$-PH	0.3465	0.3521	0.3548	0.3442
9β(D)-NC	0.3456	0.3497	0.3538	0.3257
9β(D)-EP	0.3456	0.3497	0.3538	0.3273
9β(D)-OC	0.3456	0.3497	0.3538	0.3291
9β(D)-NT	0.3456	0.3497	0.3538	0.3293
9β(D)-PH	0.3456	0.3497	0.3538	0.3305
Analytical			0.3553	

Table 3.8: Cook's beam: Tip displacement u_{2_A} (continued)

	1×4 mesh		2×8 mesh		Irregular mesh	
Element	$(-\sigma_{11})_B$	$(\sigma_{12})_C$	$(-\sigma_{11})_B$	$(\sigma_{12})_C$	$(-\sigma_{11})_B$	$(\sigma_{12})_C$
Q4	44.08	1.068	55.70	2.029	38.65	-
QC9D	63.06	2.044	61.87	2.797	56.33	-
5β-NC	60.00	3.333	60.05	3.333	54.72	-
5β-EP	60.00	3.333	60.05	3.333	58.28	-
5β-OC	60.00	3.333	60.05	3.333	55.62	-
5β-NT	60.00	3.333	60.05	3.333	58.79	-
5β-PH	60.00	3.333	60.05	3.333	60.25	-
8β(M)$*$-NC	61.63	2.865	61.20	1.035	62.05	-
8β(M)$*$-EP	61.63	2.865	61.20	1.035	63.55	-
8β(M)$*$-OC	61.63	2.865	61.20	1.035	60.43	-
8β(M)$*$-NT	61.63	2.865	61.20	1.035	63.50	-
8β(M)$*$-PH	61.63	2.865	61.20	1.035	63.99	-
8β(M)-NC	60.12	2.805	59.78	3.194	58.85	-
8β(M)-EP	60.12	2.805	59.78	3.194	61.89	-
Analytical	60.00	5.000	60.00	5.000	60.00	5.000

Table 3.9: Cook's beam: Stress analysis

	1 × 4 mesh		2 × 8 mesh		Irregular mesh	
Element	$(-\sigma_{11})_B$	$(\sigma_{12})_C$	$(-\sigma_{11})_B$	$(\sigma_{12})_C$	$(-\sigma_{11})_B$	$(\sigma_{12})_C$
8β(M)-OC	60.12	2.805	59.78	3.194	59.40	-
8β(M)-NT	60.12	2.805	59.78	3.194	61.14	-
8β(M)-PH	60.12	2.805	59.78	3.194	57.53	-
8β(D)$*$-NC	61.63	2.865	61.20	1.035	62.02	-
8β(D)$*$-EP	61.63	2.865	61.20	1.035	63.53	-
8β(D)$*$-OC	61.63	2.865	61.20	1.035	60.41	-
8β(D)$*$-NT	61.63	2.865	61.20	1.035	63.50	-
8β(D)$*$-PH	61.63	2.865	61.20	1.035	63.94	-
8β(D)-NC	60.12	2.805	59.78	3.194	58.82	-
8β(D)-EP	60.12	2.805	59.78	3.194	61.88	-
8β(D)-OC	60.12	2.805	59.78	3.194	59.39	-
8β(D)-NT	60.12	2.805	59.78	3.194	61.14	-
8β(D)-PH	60.12	2.805	59.78	3.194	57.52	-
9β(M)$*$-NC	61.63	2.865	61.20	1.035	62.18	-
9β(M)$*$-EP	61.63	2.865	61.20	1.035	62.72	-
9β(M)$*$-OC	61.63	2.865	61.20	1.035	63.44	-
9β(M)$*$-NT	61.63	2.865	61.20	1.035	62.17	-
9β(M)$*$-PH	61.63	2.865	61.20	1.035	63.53	-
9β(M)-NC	60.12	2.805	59.78	3.194	57.31	-
9β(M)-EP	60.12	2.805	59.78	3.194	57.74	-
9β(M)-OC	60.12	2.805	59.78	3.194	58.99	-
9β(M)-NT	60.12	2.805	59.78	3.194	56.19	-
9β(M)-PH	60.12	2.805	59.78	3.194	55.71	-
9β(D)$*$-NC	61.63	2.865	61.20	1.035	62.15	-
9β(D)$*$-EP	61.63	2.865	61.20	1.035	62.69	-
9β(D)$*$-OC	61.63	2.865	61.20	1.035	63.43	-
9β(D)$*$-NT	61.63	2.865	61.20	1.035	62.50	-
9β(D)$*$-PH	61.63	2.865	61.20	1.035	63.48	-
9β(D)-NC	60.12	2.805	59.78	3.194	57.29	-
9β(D)-EP	60.12	2.805	59.78	3.194	57.73	-
9β(D)-OC	60.12	2.805	59.78	3.194	58.99	-
9β(D)-NT	60.12	2.805	59.78	3.194	56.18	-
9β(D)-PH	60.12	2.805	59.78	3.194	55.70	-
Analytical	60.00	5.000	60.00	5.000	60.00	5.000

Table 3.9: Cook's beam: Stress analysis (continued)

	Center displacement u_{2_A}				Tip rotation ψ_B			
	Regular mesh		Irregular mesh		Regular mesh		Irregular mesh	
Element	LC 1	LC 2	LC 1	LC 2	LC 1	LC 2	LC 1	LC 2
Q4	0.6921	-	0.2749	-	-	-	-	-
QC9D	1.462	1.472	1.181	1.207	0.5801	0.6385	0.5243	0.6801
5β-NC	1.500	-	0.6987	-	-	-	-	-
5β-EP	1.500	-	1.405	-	-	-	-	-
5β-OC	1.500	-	1.389	-	-	-	-	-
5β-NT	1.500	-	1.418	-	-	-	-	-
5β-PH	1.500	-	1.393	-	-	-	-	-
8β(M)*-NC	1.461	1.470	2.021	2.004	0.5765	0.6377	0.8855	1.019
8β(M)*-EP	1.483	1.493	1.485	1.488	0.5876	0.6455	0.5930	0.7540
8β(M)*-OC	1.483	1.493	1.489	1.493	0.5876	0.6455	0.5943	0.7632
8β(M)*-NT	1.483	1.493	1.481	1.488	0.5876	0.6455	0.6079	0.7900
8β(M)*-PH	1.461	1.470	1.447	1.436	0.5765	0.6377	0.6160	0.8747
8β(M)-NC	1.461	1.470	1.500	1.530	0.5765	0.6377	0.7346	0.9267
8β(M)-EP	1.483	1.493	1.232	1.254	0.5876	0.6455	0.5734	0.7623
8β(M)-OC	1.483	1.493	1.233	1.257	0.5876	0.6455	0.5956	0.7971
8β(M)-NT	1.483	1.493	1.245	1.266	0.5876	0.6455	0.6068	0.8368
8β(M)-PH	1.461	1.470	1.273	1.317	0.5765	0.6377	0.6066	0.9481
8β(D)*-NC	1.461	1.470	2.011	1.991	0.5765	0.6377	0.8702	0.9925
8β(D)*-EP	1.483	1.493	1.483	1.485	0.5876	0.6455	0.5889	0.7374
8β(D)*-OC	1.483	1.493	1.487	1.491	0.5876	0.6455	0.5902	0.7450
8β(D)*-NT	1.483	1.493	1.480	1.485	0.5876	0.6455	0.6034	0.7704
8β(D)*-PH	1.461	1.470	1.445	1.432	0.5765	0.6377	0.6084	0.8428
8β(D)-NC	1.461	1.470	1.488	1.512	0.5765	0.6377	0.7150	0.8895
8β(D)-EP	1.483	1.493	1.229	1.250	0.5876	0.6455	0.5689	0.7421
8β(D)-OC	1.483	1.493	1.230	1.253	0.5876	0.6455	0.5907	0.7741
8β(D)-NT	1.483	1.493	1.243	1.262	0.5876	0.6455	0.6009	0.8106
8β(D)-PH	1.461	1.470	1.271	1.311	0.5765	0.6377	0.5959	0.9037
9β(M)*-NC	1.461	1.470	1.995	1.979	0.5765	0.6377	0.8129	1.007
9β(M)*-EP	1.483	1.493	1.480	1.483	0.5876	0.6455	0.5917	0.7534
9β(M)*-OC	1.483	1.493	1.482	1.484	0.5876	0.6455	0.5937	0.7622
9β(M)*-NT	1.483	1.493	1.473	1.481	0.5876	0.6455	0.6063	0.7886
9β(M)*-PH	1.461	1.470	1.434	1.426	0.5765	0.6377	0.6054	0.8542
9β(M)-NC	1.461	1.470	1.484	1.518	0.5765	0.6377	0.7272	0.9187
9β(M)-EP	1.483	1.493	1.228	1.253	0.5876	0.6455	0.5706	0.7616
9β(M)-OC	1.483	1.493	1.230	1.254	0.5876	0.6455	0.5949	0.7979
9β(M)-NT	1.483	1.493	1.243	1.267	0.5876	0.6455	0.6063	0.8365
9β(M)-PH	1.461	1.470	1.265	1.307	0.5765	0.6377	0.5978	0.9273
9β(D)*-NC	1.461	1.470	1.985	1.967	0.5765	0.6377	0.8580	0.9807
9β(D)*-EP	1.483	1.493	1.478	1.480	0.5876	0.6455	0.5877	0.7369
Analytical	1.500				0.600			

Table 3.10: Higher order patch test: Numerical results

	Center displacement u_{2_A}				Tip rotation ψ_B			
	Regular mesh		Irregular mesh		Regular mesh		Irregular mesh	
Element	LC 1	LC 2	LC 1	LC 2	LC 1	LC 2	LC 1	LC 2
9β(D)$*$-OC	1.483	1.493	1.480	1.482	0.5876	0.6455	0.5898	0.7442
9β(D)$*$-NT	1.483	1.493	1.472	1.479	0.5876	0.6455	0.6019	0.7691
9β(D)$*$-PH	1.461	1.470	1.433	1.422	0.5765	0.6377	0.5988	0.8251
9β(D)-NC	1.461	1.470	1.472	1.500	0.5765	0.6377	0.7079	0.8821
9β(D)-EP	1.483	1.493	1.226	1.248	0.5876	0.6455	0.5660	0.7414
9β(D)-OC	1.483	1.493	1.228	1.250	0.5876	0.6455	0.5901	0.7752
9β(D)-NT	1.483	1.493	1.241	1.262	0.5876	0.6455	0.6003	0.8103
9β(D)-PH	1.461	1.470	1.264	1.301	0.5765	0.6377	0.5881	0.8862
Analytical	1.500				0.600			

Table 3.10: Higher order patch test: Numerical results (continued)

Chapter 4

Isotropic flat shell elements

In this chapter, flat shell elements are formulated through the assembly of membrane and plate elements. The exact solution of a shell approximated by flat facets compared to the exact solution of a truly curved shell may reveal considerable differences in the distribution of bending moments, shearing forces, etc. However, for 'simple' elements the discretization error is approximately of the same order and excellent results can be obtained with the flat shell approximation [39]. Apart from being easy to define geometrically, flat shell elements will always converge to the correct deep shell solution in the limit of mesh refinement [46].

4.1 Plate formulation

For the plate component of the flat shell element the shear deformable formulation of Mindlin is employed. The final formulation is modified to include the assumed strain interpolation of Bathe and Dvorkin [47]. [1]

4.1.1 Mindlin plates: Bending theory and variational formulation

In this section the treatments of Hinton and Huang [48] and Papadopoulos and Taylor [49] are followed closely, albeit with different notations. However, the same may be found in the standard works of, for instance Hughes [38], Zienkiewicz and Taylor [39] and Bathe [50].

The simplest plate formulation which accounts for the effect of shear deformation, is presented. The transverse shear is assumed constant throughout the thickness. The assumptions of the first order Mindlin theory are

$$\sigma_{33} = 0 \tag{4.1}$$

$$u_1 = x_3\psi_1(x_1, x_2)$$

[1] From now on, the drilling degree of freedom ψ, introduced in Chapter 2, is denoted ψ_3 for reasons of clarity.

$$\begin{aligned} u_2 &= x_3\psi_2(x_1, x_2) \\ u_3 &= u_3(x_1, x_2) \end{aligned} \tag{4.2}$$

where u_1, u_2 and u_3 are the displacements components in the x_1, x_2 and x_3 directions respectively, u_3 is the lateral displacement and ψ_1 and ψ_2 are the normal rotations in the x_{13} and x_{23} planes respectively (See Figure 4.1). The element is assumed to be flat, with thickness t. Flatness of the plate is not a necessary assumption, but merely simplifies the required notation and implementation. The element area is denoted Ω.

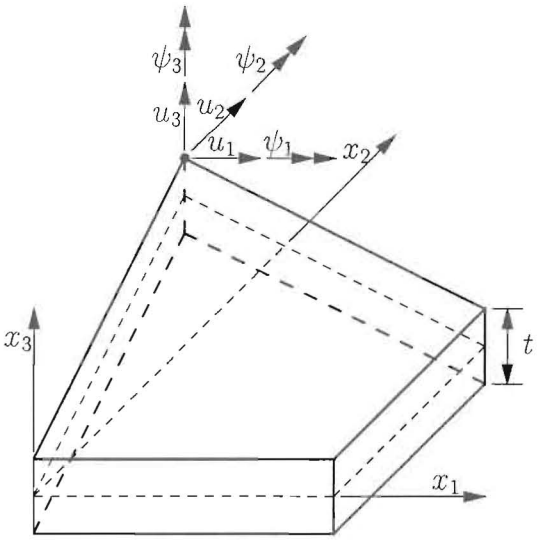

Figure 4.1: Four-node shell element

(4.1) is obviously inconsistent with three-dimensional elasticity. However, the transverse normal stress may be neglected for plates where the thickness is small compared with the other dimensions. Moreover, when a linear or constant through-the-thickness displacement assumption is made, as is customary in the shear-deformable plate theories, limited locking occurs due to the Poisson effect, when σ_{33} is restrained. (4.2) implies that straight normals to the reference surface, $x_3 = 0$, remain straight, but do not necessarily remain normal to the plate after deformation (Figure 4.2). Also, the transverse displacement u_3 is constant through the thickness.

The displacement field assumed in (4.2) yields in-plane strains of the form

$$\begin{aligned} \epsilon_{11} &= x_3\psi_{1,1} \\ \epsilon_{22} &= x_3\psi_{2,2} \\ \gamma_{12} &= x_3(\psi_{1,2} + \psi_{2,1}) \end{aligned} \tag{4.3}$$

where

$$\psi_{1,1} = \frac{\partial \psi_1}{\partial x_1}, \text{ etc.} \tag{4.4}$$

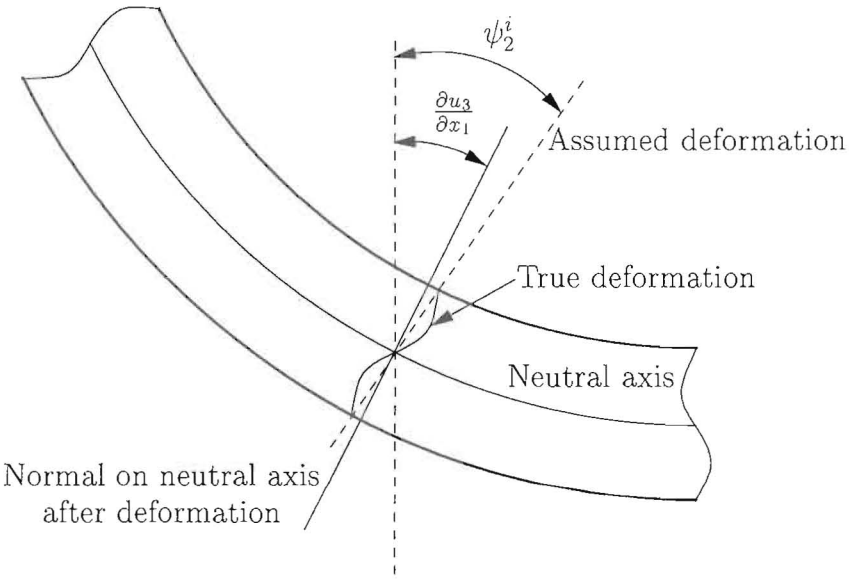

Figure 4.2: Mindlin theory

The transverse shear strains are obtained as

$$\begin{aligned} \gamma_{13} &= u_{3,1} + \psi_2 \\ \gamma_{23} &= u_{3,2} + \psi_1 \end{aligned} \tag{4.5}$$

For plane stress and linear isotropic elasticity the forgoing strain field defines the in-plane stresses as

$$\sigma_{11} = \frac{E}{1-\nu^2}[\epsilon_{11} + \nu\epsilon_{22}] \tag{4.6}$$

$$\sigma_{22} = \frac{E}{1-\nu^2}[\epsilon_{22} + \nu\epsilon_{11}] \tag{4.7}$$

$$\sigma_{12} = \sigma_{21} = G\gamma_{12} \tag{4.8}$$

where E is Young's modulus and ν is Poisson's ratio. Similarly, the out-of-plane stresses are given by

$$\sigma_{13} = \sigma_{31} = G\gamma_{13} \tag{4.9}$$

$$\sigma_{23} = \sigma_{32} = G\gamma_{23} \tag{4.10}$$

where

$$G = \frac{E}{2(1+\nu)} \tag{4.11}$$

Integrating the in-plane stresses, which vary linearly along the plate thickness, gives stress resultants of the form

$$M_{11} = \int_{-\frac{t}{2}}^{\frac{t}{2}} \sigma_{11} x_3 \, \mathrm{d}x_3 \tag{4.12}$$

$$M_{22} = \int_{-\frac{t}{2}}^{\frac{t}{2}} \sigma_{22} x_3 \, \mathrm{d}x_3 \tag{4.13}$$

$$M_{12} = M_{21} = \int_{-\frac{t}{2}}^{\frac{t}{2}} \sigma_{12} x_3 \, \mathrm{d}x_3 \tag{4.14}$$

Introducing matrix notation, the forgoing are written as

$$\boldsymbol{M} = \begin{bmatrix} M_{11} \\ M_{22} \\ M_{12} \end{bmatrix} \tag{4.15}$$

and the curvatures $\boldsymbol{\kappa}$ as

$$\boldsymbol{\kappa} = \begin{bmatrix} \psi_{1,1} \\ \psi_{2,2} \\ \psi_{1,2} + \psi_{2,1} \end{bmatrix} \tag{4.16}$$

It follows that the moment-curvature relation may be expressed as

$$\boldsymbol{M} = \boldsymbol{D}_b \boldsymbol{\kappa} \tag{4.17}$$

where

$$\boldsymbol{D}_b = \frac{Et^3}{12(1-\nu^2)} \begin{bmatrix} 1 & \nu & 0 \\ \nu & 1 & 0 \\ 0 & 0 & \frac{1-\nu}{2} \end{bmatrix} \tag{4.18}$$

Similarly, the out-of-plane stresses, when integrated along the thickness, give transverse shear forces

$$Q_{13} = \int_{-\frac{t}{2}}^{\frac{t}{2}} \sigma_{13} \, \mathrm{d}x_3 \tag{4.19}$$

$$Q_{23} = \int_{-\frac{t}{2}}^{\frac{t}{2}} \sigma_{23} \, \mathrm{d}x_3 \tag{4.20}$$

which, using matrix notation, results in

$$\boldsymbol{Q} = \boldsymbol{D}_s \boldsymbol{\gamma} \tag{4.21}$$

where

$$\boldsymbol{Q} = \begin{bmatrix} Q_{13} \\ Q_{23} \end{bmatrix} \tag{4.22}$$

$$\boldsymbol{\gamma} = \begin{bmatrix} u_{3,1} + \psi_2 \\ u_{3,2} + \psi_1 \end{bmatrix} \tag{4.23}$$

$$\boldsymbol{D}_s = Gt \begin{bmatrix} 1 & 0 \\ 0 & 1 \end{bmatrix} \tag{4.24}$$

Summation convention is implied over x_1, x_2 and x_3 for Latin indices and over x_1 and x_2 for Greek indices, so that the local equilibrium equations may be appropriately integrated through the thickness to deduce the plate equilibrium equations

$$\begin{aligned} M_{\alpha\beta,\beta} - S_\alpha &= 0 \\ S_{\alpha,\alpha} + p &= 0 \end{aligned} \tag{4.25}$$

where p denotes the transverse surface loading. The first equation relates the bending moments to the shear forces, whereas the second is a statement of transverse force equilibrium.

In the limiting case where $t \to 0$ the Kirchhoff hypothesis of zero transverse shear strains must hold. Therefore

$$\begin{aligned} u_{3,1} + \psi_2 &= 0 \\ u_{3,2} + \psi_1 &= 0 \end{aligned} \tag{4.26}$$

(4.5) imply that the transverse shear strain remains constant through the element thickness. This is inconsistent with classical theory, where the corresponding transverse shear stress varies quadratically. Also, the transverse shear strain on the plate surface is required to be zero. Consequently, a temporary modification to the displacement field is made, namely

$$u_1 = x_3\psi_1 + (x_3^3 + \beta x_3)\phi(x_1, x_2) \tag{4.27}$$

Imposing the constraint

$$\int_{-\frac{t}{2}}^{\frac{t}{2}} (x_3^3 + \beta x_3)x_3 \, \mathrm{d}x_3 = 0 \tag{4.28}$$

and setting $\gamma_{13} = 0$ on the plate faces results in

$$\gamma_{13} = \left[1 - \frac{5}{3t^2}\left(3x_3^2 - \frac{3t^2}{20}\right)\right](\psi_2 + u_{3,1}) \tag{4.29}$$

Moreover, substituting (4.29) into (4.21) leads to

$$\begin{aligned} Q_{13} &= \int_{-\frac{t}{2}}^{\frac{t}{2}} G\gamma_{13}\, \mathrm{d}x_3 \\ &= G(\psi_2 + u_{3,1}) \int_{-\frac{t}{2}}^{\frac{t}{2}} \left[1 - \frac{5}{3t^2}\left(3x_3^2 - \frac{3t^2}{20}\right)\right] \mathrm{d}x_3 \\ &= \frac{5}{6} G(\psi_2 + u_{3,1}) \end{aligned} \tag{4.30}$$

Therefore, for consistency reasons, a 'shear correction' term is introduced as

$$k = \frac{6}{5} \tag{4.31}$$

into (4.21), which now becomes

$$\boldsymbol{Q} = \bar{\boldsymbol{D}}_s \boldsymbol{\gamma} \tag{4.32}$$

where

$$\bar{\boldsymbol{D}}_s = \frac{\boldsymbol{D}_s}{k} \tag{4.33}$$

The total plate energy, based on potential energy for bending and shear, is written as

$$\boldsymbol{\Pi}(\boldsymbol{\kappa}, \boldsymbol{\gamma}) = \frac{1}{2} \int_\Omega \boldsymbol{\kappa}^T \boldsymbol{D}_b \boldsymbol{\kappa}\, d\Omega + \frac{1}{2} \int_\Omega \boldsymbol{\gamma}^T \bar{\boldsymbol{D}}_s \boldsymbol{\gamma}\, d\Omega - \boldsymbol{\Pi}_{ext} \tag{4.34}$$

where $\boldsymbol{\Pi}_{ext}$ is the potential energy of the applied loads. The thin plate Kirchhoff conditions of (4.26) should be satisfied in the finite element interpolation.

4.1.2 Finite element interpolation

The displacement in the reference surface of the element is defined by

$$\begin{pmatrix} u_1 \\ u_2 \end{pmatrix} = \sum_{i=1}^{4} N_i^e(\xi, \eta) \boldsymbol{u}_i \tag{4.35}$$

where $N_i^e(\xi, \eta)$ are the isoparametric shape functions

$$N_i^e(\xi, \eta) = \frac{1}{4}(1 + \xi_i \xi)(1 + \eta_i \eta) \quad i = 1, 2, 3, 4 \tag{4.36}$$

The sectional (normal) rotations are interpolated as

$$\psi_1 = N_i^e(\xi, \eta) \psi_1^i \tag{4.37}$$

$$\psi_2 = N_i^e(\xi, \eta) \psi_2^i \tag{4.38}$$

and the transverse mid-surface displacements are interpolated as

$$u_3 = N_i^e(\xi, \eta) u_3^i \tag{4.39}$$

where u_3^i, ψ_1^i and ψ_2^i are the nodal point values of the variables u_3, ψ_1 and ψ_2 respectively. The curvature-displacement relations are now written as

$$\boldsymbol{\kappa} = \sum_{i=1}^{4} \boldsymbol{B}_{bi} \boldsymbol{q}_i \tag{4.40}$$

The element curvature-displacement matrix is given in Appendix A. The unknowns at node i are

$$\boldsymbol{q}_i = \begin{bmatrix} u_3^i \\ \psi_1^i \\ \psi_2^i \end{bmatrix} \tag{4.41}$$

The shear strain-displacement relations are written as

$$\boldsymbol{\gamma} = \sum_{i=1}^{4} \boldsymbol{B}_{si} \boldsymbol{q}_i \tag{4.42}$$

The element shear strain-displacement matrix is given in Appendix A.

4.1.3 Assumed strain interpolations

The stationary condition of (4.34) directly results in the plate force-displacement relationship

$$\boldsymbol{K}^e \boldsymbol{q} = \boldsymbol{r} \tag{4.43}$$

where

$$\boldsymbol{K}^e = (\boldsymbol{K}_b + \bar{\boldsymbol{K}}_s) \tag{4.44}$$

with

$$\boldsymbol{K}_b = \int_\Omega \boldsymbol{\kappa}^T \boldsymbol{D}_b \boldsymbol{\kappa} \, \mathrm{d}\Omega \tag{4.45}$$

$$\bar{\boldsymbol{K}}_s = \int_\Omega \boldsymbol{\gamma}^T \bar{\boldsymbol{D}}_s \boldsymbol{\gamma} \, \mathrm{d}\Omega \tag{4.46}$$

Subscripts b and s indicate bending and shear respectively. For elements with 4 nodes, the expression for $\boldsymbol{K}_b$ is problem free, at least in terms of locking. The employed interpolation field of (4.36) in $\boldsymbol{K}_s$ results in severe locking when full integration is used.

One solution that overcomes the locking phenomena, while ensuring that the final element formulation is rank sufficient, is to incorporate the substitute assumed strain interpolation field of Bathe and Dvorkin [7, 47].

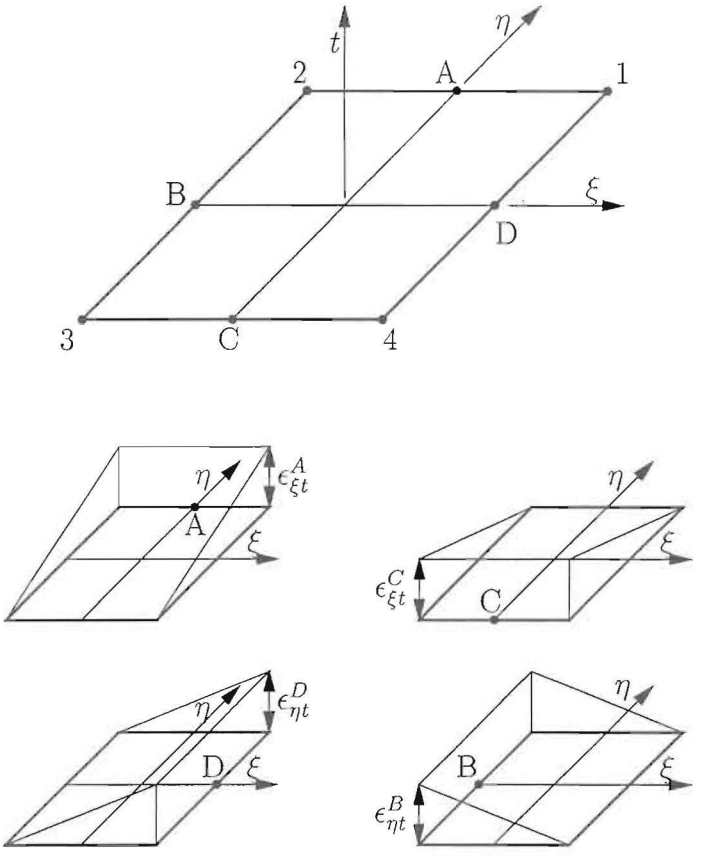

Figure 4.3: Interpolation functions for the transverse shear strains

Depicted in Figure 4.3, the assumed interpolation field of Bathe and Dvorkin is written as

$$\bar{\epsilon}_{\xi t} = \frac{1}{2}(1+\eta)\bar{\epsilon}^A_{\xi t} + \frac{1}{2}(1-\eta)\bar{\epsilon}^C_{\xi t} \tag{4.47}$$

$$\bar{\epsilon}_{\eta t} = \frac{1}{2}(1+\xi)\bar{\epsilon}^D_{\eta t} + \frac{1}{2}(1-\xi)\bar{\epsilon}^B_{\eta t} \tag{4.48}$$

where the superscripts A through D designate the sampling points for calculating the covariant shear strains. The shear strain components in the Cartesian coordinate system, $\bar{\epsilon}_{13}$ and $\bar{\epsilon}_{23}$, are obtained [51] using a transformation which in the case of a flat plate element reduces to the standard (2×2) Jacobian, $\boldsymbol{J}$

$$\begin{Bmatrix} \bar{\epsilon}_{\xi t} \\ \bar{\epsilon}_{\eta t} \end{Bmatrix} = \frac{t}{2} \begin{bmatrix} x_{1,\xi} & x_{2,\xi} \\ x_{1,\eta} & x_{2,\eta} \end{bmatrix} \begin{Bmatrix} \bar{\epsilon}_{13} \\ \bar{\epsilon}_{23} \end{Bmatrix} = \frac{t}{2} \boldsymbol{J} \bar{\boldsymbol{\epsilon}}_s \tag{4.49}$$

Therefore, the substitute shear strains $\bar{\boldsymbol{\epsilon}}_s$ are expressed as

$$\bar{\gamma} = \bar{B}_s q \tag{4.50}$$

while the associated transverse stiffness-displacement relationship becomes

$$\bar{K}_s = \int_\Omega \bar{B}_s^T \bar{D}_s \bar{B}_s \, \mathrm{d}\Omega \tag{4.51}$$

The element stiffness-displacement relationship now becomes

$$(K_b + \bar{K}_s)q = r \tag{4.52}$$

which is the final element formulation. The assumed strain interpolation satisfies the Kirchoff conditions of zero transverse shear strains in the thin plate limit, while locking is also adequately prevented.

4.2 Shell formulation

4.2.1 Element formulation

Flat shell elements are simpler than generally curved shell elements, both in terms of formulation and computer implementation. As the element Jacobian matrix is constant through the thickness, analytical through-the-thickness integration is easily performed.

The element force-displacement relationship of the 8β(M) and 9β(M) membrane families is defined by (2.80), and for the 8β(D) and 9β(D) membrane families by (2.84). These relationships are repeated here using a different notation to distinguish between the membrane and plate components. The two different force-displacement relationships for the membrane families are rewritten in a universal form to clarify the notation

$$K_m q_m = r_m \tag{4.53}$$

where

$$K_m = K + \frac{\gamma}{\Omega} h h^T \tag{4.54}$$

for the mixed formulation, and

$$K_m = K + P_\gamma \tag{4.55}$$

for the displacement formulation.

K_m denotes the membrane stiffness matrix, q_m the element displacements and r_m the element body force vector. The unknown nodal displacements q_m and the specified consistent nodal loads r_m are defined by

$$\boldsymbol{q}_m = [u_1^i \;\; u_2^i \;\; \psi_3^i]^T \tag{4.56}$$
$$\boldsymbol{r}_m = [U_1^i \;\; U_2^i \;\; M_3^i]^T \tag{4.57}$$

where ψ_3^i is the in-plane rotation and M_3^i the in-plane nodal moment.

Similarly, the Mindlin plate force-displacement relationship (see (4.52)) is rewritten as

$$(\boldsymbol{K}_b + \bar{\boldsymbol{K}}_s)\boldsymbol{q}_p = \boldsymbol{r}_p \tag{4.58}$$

The displacements $\boldsymbol{q}_p$, and the specified consistent nodal loads $\boldsymbol{r}_p$, are respectively defined by

$$\boldsymbol{q}_p = [u_3^i \;\; \psi_1^i \;\; \psi_2^i]^T \tag{4.59}$$
$$\boldsymbol{r}_p = [U_3^i \;\; M_1^i \;\; M_2^i]^T \tag{4.60}$$

Through assembly of the membrane and plate elements, the flat shell element stiffness matrix $\boldsymbol{K}^e$ is obtained in a local element coordinate system as

$$\boldsymbol{K}^e = \begin{bmatrix} \boldsymbol{K}_m & 0 \\ \text{symm} & (\boldsymbol{K}_b + \bar{\boldsymbol{K}}_s) \end{bmatrix} \tag{4.61}$$

The local shell force-displacement relationship is given by

$$\boldsymbol{K}^e \boldsymbol{q}^e = \boldsymbol{r}^e \tag{4.62}$$

where the shell nodal displacements and loads for node i respectively are

$$\boldsymbol{q}_i^e = [u_1^i \;\; u_2^i \;\; u_3^i \;\; \psi_1^i \;\; \psi_2^i \;\; \psi_3^i]^T \tag{4.63}$$
$$\boldsymbol{r}_i^e = [U_1^i \;\; U_2^i \;\; U_3^i \;\; M_1^i \;\; M_2^i \;\; M_3^i]^T \tag{4.64}$$

4.2.2 A general warped configuration

The warp correction employed in this study is the so-called 'rigid link' correction suggested by Taylor [6], which is depicted in Figure 4.4. Simple kinematic nodal relationships are used to evaluate the warp effect.

For elements with true rotational degrees of freedom the rotations about the local x_3-axes in the warped and projected planes may be taken as equal. Assuming reasonably small warp, the effect of the drilling degree on the out-of-plane bending rotations is neglected. The strain-displacement modification presented by Taylor is therefore extended by addition of the final row and column as follows [52]

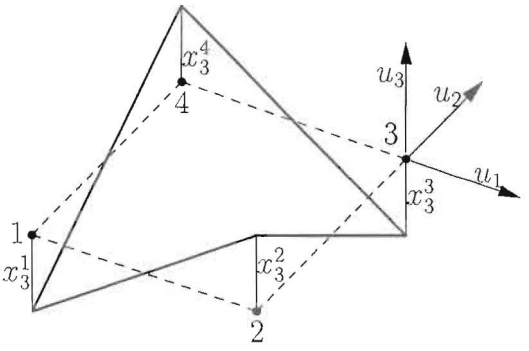

Figure 4.4: Warped and projected quadrilateral shell element

$$\begin{Bmatrix} \bar{u}_1^i \\ \bar{u}_2^i \\ \bar{u}_3^i \\ \bar{\psi}_1^i \\ \bar{\psi}_2^i \\ \bar{\psi}_3^i \end{Bmatrix} = \begin{bmatrix} 1 & 0 & 0 & 0 & 0 & 0 \\ 0 & 1 & 0 & 0 & 0 & 0 \\ 0 & 0 & 1 & 0 & 0 & 0 \\ -x_3^i & 0 & 0 & 1 & 0 & 0 \\ 0 & x_3^i & 0 & 0 & 1 & 0 \\ 0 & 0 & 0 & 0 & 0 & 1 \end{bmatrix} \begin{Bmatrix} u_1^i \\ u_2^i \\ u_3^i \\ \psi_1^i \\ \psi_2^i \\ \psi_3^i \end{Bmatrix} \tag{4.65}$$

where x_3^i defines the warp at each node and bared quantities (for example $\bar{u}_1^i$) act on the flat projection.

This correction is much simpler than for instance the correction presented by Robinson [53].

Chapter 5

Numerical results: Isotropic plates and shells

In this chapter numerical results are presented for the isotropic plate and shell elements presented in Chapter 4.

In the following,

- SA denotes the Bathe-Dvorkin assumed strain plate element [7].
- QI denotes the incompatible modes element presented by Ibrahimbegovic [54].
- QC9D/SA and QC9D*/SA denotes the flat shell elements that are formed by combining the QC9D membrane element of Ibrahimbegovic *et al.* and the Bathe-Dvorkin assumed strain plate element, respectively with and without the locking correction.
- 5β/SA denotes the flat shell element that is formed by combining the 5β-NT membrane element and the Bathe-Dvorkin assumed strain plate element.
- 8β-NC/SA, 8β-NT/SA, $8\beta*$-NC/SA and $8\beta*$-NT/SA denotes the flat shell elements that are formed by the 8β(D) membrane element combined with the Bathe-Dvorkin assumed strain plate element, respectively with and without the locking correction.
- 9β-NC/SA, 9β-NT/SA, $9\beta*$-NC/SA and $9\beta*$-NT/SA denotes the flat shell elements that are formed by the 9β(D) membrane element combined with the Bathe-Dvorkin assumed strain plate element, with and without the locking correction.

The notation '(incl. RBF)' indicates that the following residual bending flexibility correction,

$$\begin{aligned} \frac{1}{G*} &= \frac{1}{G} + \frac{l^2}{Eh^2} \\ &= \frac{1}{G}\left(1 + \frac{l^2}{2(1+\nu)h^2}\right) \end{aligned} \tag{5.1}$$

is included [13, 45, 55], where the term l^2/Eh^2 is denoted the residual bending flexibility in [55].

A shear rigid formulation is obtained by setting the shear correction factor $k \to \infty$ [52].

5.1 Plate patch tests

The plate elements used in this study passed the following patch tests:

- Constant curvature patch test (See Figure 5.1)
- Constant shear patch test with zero rotations (See Figure 5.1)
- Constant twist patch test (See Figure 5.2)

However, the constant twist patch test depicted in Figure 5.2 is passed exactly for thin plates only. Since the plate is exactly the same as the original formulation of Bathe and Dvorkin, these results are not repeated here. (See [7, 47]).

The residual bending flexibility correction is not included in the patch tests. However, the element rank stays unchanged as a result of the residual bending flexibility correction.

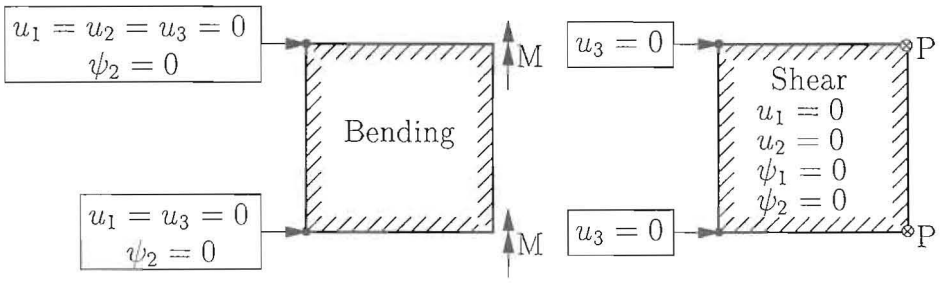

Figure 5.1: Constant curvature patch test and constant shear patch test with zero rotations

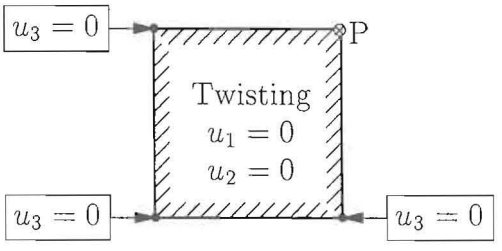

Figure 5.2: Constant twist patch test

5.2 Cantilever under transverse tip loading

This simple one-dimensional problem is taken from Bathe and Dvorkin [47]. The geometry and the material properties are depicted in Figure 5.3. Normal 4-node elements employing bi-linear bending shape functions can only represent this problem in the limit of mesh refinement, since the elements only have a constant strain capability. Table 5.1 reveals that the residual bending flexibility correction raises the capability of the 4-node element to the linear strain level for this problem.

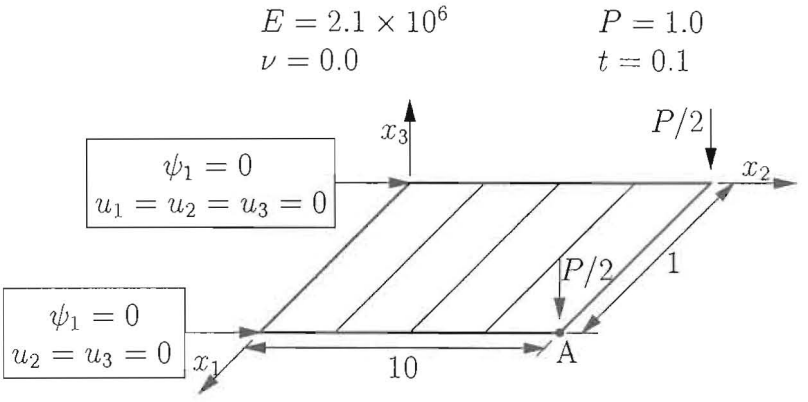

Figure 5.3: Cantilever under transverse tip loading

5.3 Thin simply supported plate under uniformly distributed load

This problem (See Figure 5.4) is included to illustrate the effect of the residual bending flexibility correction on thin plates [54]. Moreover, the effect of the degree of support at the boundaries ($x_1 = l/2$, $x_1 = -l/2$, $x_2 = l/2$ and $x_2 = -l/2$) is also illustrated. Two conditions are considered, namely hard support and soft support. For the soft supported condition the theoretical solution is unknown. The central deflection, $-u_{3_A}$, is measured.

Tables 5.2 and 5.3 show that the QI and SA(incl. RBF) elements converge from above, while the SA and SA($k \to \infty$) elements converge form below.

For both support conditions the results obtained with the SA element are superior to the results obtained with both QI and SA(incl. RBF).

5.4 Pinched hemispherical shell with 18^o hole

This problem forms part of the set proposed by MacNeal and Harder [45]. This doubly-curved shell problem is characterized by inextensible bending modes and large rigid body rotations [56]. The geometry is depicted in Figure 5.5, and tabulated numerical results are

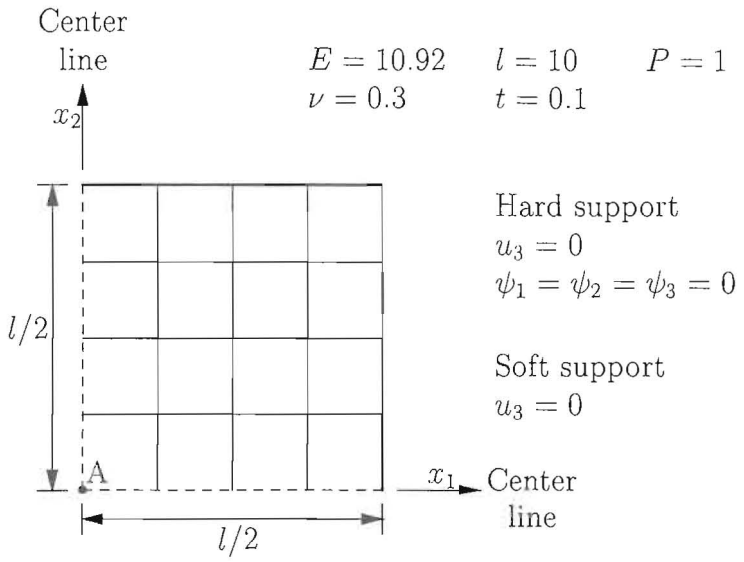

Figure 5.4: Thin simply supported plate under uniformly distributed load

presented in Table 5.4. The exact solution is 0.094 [45], although more recent analyses suggest 0.093 [20].

The results obtained with the 8β/SA and 9β/SA families are almost identical. 5β/SA outperform the 8β/SA and 9β/SA families for a coarse mesh. Note that the NC-formulations are more accurate than the NT-formulations for the coarse mesh.

The influence of γ on this problem is very small, although for small values of γ the accuracy improves slightly. The results are reflected in Table 5.5. The choice of $\gamma = G$ results in good accuracy.

For the coarse mesh the elements with the membrane locking correction using the 8-point integration scheme outperforms the other combinations of integration schemes with and without the locking correction (see Table 5.6).

5.5 Warped pinched hemisphere

In Figure 5.6 the geometry and the discretization of the warped pinched hemisphere is depicted. The chosen discretization implies that quadrilateral flat shell elements become highly warped. Mesh refinement is obtained by bisection. Note that the warpage does not disappear in the limit of mesh refinement.

The exact analytical solution was presented by Parisch [56], which compares well with the solution of the pinched hemisphere with 18° hole, since additional elements in the top of the hemisphere are expected to contribute only slightly towards the overall stiffness of the shell under pinching loads. This problem is also dominated by inextensible bending modes and large rigid body rotations [56].

Table 5.7 reveals that the 5β/SA element outperforms all the other elements for this test. Very little detrimental effect due to the out-of-plane warp is evident. Still, the warp correc-

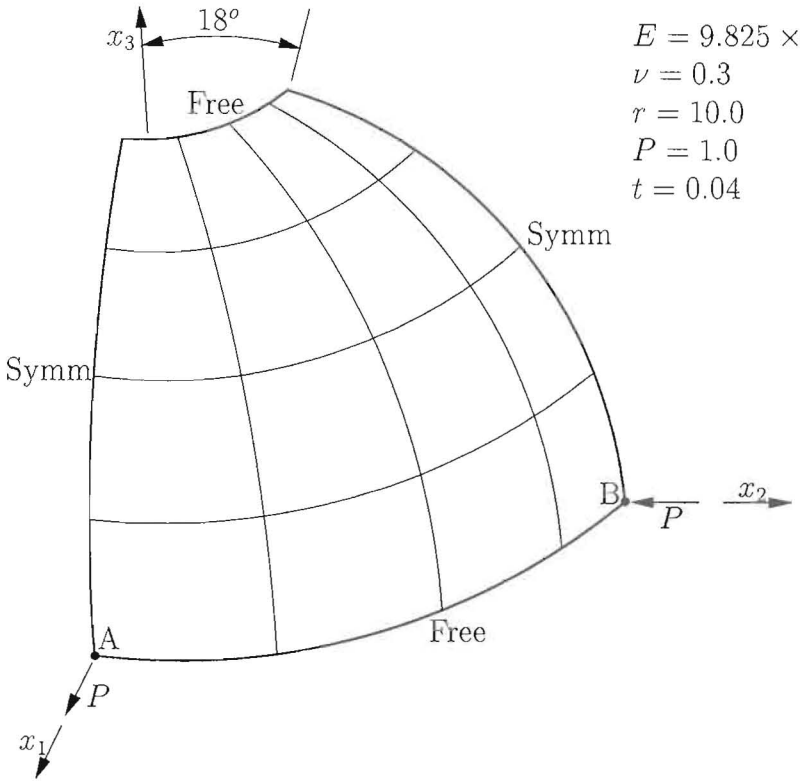

Figure 5.5: Pinched hemisphere

tion, (4.65), is crucial.

5.6 Thick pinched cylinder with open ends

The pinched cylinder problem is dominated by inextensible bending behavior and results will reveal any tendency towards membrane-bending locking [6]. In Figure 5.7 the geometry and the discretization are depicted.

Table 5.8 reveals that the NC-formulations are the most accurate for the coarse mesh. In general, the locking correction improves the element behavior for this problem.

5.7 Thin pinched cylinder with open ends

This problem is identical to the previous, except for a thiner wall thickness (Figure 5.7). Table 5.9 illustrates that all the elements tested perform almost identically, since the drilling degrees of freedom are not activated due to the pinching loads. The locking correction only slightly improves the performance of the elements.

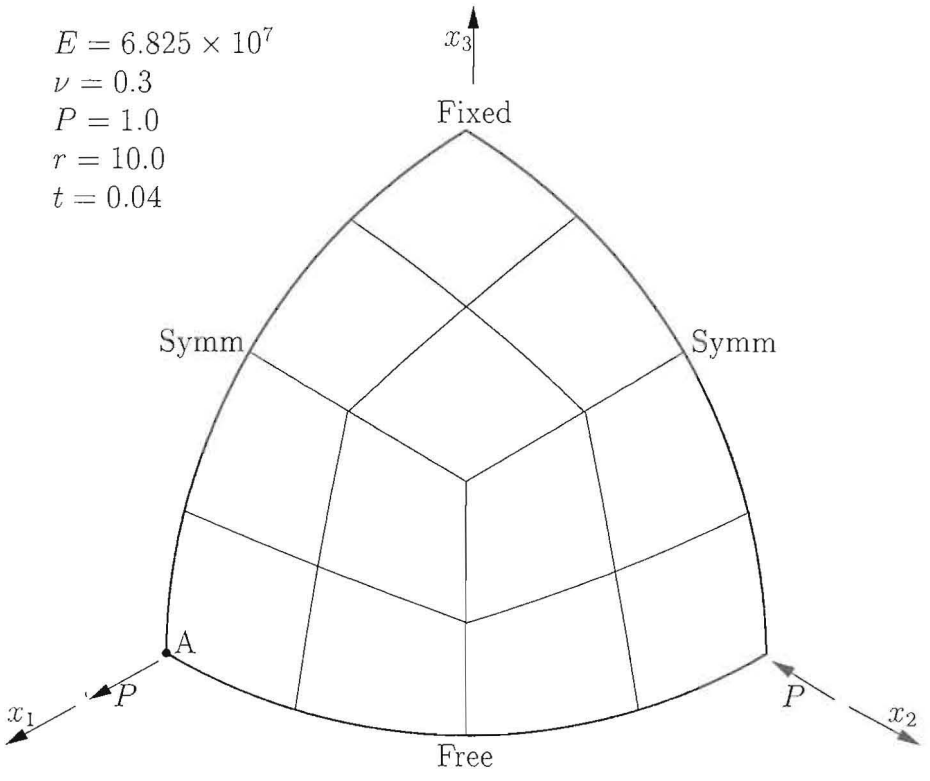

Figure 5.6: Warped pinched hemisphere

5.8 Pinched cylinder with end membranes

This problem is also dominated by inextensible bending behavior (See Figure 5.8). However, this problem is regarded as more difficult than the pinched cylinder with open ends [47].

From Table 5.10 it can be seen that that all the elements tested perform almost identically. (Once again, the drilling degrees of freedom are not activated due to the pinching loads.)

5.9 Thick pre-twisted beam

This problem is in the set proposed by MacNeal and Harder [45]. Results are presented by Taylor[6]. The thick pre-twisted beam depicted in Figure 5.9 is used to illustrate the capability of the elements for warped geometries.

Numerical results for this problem are tabulated in Table 5.11. All the elements tested perform almost identically for this test. The 5β/SA element is not included in this test, because the lack of drilling degrees of freedom complicates the use of this element for this geometry. This shows that the drilling degrees of freedom are a necessity for the problem.

$r = 4.953$
$l = 10.35$
$E = 10.5 \times 10^6$
$\nu = 0.3125$

Thick $\begin{cases} t = 0.094 \\ P = 100.0 \end{cases}$

Thin $\begin{cases} t = 0.01548 \\ P = 0.1 \end{cases}$

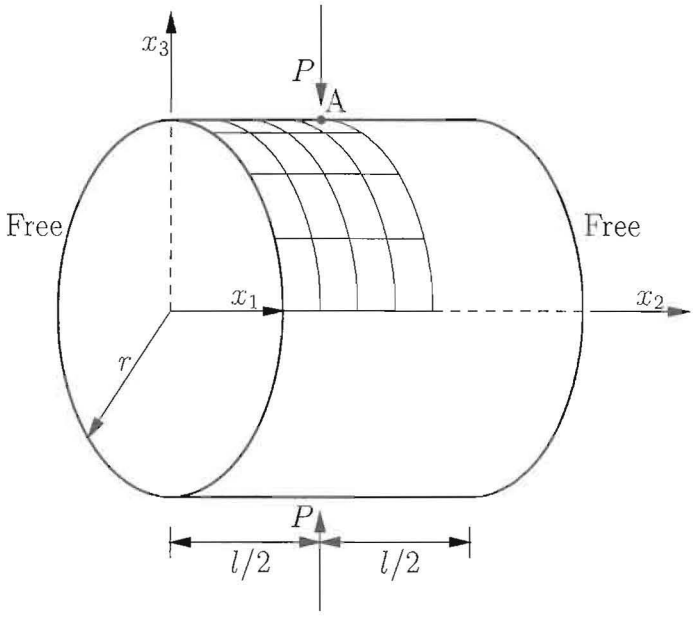

Figure 5.7: Pinched cylinder with open ends

5.10 Thin pre-twisted beam

Jetteur [16] proposed this problem, and this problem is used to evaluate locking. Results are presented by Taylor[6]. The thin pre-twisted beam is also depicted in Figure 5.9.

Numerical results for this problem are tabulated in Table 5.12. Again, all the elements perform virtually identical and are very accurate.

5.11 Scordelis-Lo roof

In Figure 5.10 the geometry and the discretization of this problem is depicted. The analytical solution of the mid-side vertical displacement, u_{3_A}, is normally taken as 0.3024 [45], even though a value of 0.3086 was originally presented by Scordelis and Lo [57].

The NT-formulations and the QC9D element outperform the other elements (Table 5.13).

5.12 Slender cantilever

MacNeal and Harder [45] proposed this problem to illustrate the effect of mesh distortion and element aspect ratio (See Figure 5.11, Table 5.14). Three shapes are considered, namely

$E = 3.0 \times 10^6$ $\quad r = 300.0$
$\nu = 0.3$ $\quad l = 600.0$
$P = 1.0$ $\quad t = 3.0$

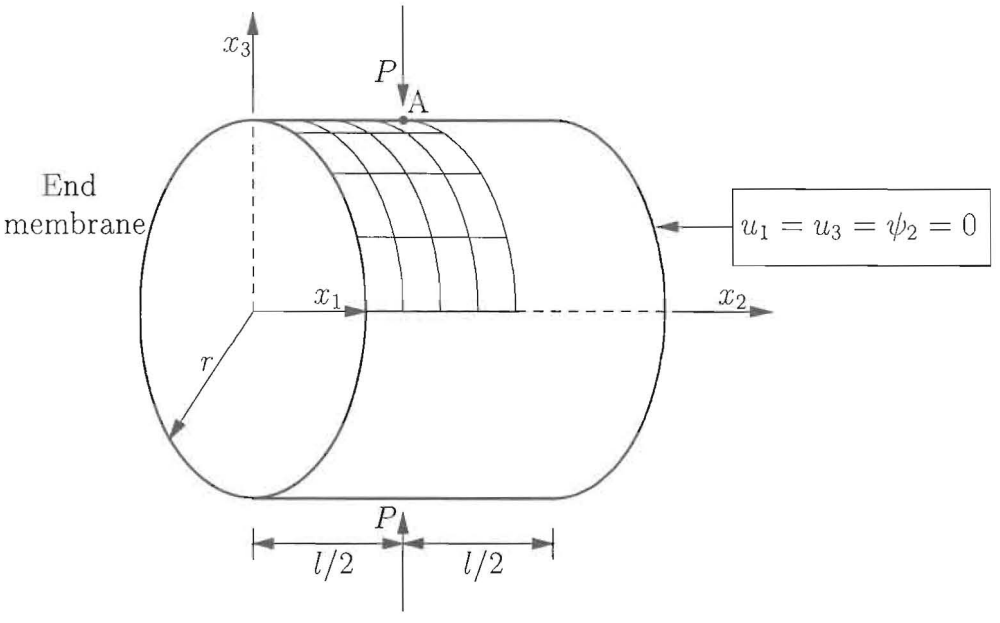

Figure 5.8: Pinched cylinder with end membranes

- regular shaped elements, $\alpha_i = 0^o$ for $i = 1, 2, 3, 4, 5$,
- parallelogram shaped elements, $\alpha_i = 45^o$ for $i = 1, 2, 3, 4, 5$, and
- trapezoidal shaped elements, $\alpha_i = 135^o$ and $\alpha_j = 45^o$ for $i = 1, 3, 5$ and $j = 2, 4$.

The clamped boundary condition prescribed by MacNeal and Harder for the beam does not allow modeling of the pure extensional force field for non-zero values for Poisson's ratio ($\nu \neq 0$) with membrane elements. For this reason the extension test was modified so that only the required restraints, two in the longitudinal and one in the thickness direction, are modeled [52].

For all the meshes all the elements converge to the exact answer for the unit extensional load case, except the NC-formulation without the locking correction for the regular mesh. For the out-of-plane shear and the twisting forces all the elements yields identical results for all the meshes. Even for the irregular meshes the elements perform very well.

For the in-plane shear test the 5β/SA element is the most accurate, while the NT-formulation are also very accurate for the regular mesh. For the irregular meshes the 5β/SA element is not accurate, while the $8\beta*$-NT/SA element still gives accurate results.

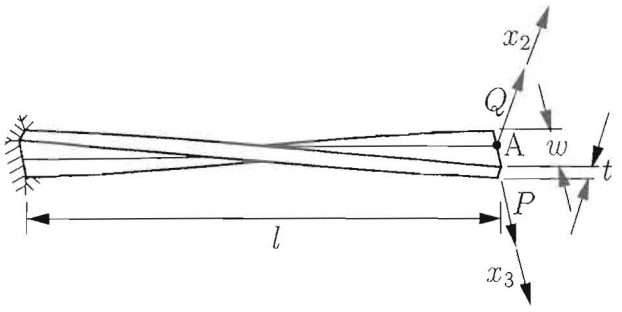

$E_{11}/E_{22} = 40$ $\quad w = 1.1$
$E_{22}/G_{23} = 2$ $\quad l = 12$
$E_{22}/G_{13} = 5/3$ $\quad$ Thick: $t = 0.32$
$E_{22}/G_{12} = 5/3$ $\quad$ Thin: $t = 0.05$
$\nu_{12} = 0.28$ $\quad P = 1$
$Q = 1$

Figure 5.9: Pre-twisted beam

$E = 432 \times 10^6$ $\quad l = 50.00$
$\nu = 0.0$ $\quad r = 25.0$
Load =90/unit shell area (weight) $\quad t = 0.25$

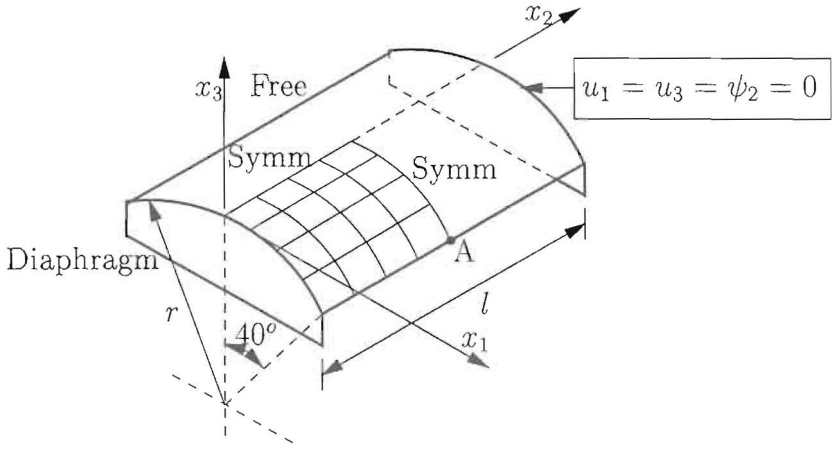

Figure 5.10: Scordelis-Lo roof

Element	1×1	1×4
SA	1.429	1.875
SA(incl. RBF)	1.905	1.905
Exact solution	1.905	

Table 5.1: Cantilever under transverse tip loading: Tip displacement u_{3_A}

$E = 1.0 \times 10^7$ $P = 1$ $t = 0.1$
$\nu = 0.30$ $l = 6.0$ $h = 0.2$

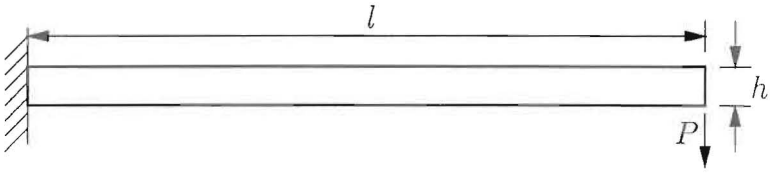

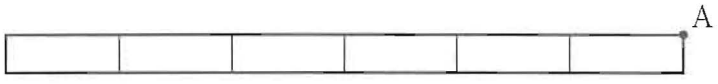

Regular mesh

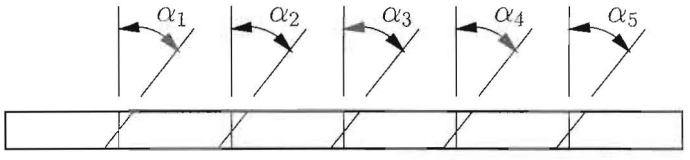

Irregular mesh

Figure 5.11: Slender cantilever

Element	2×2	4×4	8×8	16×16	32×32
SA	39712	40436	40593	40632	40641
SA($k \to \infty$)	39690	40414	40572	40612	40625
SA(incl. RBF)	44141	41499	40854	40694	40654
QI [54]	42512	41115	40761	40673	40651
Plate theory [58]			40644		

Table 5.2: Thin simply supported plate under uniformly distributed load (Hard supported): Center displacement $-u_{3_A}$

Element	2×2	4×4	8×8	16×16	32×32
SA	39728	40466	40653	40747	40841
SA($k \to \infty$)	39690	40414	40572	40612	40625
SA(incl. RBF)	46550	42774	41533	41089	40948
QI [54]	44613	42273	41395	41060	40961

Table 5.3: Thin simply supported plate under uniformly distributed load (Soft supported): Center displacement $-u_{3_A}$

Element	2×2	4×4	8×8	16×16	32×32
5β/SA	0.08420	0.09330	0.09292	0.09313	0.09346
QC9D/SA	0.006745	0.01135	0.05953	0.08987	0.09318
8β-NC/SA	0.01202	0.05681	0.08483	0.09278	0.09348
8β-NT/SA	0.007731	0.01304	0.06408	0.09053	0.09322
9β-NC/SA	0.01185	0.05606	0.08459	0.09276	0.09348
9β-NT/SA	0.006939	0.01226	0.06145	0.09015	0.09320
QC9D$*$-SA	0.006554	0.01047	0.05905	0.08998	0.09324
$8\beta*$-NC/SA	0.009182	0.03363	0.08394	0.09297	0.09355
$8\beta*$-NT/SA	0.007268	0.01177	0.06329	0.09063	0.09328
$9\beta*$-NC/SA	0.008982	0.03334	0.08372	0.09295	0.09355
$9\beta*$-NT/SA	0.006809	0.01116	0.06087	0.09026	0.09326
Best known [20]			0.09300		

Table 5.4: Pinched Hemisphere with 18^o Hole: Radial displacement u_{1_A}

γ	2×2
$G \times 10^{-3}$	0.008067
$G \times 10^{-2}$	0.008057
$G \times 10^{-1}$	0.007975
$G \times 10^{0}$	0.007731
$G \times 10^{1}$	0.007605
$G \times 10^{2}$	0.007586
$G \times 10^{3}$	0.007584
Best known	0.093000

Table 5.5: Pinched Hemisphere with 18^o Hole: Influence of γ for the 2×2 mesh

Element	2×2	4×4	8×8	16×16
5 point integration				
$8\beta*$-NC/SA	0.01087	0.05721	0.09174	0.09362
$8\beta*$-EP/SA	0.008424	0.03635	0.08937	0.09312
$8\beta*$-OC/SA	0.007254	0.03604	0.08939	0.09312
$8\beta*$-NT/SA	0.007338	0.03612	0.08939	0.09312
$8\beta*$-PH/SA	0.007274	0.03492	0.08926	0.09311
8β-NC/SA	0.02543	0.08607	0.09311	0.09343
8β-EP/SA	0.02981	0.08757	0.09270	0.09307
8β-OC/SA	0.02600	0.08707	0.09272	0.09308
8β-NT/SA	0.02603	0.08707	0.09272	0.09308
8β-PH/SA	0.01494	0.08287	0.09262	0.09307
8 point integration				
$8\beta*$-NC/SA	0.01088	0.05733	0.09175	0.09362
$8\beta*$-EP/SA	0.008416	0.03601	0.08922	0.09311
$8\beta*$-OC/SA	0.007309	0.03598	0.08926	0.09311
$8\beta*$-NT/SA	0.007430	0.03607	0.08926	0.09311
$8\beta*$-PH/SA	0.007276	0.03457	0.08909	0.09310
8β-NC/SA	0.02530	0.08596	0.09312	0.09344
8β-EP/SA	0.02452	0.08532	0.09253	0.09306
8β-OC/SA	0.03495	0.08610	0.09257	0.09307
8β-NT/SA	0.03507	0.08612	0.09257	0.09307
8β-PH/SA	0.01425	0.08045	0.09243	0.09306
Full integration				
$8\beta*$-NC/SA	0.009182	0.03363	0.08394	0.09297
$8\beta*$-EP/SA	0.007056	0.01176	0.06330	0.09063
$8\beta*$-OC/SA	0.007299	0.01182	0.06333	0.09063
$8\beta*$-NT/SA	0.007268	0.01177	0.06329	0.09063
$8\beta*$-PH/SA	0.006586	0.01120	0.06141	0.09035
8β-NC/SA	0.01202	0.05681	0.08483	0.09278
8β-EP/SA	0.007667	0.01306	0.06409	0.09053
8β-OC/SA	0.008486	0.01311	0.06411	0.09053
8β-NT/SA	0.007731	0.01304	0.06408	0.09053
8β-PH/SA	0.006829	0.01239	0.06208	0.09025
Best known		0.093		

Table 5.6: Pinched Hemisphere with 18° Hole: Effect of integration scheme order

Element	2×2	4×4	8×8	16×16
5β/SA	0.08549	0.09086	0.09154	0.09185
QC9D/SA	0.0005911	0.006161	0.04522	0.08607
8β-NC/SA	0.001446	0.02180	0.07363	0.09068
8β-NT/SA	0.0006833	0.007153	0.04885	0.08692
9β-NC/SA	0.001439	0.02153	0.07339	0.09066
9β-NT/SA	0.0006833	0.006864	0.04805	0.08674
QC9D$*$/SA	0.0004999	0.005915	0.04471	0.08614
$8\beta*$-NC/SA	0.001410	0.01910	0.07212	0.09085
$8\beta*$-NT/SA	0.0005637	0.006761	0.04813	0.08697
$9\beta*$-NC/SA	0.001402	0.01890	0.07190	0.09083
$9\beta*$-NT/SA	0.0005637	0.006519	0.04736	0.08680
Analytical [56]		0.09240		

Table 5.7: Warped pinched hemisphere: Radial displacement u_{1_A}

Element	2×2	4×4	8×8	16×16
5β/SA	0.07026	0.1002	0.1100	0.1128
QC9D/SA	0.07005	0.09980	0.1099	0.1128
8β-NC/SA	0.07088	0.1005	0.1101	0.1129
8β-NT/SA	0.07008	0.09990	0.1099	0.1128
9β-NC/SA	0.07088	0.1005	0.1101	0.1129
9β-NT/SA	0.07005	0.09982	0.1099	0.1128
QC9D$*$/SA	0.07001	0.09979	0.1099	0.1128
$8\beta*$-NC/SA	0.07019	0.1007	0.1102	0.1129
$8\beta*$-NT/SA	0.07002	0.09986	0.1099	0.1128
$9\beta*$-NC/SA	0.07019	0.1007	0.1102	0.1129
$9\beta*$-NT/SA	0.07001	0.09981	0.1099	0.1128
Jaamei [17]		0.094		

Table 5.8: Thick pinched cylinder with open ends: Radial displacement $-u_{3_A}$

Element	2×2	4×4	8×8	16×16
5β/SA	0.01562	0.02196	0.02383	0.02440
QC9D/SA	0.01561	0.02194	0.02380	0.02439
8β-NC/SA	0.01562	0.02200	0.02387	0.02442
8β-NT/SA	0.01561	0.02194	0.02381	0.02439
9β-NC/SA	0.01562	0.02200	0.02387	0.02442
9β-NT/SA	0.01561	0.02194	0.02380	0.02439
QC9D$*$/SA	0.01561	0.02194	0.02380	0.02440
$8\beta*$-NC/SA	0.01562	0.02197	0.02389	0.02443
$8\beta*$-NT/SA	0.01561	0.02194	0.02381	0.02440
$9\beta*$-NC/SA	0.01562	0.02197	0.02389	0.02443
$9\beta*$-NT/SA	0.01561	0.02194	0.02380	0.02440
Jaamei [17]		0.01548		

Table 5.9: Thin pinched cylinder with open ends: Radial displacement $-u_{3_A}$

Element	4×4	8×8	16×16
5β/SA	0.7175E-05	1.376E-05	1.792E-05
QC9D/SA	0.6824E-05	1.396E-05	1.787E-05
8β-NC/SA	0.8138E-05	1.412E-05	1.802E-05
8β-NT/SA	0.6888E-05	1.355E-05	1.787E-05
9β-NC/SA	0.8138E-05	1.412E-05	1.802E-05
9β-NT/SA	0.6831E-05	1.351E-05	1.787E-05
QC9D$*$/SA	0.6930E-05	1.350E-05	1.785E-05
$8\beta*$-NC/SA	0.8078E-05	1.411E-05	1.801E-05
$8\beta*$-NT/SA	0.6956E-05	1.354E-05	1.786E-05
$9\beta*$-NC/SA	0.8078E-05	1.411E-05	1.801E-05
$9\beta*$-NT/SA	0.6938E-05	1.352E-05	1.786E-05
Jaamei [17]		1.8248E-05	

Table 5.10: Pinched cylinder with end membranes: Radial displacement $-u_{3_A}$

Element	1×6	2×12	4×24	8×48
In-plane shear: u_{3_A}				
QC9D/SA	5.387E-03	5.405E-03	5.412E-03	5.416E-03
8β-NC/SA	5.387E-03	5.405E-03	5.412E-03	5.416E-03
8β-NT/SA	5.388E-03	5.405E-03	5.412E-03	5.416E-03
9β-NC/SA	5.387E-03	5.405E-03	5.412E-03	5.416E-03
9β-NT/SA	5.388E-03	5.405E-03	5.412E-03	5.416E-03
QC9D$*$/SA	5.387E-03	5.405E-03	5.412E-03	5.416E-03
$8\beta*$-NC/SA	5.387E-03	5.405E-03	5.412E-03	5.416E-03
$8\beta*$-NT/SA	5.388E-03	5.405E-03	5.412E-03	5.416E-03
$9\beta*$-NC/SA	5.387E-03	5.405E-03	5.412E-03	5.416E-03
$9\beta*$-NT/SA	5.388E-03	5.405E-03	5.412E-03	5.416E-03
Analytical [45]		5.429E-03		
Out-of-plane shear: u_{2_A}				
QC9D/SA	1.758E-03	1.755E-03	1.752E-03	1.753E-03
8β-NC/SA	1.757E-03	1.755E-03	1.752E-03	1.753E-03
8β-NT/SA	1.761E-03	1.756E-03	1.753E-03	1.753E-03
9β-NC/SA	1.757E-03	1.755E-03	1.752E-03	1.753E-03
9β-NT/SA	1.761E-03	1.756E-03	1.753E-03	1.753E-03
QC9D$*$/SA	1.758E-03	1.754E-03	1.752E-03	1.753E-03
$8\beta*$-NC/SA	1.757E-03	1.754E-03	1.752E-03	1.753E-03
$8\beta*$-NT/SA	1.761E-03	1.755E-03	1.753E-03	1.753E-03
$9\beta*$-NC/SA	1.757E-03	1.754E-03	1.752E-03	1.753E-03
$9\beta*$-NT/SA	1.761E-03	1.755E-03	1.753E-03	1.753E-03
Analytical [45]		1.750E-03		

Table 5.11: Thick pre-twisted beam: Numerical results

Element	1×6	2×12	4×24	8×48
In-plane shear: u_{3_A}				
QC9D/SA	1.383	1.384	1.386	1.387
8β-NC/SA	1.383	1.384	1.386	1.387
8β-NT/SA	1.383	1.384	1.386	1.387
9β-NC/SA	1.383	1.384	1.386	1.387
9β-NT/SA	1.383	1.384	1.386	1.387
QC9D*/SA	1.383	1.384	1.386	1.387
8β*-NC/SA	1.383	1.384	1.386	1.387
8β*-NT/SA	1.383	1.384	1.386	1.387
9β*-NC/SA	1.383	1.384	1.386	1.387
9β*-NT/SA	1.383	1.384	1.386	1.387
Isoparametric solid elements [16]			1.3857	
Out-of-plane shear: u_{2_A}				
QC9D/SA	0.3442	0.3434	0.3429	0.3429
8β-NC/SA	0.3442	0.3434	0.3429	0.3429
8β-NT/SA	0.3443	0.3434	0.3429	0.3429
9β-NC/SA	0.3442	0.3433	0.3429	0.3429
9β-NT/SA	0.3443	0.3434	0.3429	0.3429
QC9D*/SA	0.3442	0.3432	0.3429	0.3429
8β*-NC/SA	0.3442	0.3432	0.3429	0.3429
8β*-NT/SA	0.3443	0.3432	0.3429	0.3429
9β*-NC/SA	0.3442	0.3432	0.3429	0.3429
9β*-NT/SA	0.3443	0.3432	0.3429	0.3429
Isoparametric solid elements [16]			0.3427	

Table 5.12: Thin pre-twisted beam: Numerical results

Element	4×4	8×8	16×16
5β/SA	0.3162	0.3052	0.3074
QC9D/SA	0.3159	0.3038	0.3016
8β-NC/SA	0.3417	0.3107	0.3034
8β-NT/SA	0.3159	0.3038	0.3016
9β-NC/SA	0.3417	0.3107	0.3034
9β-NT/SA	0.3159	0.3038	0.3016
QC9D*/SA	0.3168	0.3041	0.3017
8β*-NC/SA	0.3428	0.3110	0.3034
8β*-NT/SA	0.3169	0.3041	0.3017
9β*-NC/SA	0.3428	0.3110	0.3034
9β*-NT/SA	0.3169	0.3041	0.3017
Analytical		0.3024	

Table 5.13: Scordelis-Lo roof: Center displacement u_{3_A}

Element	Unit extensional u_{1_A}	In-plane shear u_{2_A}	Out-of-plane shear u_{3_A}	Twisting forces ψ_{1_A}
Regular mesh				
5β/SA	0.3000E-04	0.1073	0.4235	0.03015
QC9D/SA	0.3000E-04	0.1055	0.4235	0.03015
8β-NC/SA	0.3000E-04	0.3794	0.4235	0.03015
8β-NT/SA	0.3000E-04	0.1072	0.4235	0.03015
9β-NC/SA	0.3000E-04	0.3794	0.4235	0.03015
9β-NT/SA	0.3000E-04	0.1072	0.4235	0.03015
QC9D*/SA	0.3000E-04	0.1055	0.4235	0.03015
8β*-NC/SA	0.3025E-03	0.3794	0.4235	0.03015
8β*-NT/SA	0.3000E-04	0.1072	0.4235	0.03015
9β*-NC/SA	0.3543E-03	0.3794	0.4235	0.03015
9β*-NT/SA	0.3000E-04	0.1072	0.4235	0.03015
Parallelograms				
5β/SA	0.3000E-4	0.06858	0.4226	0.02722
QC9D/SA	0.3000E-4	0.05519	0.4226	0.02722
8β-NC/SA	0.3000E-4	0.1530	0.4226	0.02722
8β-NT/SA	0.3000E-4	0.06640	0.4226	0.02722
9β-NC/SA	0.3000E-4	0.1519	0.4226	0.02722
9β-NT/SA	0.3000E-4	0.06169	0.4226	0.02722
QC9D*/SA	0.3000E-4	0.09868	0.4226	0.02722
8β*-NC/SA	0.3000E-4	0.2838	0.4226	0.02722
8β*-NT/SA	0.3000E-4	0.1061	0.4226	0.02722
9β*-NC/SA	0.3000E-4	0.2837	0.4226	0.02722
9β*-NT/SA	0.3000E-4	0.1048	0.4226	0.02722
Trapezoidals				
5β/SA	0.3000E-4	0.005859	0.4163	0.02834
QC9D/SA	0.3000E-4	0.004612	0.4163	0.02834
8β-NC/SA	0.3000E-4	0.01685	0.4163	0.02834
8β-NT/SA	0.3000E-4	0.005226	0.4163	0.02834
9β-NC/SA	0.3000E-4	0.01685	0.4163	0.02834
9β-NT/SA	0.3000E-4	0.005022	0.4163	0.02834
QC9D*/SA	0.3000E-4	0.09494	0.4163	0.02834
8β*-NC/SA	0.3000E-4	0.2611	0.4163	0.02834
8β*-NT/SA	0.3000E-4	0.1064	0.4163	0.02834
9β*-NC/SA	0.3000E-4	0.2610	0.4163	0.02834
9β*-NT/SA	0.3000E-4	0.1063	0.4163	0.02834
Beam theory	0.3000E-4	0.1081	0.4321	0.03208

Table 5.14: Slender cantilever: Numerical results

Chapter 6

Orthotropic flat shell elements

In this chapter, the constitutive relationship is extended to incorporate orthotropy.

Layered orthotropic materials are particularly demanding in terms of the kinematic requirements of finite elements, since the transverse shear flexibility could be significant. Therefore, a shear flexible through-thickness formulation is called for. The Mindlin theory includes shear deformations, and C^0 continuity of the shape functions only is required.

Hence, the 5β/SA, 8β/SA and 9β/SA elements developed in previous chapters are suitable candidates for orthotropic problems.

6.1 Constitutive relationship

The linear elastic three-dimensional stress-strain relation defined by

$$\sigma_{ij} = E_{ijkl}\epsilon_{kl} \tag{6.1}$$

is used as the basic building brick for laminated orthotropic materials. It is assumed in the plate theory of laminated orthotropic materials that the normal stress in each laminate vanishes, i.e. it is assumed that (6.1) reduces to

$$\begin{Bmatrix} \sigma_{xx} \\ \sigma_{yy} \\ \sigma_{xy} \\ \sigma_{xz} \\ \sigma_{yz} \end{Bmatrix} = \begin{bmatrix} Q_{11} & Q_{12} & Q_{16} & 0 & 0 \\ & Q_{22} & Q_{26} & 0 & 0 \\ & & Q_{66} & 0 & 0 \\ & & & Q_{44} & Q_{45} \\ Symm & & & & Q_{55} \end{bmatrix} \begin{Bmatrix} \epsilon_{xx} \\ \epsilon_{yy} \\ \epsilon_{xy} \\ \epsilon_{xz} \\ \epsilon_{yz} \end{Bmatrix} \tag{6.2}$$

where the stress-strain relations are written with respect to the reference coordinate system. The laminate staking convention is depicted in Figure 6.1.

Since the orthotropic layers are generally rotated with respect to the reference coordinate axis (see Figure 6.2), Q_{ij} relates the principal directions of the material orthotropy to the reference coordinate system. Q_{ij} is defined by

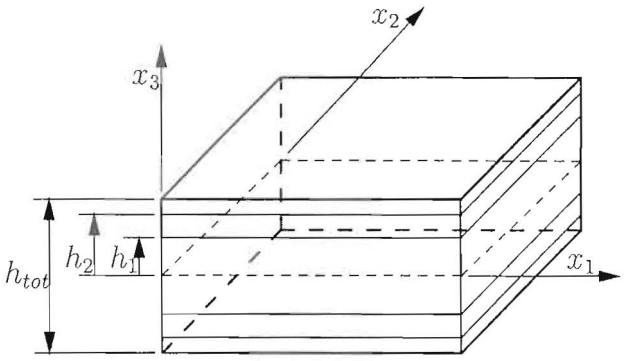

Figure 6.1: Laminate staking convention

$$
\begin{aligned}
Q_{11} &= c^4E_{1111} + 2c^2s^2E_{1122} + s^4E_{2222} + 4s^2c^2E_{1212} \\
Q_{12} &= c^2s^2E_{1111} + s^4E_{1122} + c^4E_{1122} + s^2c^2E_{2222} - 4s^2c^2E_{1212} \\
Q_{16} &= sc^3E_{1111} + s^3cE_{1122} - sc^3E_{1122} - s^3cE_{2222} + 2sc(s^2 - c^2)E_{1212} \\
Q_{22} &= s^4E_{1111} + 2s^2c^2E_{1122} + c^4E_{2222} + 4s^2c^2E_{1212} \\
Q_{26} &= cs^3E_{1111} + c^3sE_{1122} - cs^3E_{1122} - c^3sE_{2222} + 2sc(c^2 - s^2)E_{1212} \\
Q_{66} &= s^2c^2E_{1111} - 2s^2c^2E_{1122} + s^2c^2E_{2222} + (c^4 - 2s^2c^2 + s^4)E_{1212} \\
Q_{44} &= c^2E_{1313} + s^2E_{2323} \\
Q_{45} &= csE_{1313} - csE_{2323} \\
Q_{55} &= s^2E_{1313} + c^2E_{2323}
\end{aligned} \tag{6.3}
$$

where c and s respectively indicate $\cos\theta$ and $\sin\theta$, while θ indicates the fiber ply angle in respect to the positive x_1-axis (See Figure 6.2).

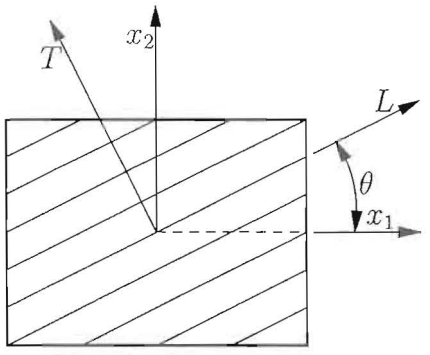

Figure 6.2: Local coordinate system for laminated structures

For orthotropic layered laminates E_{ijkl} are obtainable as

$$E_{1111} = \frac{E_L}{(1 - \nu_{LT}\nu_{TL})}$$

$$\begin{aligned} E_{2222} &= \frac{E_T}{(1-\nu_{LT}\nu_{TL})} \\ E_{1122} &= \frac{\nu_{LT}E_T}{(1-\nu_{LT}\nu_{TL})} \\ E_{1212} &= G_{LT} \\ E_{1313} &= G_{LO} \\ E_{2323} &= G_{TO} \end{aligned} \tag{6.4}$$

where the subscripts L and T indicate the in-plane longitudinal and transverse directions of the fibers, and O indicates the out-of-plane transverse direction. E_i denote the Young's moduli, G_{ij} denote the shear moduli and ν_{ij} denote the Poisson's ratio's.

Integration of the shell stresses yields the shell resultants as

$$\begin{aligned} N_{ij} &= \int_{\frac{-h}{2}}^{\frac{h}{2}} \sigma_{ij}\, \mathrm{d}z \qquad i,j=1,2 \\ M_{ij} &= \int_{\frac{-h}{2}}^{\frac{h}{2}} z\sigma_{ij}\, \mathrm{d}z \qquad i,j=1,2 \\ V_{ij} &= \int_{\frac{-h}{2}}^{\frac{h}{2}} \sigma_{ij}\, \mathrm{d}z \qquad i=1,2; j=3 \end{aligned} \tag{6.5}$$

For isotropic materials the relevant constitutive relationships are given in (2.13), (4.18) and (4.24) respectively. For orthotropy the constitutive relationships are given by [59]

$$\begin{aligned} C^m_{ij} &= \textstyle\sum_{k=1}^{n}(Q_{ij})_k(h_{k+1}-h_k) \qquad i,j=1,2,6 \\ C^b_{ij} &= \tfrac{1}{3}\textstyle\sum_{k=1}^{n}(Q_{ij})_k(h^3_{k+1}-h^3_k) \qquad i,j=1,2,6 \\ C^s_{ij} &= \textstyle\sum_{k=1}^{n}(Q_{ij})_k(h_{k+1}-h_k) \qquad i,j=4,5 \end{aligned} \tag{6.6}$$

6.2 Compliance matrix

Complementary to the general relationship between stress and strain, (6.1), one can define the inverse relationships as:

$$\epsilon_{ij} = S_{ijkl}\sigma_{kl} \tag{6.7}$$

where S_{ijkl} is the 'compliance tensor'. (6.1) and (6.7) can be rewritten in matrix form

$$\boldsymbol{\sigma} = \boldsymbol{E}\boldsymbol{\epsilon} \tag{6.8}$$

$$\boldsymbol{\epsilon} = \boldsymbol{S}\boldsymbol{\sigma} \tag{6.9}$$

This means that $\boldsymbol{S}$ is the inverse of $\boldsymbol{E}$. Therefore, S_{ijkl} has the same symmetries as E_{ijkl}. (6.7) now reduces to

$$\begin{Bmatrix} \epsilon_{xx} \\ \epsilon_{yy} \\ \epsilon_{xy} \\ \epsilon_{xz} \\ \epsilon_{yz} \end{Bmatrix} = \begin{bmatrix} S_{11} & S_{12} & S_{16} & 0 & 0 \\ & S_{22} & S_{26} & 0 & 0 \\ & & S_{66} & 0 & 0 \\ & & & S_{44} & S_{45} \\ Symm & & & & S_{55} \end{bmatrix} \begin{Bmatrix} \sigma_{xx} \\ \sigma_{yy} \\ \sigma_{xy} \\ \sigma_{xz} \\ \sigma_{yz} \end{Bmatrix} \tag{6.10}$$

S_{ij} relates the principal directions of the material orthotropy to the reference coordinate system and are defined by

$$\begin{aligned}
S_{11} &= c^4 S_{1111} + 2c^2 s^2 S_{1122} + s^4 S_{2222} + s^2 c^2 S_{1212} \\
S_{12} &= c^2 s^2 S_{1111} + s^4 S_{1122} + c^4 S_{1122} + s^2 c^2 S_{2222} - s^2 c^2 S_{1212} \\
S_{16} &= 2sc^3 S_{1111} + 2s^3 c S_{1122} - 2sc^3 S_{1122} - 2s^3 c S_{2222} - sc(c^2 - s^2) S_{1212} \\
S_{22} &= s^4 S_{1111} + 2s^2 c^2 S_{1122} + c^4 S_{2222} + s^2 c^2 S_{1212} \\
S_{26} &= 2cs^3 S_{1111} + 2c^3 s S_{1122} - 2cs^3 S_{1122} - 2c^3 s S_{2222} + sc(c^2 - s^2) S_{1212} \\
S_{66} &= 4s^2 c^2 S_{1111} - 8s^2 c^2 S_{1122} + 4s^2 c^2 S_{2222} + (c^4 - 2s^2 c^2 + s^4) S_{1212} \\
S_{44} &= c^2 S_{1313} + s^2 S_{2323} \\
S_{45} &= cs S_{1313} - cs S_{2323} \\
S_{55} &= s^2 S_{1313} + c^2 S_{2323}
\end{aligned} \tag{6.11}$$

where c and s respectively indicate $\cos\theta$ and $\sin\theta$, while θ indicates the fiber ply angle in respect to the positive x_1-axis (See Figure 6.2).

For orthotropic layered laminates S_{ijkl} are obtainable as

$$\begin{aligned}
S_{1111} &= \frac{1}{E_L} \\
S_{2222} &= \frac{1}{E_T} \\
S_{1122} &= \frac{-\nu_{LT}}{E_T} \\
S_{1212} &= \frac{1}{G_{LT}} \\
S_{1313} &= \frac{1}{G_{LO}} \\
S_{2323} &= \frac{1}{G_{TO}}
\end{aligned} \tag{6.12}$$

where the subscripts L and T indicate the in-plane longitudinal and transverse directions of the fibers, and O indicates the out-of-plane transverse direction. E_i denote the Young's moduli, G_{ij} denote the shear moduli and ν_{ij} denote the Poisson's ratio's.

Chapter 7

Numerical results: Orthotropic problems

7.1 Plane stress membrane cantilever under transverse tip loading

The plane stress membrane cantilever is depicted in Figure 7.1. $-u_{2_A}$ represents the reference displacement. Beam theory need not be exact.

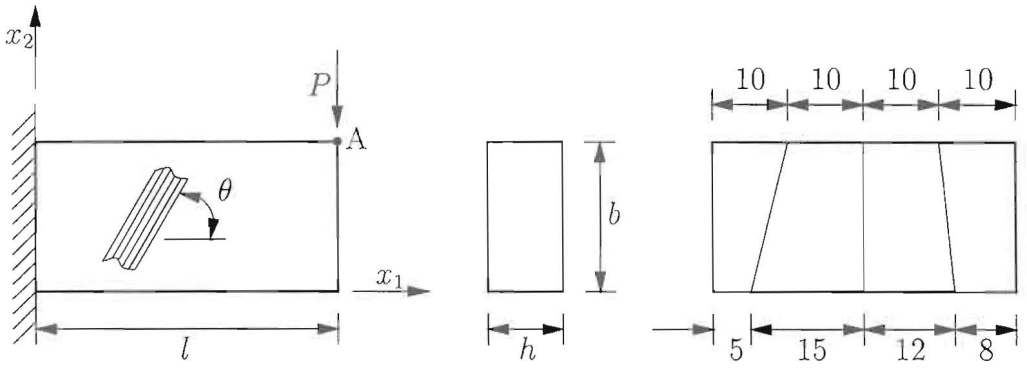

Figure 7.1: Cantilever under transverse tip loading and irregular mesh

7.1.1 Stacking sequence [0]

Table 7.1 reveals that for the regular mesh the 5β-NT element outperforms the other elements. For the irregular mesh the $8\beta*$-NT element is by far the most accurate. The 5β-NT element performs badly for this highly distorted mesh. For the irregular mesh the QC9D* element also outperforms the 5β-NT element.

For this stacking sequence, Table 7.2 reveals that small values of γ predict more accurate displacements. For values of $\gamma > G_{12}$ the accuracy decreases drastically. The results with the choice of $\gamma = G_{12}$ are acceptable.

From the results presented in Table 7.3 it is clear that there is no significant influence of the integration schemes for the regular meshes. However, for the irregular mesh the $8\beta*$-NT element with full integration is the most accurate.

7.1.2 Stacking sequence [30]

As before, the 5β-NT element performs very well for the regular mesh, but for the irregular mesh the $8\beta*$-NT element is the most accurate (See Table 7.4). Note that the QC9D* and the 5β-NT elements yield results an order of magnitude lower that the beam theory solution.

This stacking sequence is very sensitive to the value of γ (see Table 7.5). The best accuracy is obtained when γ is very small. With $\gamma = G_{12}$, the results are acceptable.

Table 7.6 reveals that for the regular meshes, the 5-point and 8-point integration schemes in combination with the locking correction outperform the other combinations without the locking correction. However, for the irregular mesh the $8\beta*$-NT element with full integration is again the most accurate.

7.1.3 Stacking sequence $[0/90]_s$

Numerical results for this stacking sequence are tabulated in Table 7.7. For the regular mesh all the elements are very accurate, except Q4. For the irregular mesh the $8\beta*$-NT element is the most accurate. Note that the 5β-NT element again yield results an order of magnitude lower that the beam theory solution. QC9D* yields accurate results for this problem.

7.1.4 Stacking sequence $[30/-30]_s$

For this staking sequence the 5β-NT, $8\beta*$-NT and $9\beta*$-NT all yields very accurate results (See Table 7.8). For the irregular mesh the $8\beta*$-NT element is again the most accurate with the 5β-NT formulation an order of magnitude lower than the theoretical solution.

7.1.5 Stacking sequence $[0/45/-45/90]_s$

For the coarse meshes Table 7.9 reveals that the QC9D* element is the most accurate, and for the refined meshes the 5β-NT element is the most accurate. For the irregular mesh the $8\beta*$-NT element is again the most accurate with the 5β-NT formulation an order of magnitude lower than the theoretical solution.

7.2 Clamped cylinder under internal pressure

Depicted in Figure 7.2, this problem was proposed by Haas and Lee [60]. u_{1_A} at $l/2$ is the reference displacement of interest.

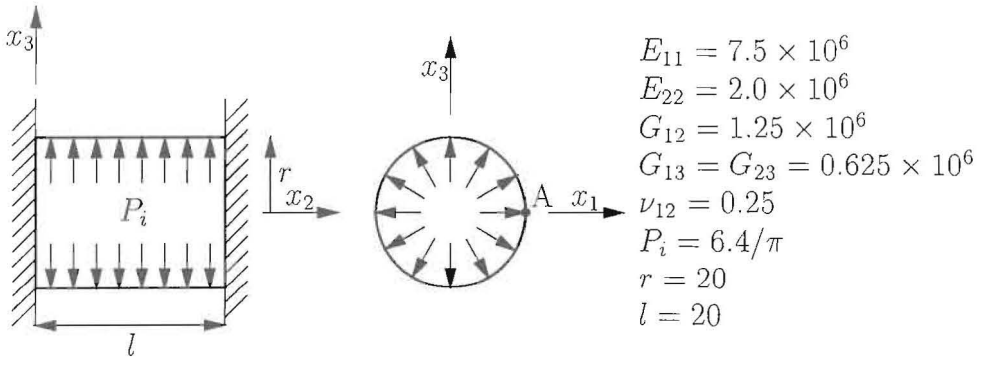

Figure 7.2: Clamped cylinder under internal pressure

7.2.1 Stacking sequence [90]

Numerical results for this stacking sequence are tabulated in Table 7.10. For $r/t = 20$ all the elements yields accurate results, with the $8\beta*$-NT/SA results slightly superior. For $r/t = 100$ the Q4/SA element yields highly accurate results. $8\beta*$-NT/SA compares very well with Q4/SA for all the meshes.

7.2.2 Stacking sequence $[-45/45]_s$

Numerical results for this stacking sequence are tabulated in Table 7.11. For $r/t = 20$ the $8\beta*$-NT/SA element yields the most accurate results. For $r/t = 100$ the $8\beta*$-NT/SA element with the 4×4 mesh is virtually converged. All the other elements yields comparable results for the 8×8 mesh.

7.2.3 Stacking sequence $[90/0]_s$

Numerical results for this stacking sequence are tabulated in Table 7.12. For $r/t = 20$ the Q4/SA element is the most accurate. All the elements converge from above. For $r/t = 100$ all the elements, except $8\beta*$-NT/SA, converge from above. The $8\beta*$-NT/SA element results are virtually converged for the coarse 4×4 mesh.

7.2.4 Stacking sequence $[0/90]_s$

Numerical results for this stacking sequence are tabulated in Table 7.13. Haas and Lee [60] did not perform this stacking sequence. For $r/t = 20$ all the elements converges mono-

tonically from above. For $r/t = 100$ all the elements, except Q4/SA, oscillate around approximately 0.0008450. Q4/SA converge monotonically from above.

7.2.5 Stacking sequence [0]

Numerical results for stacking sequence are tabulated in Table 7.14. Again, Haas and Lee [60] did not perform this test. For $r/t = 20$ all the elements converge monotonically from above. For $r/t = 100$ QC9D$*$/SA and 8$\beta*$-NT/SA converge monotonically from above. Q4/SA and 9$\beta*$-NT/SA oscillate around approximately 0.0005364.

7.3 Clamped hemisphere with 30^o hole

This problem was suggested by Moser and Schmid [61], and is depicted in Figure 7.3, showing the graded mesh proposed by Moser and Schmid. In this study, the benefit of the graded mesh is not exploited. Instead, the meshes are constructed using bisection.

7.3.1 Ply orientation $E_\theta = E_{11}$

Numerical results for this ply orientation are tabulated in Table 7.18. For the coarse mesh the 8$\beta*$-NT/SA element is the most accurate at points A and C. At point B the Q4/SA element is the most accurate. Note that the Q4/SA element is the most accurate for the refined mesh at points A and C.

Table 7.16 reveals that for small values of γ the displacement at points A and B are the most accurate, while the best results are obtained at point C when γ is large.

Results in Table 7.17 shows that at point A the 8$\beta*$-NT/SA element with the 8-point integration scheme is the most accurate for the coarse mesh. The performance of the elements with the locking correction is improved with the use of reduced integration. At points B and C the 8β-NT/SA element with the 8-point integration scheme is the most accurate for the coarse mesh. In general, the 8β-NT/SA element with the 8-point integration scheme is the most accurate.

7.3.2 Ply orientation $E_\phi = E_{11}$

Numerical results for this ply orientation are tabulated in Table 7.18. For the coarse mesh the Q4/SA element yields the most accurate results. For the refined meshes 8$\beta*$-NT/SA is the most accurate at point C.

This ply orientation is insensitive to the value of γ. However, note that for both large and small values of γ the best displacement at point C is obtained (see Table 7.19).

Results in Table 7.20 shows that the 8β-NT/SA with the 8-point integration scheme gives the most accurate results in points A, B and C.

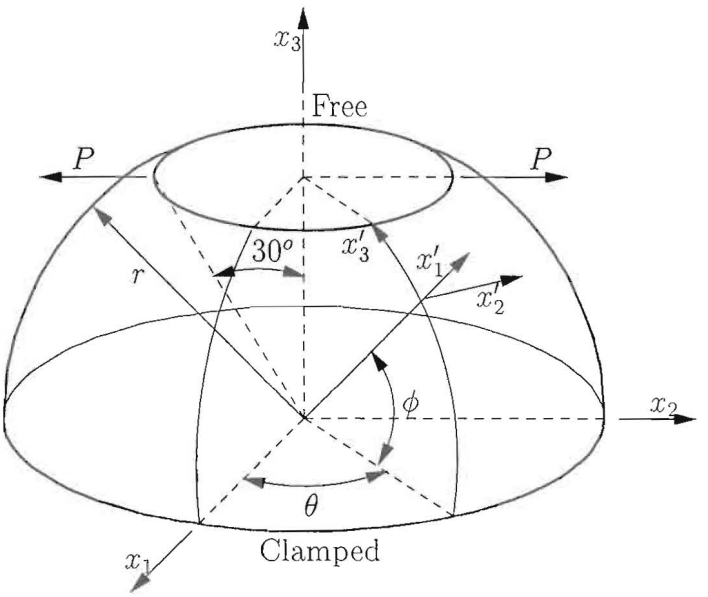

$E_{11} = 7.5 \times 10^6$ $P = 2.0$ Case 1 : $E_\theta = E_{x_2'} = E_{11}$
$E_{22} = 2.0 \times 10^6$ $t = 1.0$ Case 2 : $E_\phi = E_{x_3'} = E_{11}$
$G_{12} = 1.25 \times 10^6$ $r = 100.0$
$\nu_{12} = 0.25$
$\nu_{23} = 0.45$

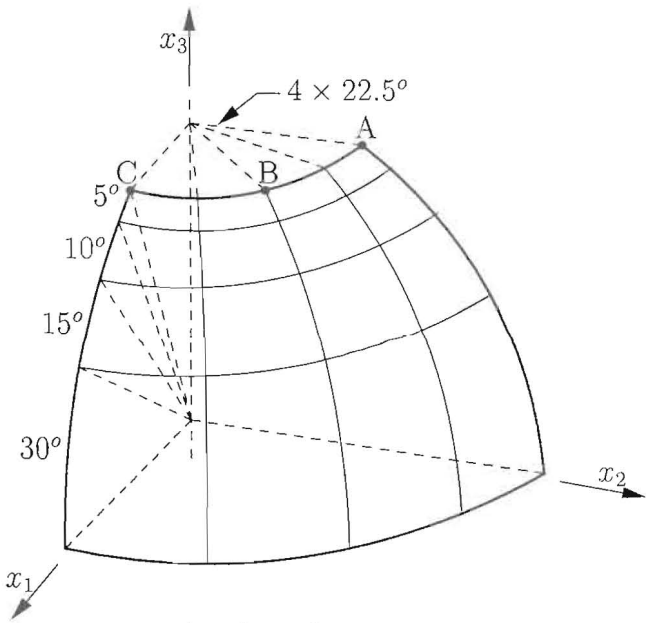

4×4 mesh

Figure 7.3: Clamped hemisphere with 30^o hole

7.4 Pre-twisted beam

The pre-twisted beam depicted in Figure 5.9 is used to illustrate the capability of the elements for warped geometries. For this new problems there are no known exact solutions. ($E_{11} = 30\times10^6$, $E_{22} = 0.75\times10^6$, $\nu_{12} = 0.28$, $G_{12} = 0.45\times10^6$, $G_{13} = 0.45\times10^6$ and $G_{23} = 0.375\times10^6$)

7.4.1 Stacking sequence $[0/90]_s$

Numerical results for this stacking sequence are tabulated in Table 7.21. All the elements converge monotonically from below for the in-plane shear loading condition (≈ 0.3545). For the out-of-plane shear loading condition all the elements converge monotonically from above. All the elements yield approximately converged results for the coarse 1×6 mesh (≈ 0.009544).

7.4.2 Stacking sequence $[-45/45]_s$

Numerical results for this stacking sequence are tabulated in Table 7.22. All the elements converge monotonically from below. In addition, the results predicted by the elements are very similar (≈ 0.08723 for u_{3_A} and ≈ 0.03006 for u_{2_A}).

7.4.3 Stacking sequence $[30/60]_s$

Numerical results for this stacking sequence are tabulated in Table 7.23. All the elements converge monotonically from below to roughly 0.08939 for the in-plane shear and to roughly 0.02878 for the out-of plane shear.

Element	1×4	2×8	4×16	8×32	Irregular Mesh
Q4	0.03447	0.06269	0.07893	0.08440	0.01545
QC9D*	0.08485	0.08607	0.08632	0.08637	0.07768
5β-NT	0.08489	0.08588	0.08626	0.08636	0.03069
8β*-NT	0.08489	0.08620	0.08637	0.08638	0.08217
9β*-NT	0.08488	0.08612	0.08635	0.08638	0.08184
Beam theory			0.08533		

Table 7.1: Plane stress membrane cantilever (Stacking sequence [0]): Tip displacement $-u_{2_A}$

γ	Irregular mesh
$G_{12} \times 10^{-3}$	0.02992
$G_{12} \times 10^{-2}$	0.02990
$G_{12} \times 10^{-2}$	0.02972
$G_{12} \times 10^{0}$	0.02855
$G_{12} \times 10^{1}$	0.02549
$G_{12} \times 10^{2}$	0.02019
$G_{12} \times 10^{3}$	0.01750
Beam theory	0.08533

Table 7.2: Plane stress membrane cantilever (Stacking sequence [0]): Influence of γ on irregular mesh

Element	1×4	2×8	4×16	Irregular mesh
5 point integration				
$8\beta*$-NT	0.08489	0.08620	0.08637	0.07810
8β-NT	0.08488	0.08588	0.08626	0.02692
8 point integration				
$8\beta*$-NT	0.08489	0.08620	0.08637	0.07968
8β-NT	0.08488	0.08588	0.08626	0.02707
Full integration				
$8\beta*$-NT	0.08489	0.08620	0.08637	0.08217
8β-NT	0.08488	0.08588	0.08626	0.02855
Beam theory			0.08533	

Table 7.3: Plane stress membrane cantilever (Stacking sequence [0]): Effect of integration scheme order

Element	1×4	2×8	4×16	8×32	Irregular Mesh
Q4	0.004815	0.01734	0.06465	0.2221	0.002128
QC9D*	0.6114	0.9179	1.160	1.250	0.2938
5β-NT	1.300	1.296	1.293	1.295	0.1133
$8\beta*$-NT	1.230	1.130	1.220	1.270	1.250
$9\beta*$-NT	1.137	1.080	1.210	1.267	1.194
Beam theory			1.320		

Table 7.4: Plane stress membrane cantilever (Stacking sequence [30]): Tip displacement $-u_{2_A}$

γ	Irregular mesh
$G_{12} \times 10^{-3}$	0.09082
$G_{12} \times 10^{-2}$	0.08417
$G_{12} \times 10^{-2}$	0.07596
$G_{12} \times 10^{0}$	0.05908
$G_{12} \times 10^{1}$	0.03975
$G_{12} \times 10^{2}$	0.03509
$G_{12} \times 10^{3}$	0.03456
Beam theory	1.320

Table 7.5: Plane stress membrane cantilever (Stacking sequence [30]): Influence of γ on irregular mesh

Element	1×4	2×8	4×16	Irregular mesh
5 point integration				
8β*-NT	1.230	1.130	1.220	1.137
8β-NT	1.299	1.262	1.259	0.06053
8 point integration				
8β*-NT	1.230	1.130	1.220	1.182
8β-NT	1.299	1.262	1.259	0.06076
Full integration				
8β*-NT	1.230	1.130	1.220	1.250
8β-NT	1.290	1.254	1.257	0.05908
Beam theory			1.320	

Table 7.6: Plane stress membrane cantilever (Stacking sequence [30]): Effect of integration scheme order

Element	1×4	2×8	4×16	8×32	Irregular Mesh
Q4	0.04261	0.09658	0.1414	0.1600	0.01660
QC9D*	0.1645	0.1665	0.1671	0.1673	0.1407
5β-NT	0.1646	0.1665	0.1671	0.1673	0.04056
8β*-NT	0.1646	0.1668	0.1672	0.1673	0.1576
9β*-NT	0.1646	0.1665	0.1672	0.1673	0.1556
Beam theory			0.1663		

Table 7.7: Plane stress membrane cantilever (Stacking sequence $[0/90]_s$): Tip displacement $-u_{2_A}$

Element	1×4	2×8	4×16	8×32	Irregular Mesh
Q4	0.004276	0.01651	0.05879	0.1654	0.001777
QC9D*	0.3126	0.3707	0.3998	0.4136	0.1021
5β-NT	0.4226	0.4034	0.4143	0.4208	0.03139
8β*-NT	0.4081	0.4181	0.4151	0.4184	0.3831
9β*-NT	0.4081	0.4067	0.4128	0.4180	0.3752
Beam theory			0.4292		

Table 7.8: Plane stress membrane cantilever (Stacking sequence $[30/-30]_s$): Tip displacement $-u_{2_A}$

Element	1×4	2×8	4×16	8×32	Irregular Mesh
Q4	0.006177	0.02293	0.07128	0.1510	0.002386
QC9D*	0.2329	0.2380	0.2399	0.2405	0.1052
5β-NT	0.2373	0.2382	0.2397	0.2404	0.02269
8β*-NT	0.2373	0.2400	0.2406	0.2408	0.2229
9β*-NT	0.2373	0.2392	0.2403	0.2407	0.2141
Beam theory			0.2351		

Table 7.9: Plane stress membrane cantilever (Stacking sequence $[0/45/-45/90]_s$): Tip displacement $-u_{2_A}$

Element	4×4	8×8	16×16
$r/t = 20.0$			
Q4/SA	0.0003596	0.0003699	0.0003727
QC9D*/SA	0.0003641	0.0003736	0.0003738
8β*-NT/SA	0.0003764	0.0003744	0.0003739
9β*-NT/SA	0.0003643	0.0003737	0.0003738
Haas and Lee		0.0003781	
$r/t = 100.0$			
Q4/SA	0.002040	0.002055	0.002051
QC9D*/SA	0.002225	0.002077	0.002052
8β*-NT/SA	0.002081	0.002055	0.002050
9β*-NT/SA	0.002225	0.002076	0.002052
Haas and Lee		0.002044	

Table 7.10: Clamped cylinder under internal pressure (Stacking sequence [90]): Radial displacement u_{1_A}

Element	4×4	8×8
$r/t = 20.0$		
Q4/SA	0.0002250	0.0002307
QC9D$*$/SA	0.0002352	0.0002334
8$\beta*$-NT/SA	0.0002369	0.0002335
9$\beta*$-NT/SA	0.0002355	0.0002335
Haas and Lee	0.0002402	
$r/t = 100.0$		
Q4/SA	0.001088	0.001068
QC9D$*$/SA	0.001137	0.001063
8$\beta*$-NT/SA	0.001063	0.001061
9$\beta*$-NT/SA	0.001129	0.001062
Haas and Lee	0.001068	

Table 7.11: Clamped cylinder under internal pressure (Stacking sequence $[-45/45]_s$): Radial displacement u_{1_A}

Element	4×4	8×8	16×16
$r/t = 20.0$			
Q4/SA	0.0001797	0.0001788	0.0001786
QC9D$*$/SA	0.0001797	0.0001791	0.0001787
8$\beta*$-NT/SA	0.0001811	0.0001792	0.0001787
9$\beta*$-NT/SA	0.0001797	0.0001791	0.0001787
Haas and Lee		0.0001783	
$r/t = 100.0$			
Q4/SA	0.0008455	0.0008447	0.0008441
QC9D$*$/SA	0.0008904	0.0008450	0.0008439
8$\beta*$-NT/SA	0.0008435	0.0008439	0.0008439
9$\beta*$-NT/SA	0.0008900	0.0008450	0.0008439
Haas and Lee		0.0008422	

Table 7.12: Clamped cylinder under internal pressure (Stacking sequence $[90/0]_s$): Radial displacement u_{1_A}

Element	4×4	8×8	16×16
$r/t = 20.0$			
Q4/SA	0.0001841	0.0001822	0.0001818
QC9D$*$/SA	0.0001856	0.0001825	0.0001819
8$\beta*$-NT/SA	0.0001854	0.0001825	0.0001818
9$\beta*$-NT/SA	0.0001856	0.0001825	0.0001819
$r/t = 100.0$			
Q4/SA	0.0008630	0.0008462	0.0008453
QC9D$*$/SA	0.0008817	0.0008444	0.0008452
8$\beta*$-NT/SA	0.0008442	0.0008459	0.0008453
9$\beta*$-NT/SA	0.0008812	0.0008444	0.0008452

Table 7.13: Clamped cylinder under internal pressure (Stacking sequence $[0/90]_s$): Radial displacement u_{1_A}

Element	4×4	8×8	16×16
$r/t = 20.0$			
Q4/SA	0.0001141	0.0001123	0.0001119
QC9D$*$/SA	0.0001147	0.0001123	0.0001119
8$\beta*$-NT/SA	0.0001139	0.0001122	0.0001119
9$\beta*$-NT/SA	0.0001146	0.0001123	0.0001119
$r/t = 100.0$			
Q4/SA	0.0005340	0.0005370	0.0005364
QC9D$*$/SA	0.0005630	0.0005371	0.0005364
8$\beta*$-NT/SA	0.0005417	0.0005371	0.0005364
9$\beta*$-NT/SA	0.0005340	0.0005370	0.0005364

Table 7.14: Clamped cylinder under internal pressure (Stacking sequence $[0]$): Radial displacement u_{1_A}

Element	4×4	8×8	16×16
Radial displacement at A			
Q4/SA	0.7099E-04	1.034E-04	1.151E-04
QC9D$*$/SA	0.7151E-04	1.035E-04	1.141E-04
$8\beta*$-NT/SA	0.7268E-04	1.036E-04	1.142E-04
$9\beta*$-NT/SA	0.7170E-04	1.035E-04	1.141E-04
Moser and Schmid		$\approx 1.15E-04$	
Radial displacement at B			
Q4/SA	-0.3804E-04	-0.4316E-04	-0.4463E-04
QC9D$*$/SA	-0.3535E-04	-0.4285E-04	-0.4428E-04
$8\beta*$-NT/SA	-0.3563E-04	-0.4287E-04	-0.4429E-04
$9\beta*$-NT/SA	-0.3543E-04	-0.4286E-04	-0.4428E-04
Moser and Schmid		$\approx -0.44E-04$	
Radial displacement at C			
Q4/SA	0.04328E-04	0.1242E-04	0.1208E-04
QC9D$*$/SA	0.08398E-04	0.1283E-04	0.1213E-04
$8\beta*$-NT/SA	0.08456E-04	0.1280E-04	0.1212E-04
$9\beta*$-NT/SA	0.08442E-04	0.1283E-04	0.1212E-04
Moser and Schmid		$\approx 0.12E-04$	

Table 7.15: Clamped hemisphere with 30^o hole (Ply orientation $E_\theta = E_{11}$): Radial displacement

Element	4×4
Radial displacement at A	
$G_{12} \times 10^{-3}$	0.6929E-04
$G_{12} \times 10^{-2}$	0.6928E-04
$G_{12} \times 10^{-2}$	0.6917E-04
$G_{12} \times 10^{0}$	0.6879E-04
$G_{12} \times 10^{1}$	0.6843E-04
$G_{12} \times 10^{2}$	0.6836E-04
$G_{12} \times 10^{3}$	0.6834E-04
Moser and Schmid	$\approx 1.15E-04$
Radial displacement at B	
$G_{12} \times 10^{-3}$	-0.3580E-04
$G_{12} \times 10^{-2}$	-0.3580E-04
$G_{12} \times 10^{-2}$	-0.3577E-04
$G_{12} \times 10^{0}$	-0.3567E-04
$G_{12} \times 10^{1}$	-0.3561E-04
$G_{12} \times 10^{2}$	-0.3561E-04
$G_{12} \times 10^{3}$	-0.3561E-04
Moser and Schmid	$\approx -0.44E-04$
Radial displacement at C	
$G_{12} \times 10^{-3}$	0.1033E-04
$G_{12} \times 10^{-2}$	0.1033E-04
$G_{12} \times 10^{-2}$	0.1037E-04
$G_{12} \times 10^{0}$	0.1052E-04
$G_{12} \times 10^{1}$	0.1073E-04
$G_{12} \times 10^{2}$	0.1079E-04
$G_{12} \times 10^{3}$	0.1080E-04
Moser and Schmid	$\approx 0.12E-04$

Table 7.16: Clamped hemisphere with 30^o hole (Ply orientation $E_\theta = E_{11}$): Influence of γ on 4×4 mesh

Element	4×4	8×8
Radial displacement at A		
5 point integration		
$8\beta*$-NT/SA	0.7470E-04	1.039E-04
8β-NT/SA	0.7150E-04	1.032E-04
8 point integration		
$8\beta*$-NT/SA	0.7472E-04	1.039E-04
8β-NT/SA	0.7152E-04	1.032E-04
Full integration		
$8\beta*$-NT/SA	0.7268E-04	1.036E-04
8β-NT/SA	0.6879E-04	1.029E-04
Moser and Schmid	$\approx 1.15E-04$	
Radial displacement at B		
5 point integration		
$8\beta*$-NT/SA	-0.3691E-04	-0.4301E-04
8β-NT/SA	-0.3765E-04	-0.4384E-04
8 point integration		
$8\beta*$-NT/SA	-0.3693E-04	-0.4301E-04
8β-NT/SA	-0.3766E-04	-0.4284E-04
Full integration		
$8\beta*$-NT/SA	-0.3563E-04	-0.4287E-04
8β-NT/SA	-0.3567E-04	-0.4268E-04
Moser and Schmid	$\approx -0.44E-04$	
Radial displacement at C		
5 point integration		
$8\beta*$-NT/SA	0.09401E-04	0.1290E-04
8β-NT/SA	0.1203E-04	0.1266E-04
8 point integration		
$8\beta*$-NT/SA	0.09410E-04	0.1289E-04
8β-NT/SA	0.1203E-04	0.1266E-04
Full integration		
$8\beta*$-NT/SA	0.08456E-04	0.1280E-04
8β-NT/SA	0.1052E-04	0.1260E-04
Moser and Schmid	$\approx 0.12E-04$	

Table 7.17: Clamped hemisphere with 30^o hole (Ply orientation $E_\theta = E_{11}$): Effect of integration scheme order

Element	4×4	8×8	16×16
Radial displacement at A			
Q4/SA	1.102E-04	1.600E-04	1.766E-04
QC9D$*$/SA	0.9654E-04	1.617E-04	1.769E-04
8$\beta*$-NT/SA	1.041E-04	1.627E-04	1.769E-04
9$\beta*$-NT/SA	0.9743E-04	1.617E-04	1.769E-04
Moser and Schmid		$\approx 1.8E-04$	
Radial displacement at B			
Q4/SA	-0.6605E-04	-0.6850E-04	-0.7056E-04
QC9D$*$/SA	-0.5242E-04	-0.6950E-04	-0.7074E-04
8$\beta*$-NT/SA	-0.5705E-04	-0.7004E-04	-0.7078E-04
9$\beta*$-NT/SA	-0.5301E-04	-0.6953E-04	-0.7075E-04
Moser and Schmid		$\approx -0.7E-04$	
Radial displacement at C			
Q4/SA	0.3680E-04	0.3952E-04	0.3792E-04
QC9D$*$/SA	0.2594E-04	0.3791E-04	0.3833E-04
8$\beta*$-NT/SA	0.2972E-04	0.3996E-04	0.3836E-04
9$\beta*$-NT/SA	0.2636E-04	0.3954E-04	0.3833E-04
Moser and Schmid		$\approx 0.4E-04$	

Table 7.18: Clamped hemisphere with 30^o hole: (Ply orientation $E_\phi = E_{11}$): Radial displacement

Element	4×4
Radial displacement at A	
$G_{12} \times 10^{-3}$	1.094E-04
$G_{12} \times 10^{-2}$	1.094E-04
$G_{12} \times 10^{-2}$	1.093E-04
$G_{12} \times 10^{0}$	1.090E-04
$G_{12} \times 10^{1}$	1.088E-04
$G_{12} \times 10^{2}$	1.088E-04
$G_{12} \times 10^{3}$	1.088E-04
Moser and Schmid	$\approx 1.8E-04$
Radial displacement at B	
$G_{12} \times 10^{-3}$	-0.6335E-04
$G_{12} \times 10^{-2}$	-0.6333E-04
$G_{12} \times 10^{-2}$	-0.6329E-04
$G_{12} \times 10^{0}$	-0.6315E-04
$G_{12} \times 10^{1}$	-0.6307E-04
$G_{12} \times 10^{2}$	-0.6306E-04
$G_{12} \times 10^{3}$	-0.6305E-04
Moser and Schmid	$\approx -0.7E-04$
Radial displacement at C	
$G_{12} \times 10^{-3}$	0.3641E-04
$G_{12} \times 10^{-2}$	0.3641E-04
$G_{12} \times 10^{-2}$	0.3639E-04
$G_{12} \times 10^{0}$	0.3637E-04
$G_{12} \times 10^{1}$	0.3642E-04
$G_{12} \times 10^{2}$	0.3643E-04
$G_{12} \times 10^{3}$	0.3643E-04
Moser and Schmid	$\approx 0.4E-04$

Table 7.19: Clamped hemisphere with 30^o hole (Ply orientation $E_\phi = E_{11}$): Influence of γ on 4×4 mesh

Element	4×4	8×8
Radial displacement at A		
5 point integration		
$8\beta*$-NT/SA	1.067E-04	1.631E-04
8β-NT/SA	1.144E-04	1.632E-04
8 point integration		
$8\beta*$-NT/SA	1.068E-04	1.631E-04
8β-NT/SA	1.144E-04	1.632E-04
Full integration		
$8\beta*$-NT/SA	1.041E-04	1.627E-04
8β-NT/SA	1.090E-04	1.626E-04
Moser and Schmid	$\approx 1.8E-04$	
Radial displacement at B		
5 point integration		
$8\beta*$-NT/SA	-0.5882E-04	-0.7026E-04
8β-NT/SA	-0.6696E-04	-0.6999E-04
8 point integration		
$8\beta*$-NT/SA	-0.5884E-04	-0.7026E-04
8β-NT/SA	-0.6699E-04	-0.6999E-04
Full integration		
$8\beta*$-NT/SA	-0.5705E-04	-0.7004E-04
8β-NT/SA	-0.6315E-04	-0.6973E-04
Moser and Schmid	$\approx -0.7E-04$	
Radial displacement at C		
5 point integration		
$8\beta*$-NT/SA	0.3113E-04	0.4009E-04
8β-NT/SA	0.3922E-04	0.3981E-04
8 point integration		
$8\beta*$-NT/SA	0.3114E-04	0.4009E-04
8β-NT/SA	0.3924E-04	0.3981E-04
Full integration		
$8\beta*$-NT/SA	0.2972E-04	0.3996E-04
8β-NT/SA	0.3637E-04	0.3974E-04
Moser and Schmid	$\approx 0.4E-04$	

Table 7.20: Clamped hemisphere with 30^o hole (Ply orientation $E_\phi = E_{11}$): Effect of integration scheme order

Element	1×6	2×12	4×24	8×48
In-plane shear: u_{3_A}				
QC9D$*$/SA	0.03525	0.03533	0.03535	0.03535
8$\beta*$-NT/SA	0.03532	0.03542	0.03544	0.03545
9$\beta*$-NT/SA	0.03532	0.03541	0.03544	0.03545
Out-of-plane shear: u_{2_A}				
QC9D$*$/SA	0.009570	0.009548	0.009520	0.009518
8$\beta*$-NT/SA	0.009594	0.009574	0.009547	0.009544
9$\beta*$-NT/SA	0.009594	0.009573	0.009546	0.009544

Table 7.21: Pre-twisted beam (Stacking sequence $[0/90]_s$): Numerical results

Element	1×6	2×12	4×24	8×48
In-plane shear: u_{3_A}				
QC9D$*$/SA	0.06968	0.07973	0.08489	0.08721
8$\beta*$-NT/SA	0.07000	0.07990	0.08495	0.08723
9$\beta*$-NT/SA	0.06998	0.07990	0.08495	0.08723
Out-of-plane shear: u_{2_A}				
QC9D$*$/SA	0.02445	0.02763	0.02928	0.02997
8$\beta*$-NT/SA	0.02542	0.02838	0.02956	0.03006
9$\beta*$-NT/SA	0.02542	0.02836	0.02955	0.03006

Table 7.22: Pre-twisted beam (Stacking sequence $[-45/45]_s$): Numerical results

Element	1×6	2×12	4×24	8×48
In-plane shear: u_{3_A}				
QC9D$*$/SA	0.08230	0.08779	0.08899	0.08938
8$\beta*$-NT/SA	0.08552	0.08815	0.08903	0.08939
9$\beta*$-NT/SA	0.08487	0.08809	0.08902	0.08939
Out-of-plane shear: u_{2_A}				
QC9D$*$/SA	0.02669	0.02834	0.02867	0.02877
8$\beta*$-NT/SA	0.02823	0.02857	0.02872	0.02878
9$\beta*$-NT/SA	0.02794	0.02855	0.02872	0.02878

Table 7.23: Pre-twisted beam (Stacking sequence $[30/60]_s$): Numerical results

Chapter 8

Conclusions and recommendations

In this chapter the capabilities of the newly implemented elements are summarized. A proposed formulation for general use is also suggested.

8.1 Isotropic membrane elements

The 8β and 9β families perform almost identical. However, since the formulation of the 8β family is simpler than that of the 9β family, the 8β family is preferable to the 9β family.

The difference between the mixed and displacement formulations is, (in terms of numerical accuracy), insignificant, and is a result of the rank one update of the mixed formulation. Once again, since the displacement formulation is simpler, this formulation is preferred above the mixed formulation.

In general, the NT-formulations outperform the other formulations and are, therefore, the preferred formulation for constraining the higher order stress field.

In general, the performance of the elements is increased if the locking correction is excluded, albeit at the cost of additional complexity in the formulation of the consistent nodal loads. In particular, exclusion of the locking correction increases the accuracy for highly distorted meshes. Notwithstanding the foregoing, the results are still acceptable if the correction is included, and membrane-bending locking is prevented. Hence, it is suggested that the locking correction is in general included. This has the additional advantage that the consistent nodal loads reduce to those of a 'standard' quadrilateral finite element with only two (translational) degrees of freedom per node.

Reduced integration improves the behavior of the elements when the locking correction is used, due to the introduction of a soft higher order deformation mode. However, for highly distorted geometries, full integration can be beneficial.

Finally, the formulation reveals some sensitivity to the numerical value of the stability parameter γ. However, the results obtained with the choice of $\gamma = G$ for the large range of problems evaluated are all acceptable, and this value is suggested for practical analyses. It is reiterated that the patch test is passed for any $\gamma > 0$. Hence, the value of γ ($\gamma > 0$) becomes irrelevant in the limit of mesh refinement.

8.2 Isotropic plate elements

The assumed strain plate element proposed by Bathe and Dvorkin is highly accurate, and almost free from locking. The element has extensively been used and tested by numerous researchers previously, and is relatively problem-free. Hence this element is an ideal plate component for flat shells which require a first order shear deformation theory, as is the case with orthotropic laminates.

For one-dimensional problems, (e.g. a simple cantilever), the residual bending flexibility (RBF) correction can be included to raise the capability of the elements to exactly the linear strain level.

However, for two-dimensional problems, selection of the characteristic lengths is not simple, and some over displacement is noted for meshes of intermediate refinement. Hence, and notwithstanding the fact that the effect of the correction disappears in the limit of mesh refinement, it is suggested that the formulation of Bathe and Dvorkin is in general used without the residual bending flexibility correction.

8.3 Isotropic shell elements

The 8β/SA and 9β/SA families perform very well for the test problems considered in this study, with the settings for the 8β and 9β membrane elements suggested in Section 8.1. Viz, the membrane locking correction is included, the displacement formulation is used and full integration is used.

The competing 5β/SA family proposed by Di and Ramm performs very well for the regular meshes, and in general even outperforms the 8β/SA and 9β/SA families. However, the 5β/SA family becomes increasingly inaccurate for distorted meshes. In addition, the 5β/SA family is ineffective for warped geometries, since the lack of drilling degrees of freedom complicates the use of this family for warped geometries.

8.4 Orthotropic formulation

For an orthotropic constitutive relationship, the 8β/SA and 9β/SA families proposed herein perform very well. However, the sensitivity to the value of γ, and the effect of the membrane locking correction become more pronounced. Nevertheless, the value of $\gamma = G_{12}$ suffices, and is recommended for general use.

As opposed to the isotropic formulation, it is suggested that the membrane locking correction *may* be excluded for the combination of computationally expensive orthotropic problems and highly distorted meshes. Viz, if the 8β/SA family is used in a global optimization infrastructure, it might well be beneficial to accept the increased complexity in the formulation of the consistent nodal loads when the locking correction is excluded, at the gain of a dramatic increase in accuracy.

Finally, it is noted that the superiority of the 8β/SA and the 9β/SA families over the

5β/SA family for distorted geometries becomes even more pronounced for orthotropy than for isotropy.

8.5 Recommendations

As opposed to the general trend to use higher order finite elements for the analysis of orthotropic structures, it is demonstrated that the relatively simple flat shell finite elements with an assumed stress membrane interpolation, drilling degrees of freedom and an assumed strain plate interpolation recommended in this study, suffice. This, potentially, significantly reduces the cost of orthotropic analyses.

- It is recommended that the 8β/SA element proposed herein is used for the analysis of orthotropic shell problems, with $\gamma = G_{12}$, full integration, and inclusion of the membrane locking correction.

  For coarse, highly distorted meshes, the locking correction could be excluded to increase accuracy (e.g. when using the elements in an optimization algorithm).

- An investigation into low order enhanced strain formulations is suggested as a fruitful research area to further investigate the efficiency of low order finite elements for the analysis of orthotropic structures.

- The formulation of a non-flat shell element with in-plane drilling degrees of freedom, and a formulation for geometric and material non-linearity would be desirable.

Bibliography

[1] H.H. Dovey. *Extension of three dimensional analysis to shell structures using the finite element idealization.* PhD dissertation, University of California, Berkeley, 1974. (Report no. UC SESM 74-2).

[2] K.B. Armstrong and R.T Barrett. *Care and repair of advanced composites.* Society of automative engineers, Warrendale, 1998.

[3] A.A. Groenwold and N. Stander. A 24 d.o.f. 4-node flat shell finite element for general unsymmetric orthotropic layered composites. *Eng. Comput.*, 15:518–543, 1998.

[4] A.K. Noor and M.D. Mathers. Finite element analysis of anisotropic plates. *Int. J. Numer. Methods Eng.*, 11:289–307, 1977.

[5] T.J.R. Hughes and F. Brezzi. On drilling degrees of freedom. *Comp. Methods Appl. Mech. Eng.*, 72:105–121, 1989.

[6] R.L. Taylor. Finite element analysis of linear shell problems. In J.R. Whiteman, editor, *Proceedings of the Mathematics in Finite Elements and Applications*, pages 191–203, New York, 1987. Academic Press.

[7] K.-J. Bathe and E.N. Dvorkin. A four node plate bending element based on Mindlin-Reissner plate theory and a mixed interpolation. *Int. J. Numer. Methods Eng.*, 21:367–383, 1985.

[8] W. Feng, S.V. Hoa, and Q. Huang. Classification of stress modes in assumed stress fields of hybrid finite elements. *Int. J. Numer. Methods Eng.*, 40:4313–4339, 1997.

[9] A.A. Groenwold and S. Geyer. Two hybrid stress membrane finite element families with drilling rotations. Submitted.

[10] F. Frey. Shell finite elements with six degrees of freedom per node. In *ASME Winter Annual Meeting*, San Francisco, 1989.

[11] P.G. Bergan and C.A. Felippa. A triangular membrane element with rotational degrees of freedom. *Comp. Meth. Applied Mech. Eng.*, 50:25–69, 1985.

[12] D.J. Allman. A compatible triangular element including vertex rotations for plane elasticity analysis. *Comp. Struc.*, 19:1–8, 1984.

[13] R.H. MacNeal and R.L. Harder. A refined four-noded membrane element with rotational degrees of freedom. *Comp. Struct.*, 18:75–84, 1988.

[14] R.D. Cook. On the allman triangle and a related quadrilateral element. *Comp. Struc.*, 22:1065–1067, 1986.

[15] D.J. Allman. A quadrilateral finite element including vertex rotations for plane elasticity analysis. *Int. J. Numer. Methods Eng.*, 26:717–730, 1988.

[16] P. Jetteur. A shallow shell element with in-plane rotational degrees of freedom. IREM Internal Report 86/3, Ecole Polytechnique Federale de Lausanne, 1986.

[17] S. Jaamei. "Jet" thin shell finite element with drilling rotations. IREM Internal Report 88/7, Ecole Polytechnique Federale de Lausanne, 1988.

[18] P. Jetteur. Improvement of the quadrilateral "JET" shell element for a particular class of shell problems. IREM Internal Report 87/1, Ecole Polytechnique Federale de Lausanne, 1987.

[19] R.L. Taylor and J.C. Simo. Bending and membrane elements for analysis of thick and thin shells. In *Proceedings of NUMETA Conference*, Swansea, 1985.

[20] J.C. Simo, D.D. Fox, and M.S. Rifai. On a stress resultant geometrically exact shell model, Part II: The linear theory; computational aspects. *Comp. Meth. Applied Mech. Eng.*, 73:53–92, 1989.

[21] E. Reissner. A note on variational principles in elasticity. *Int. J. Solids. Struct.*, 1:93–95, 1965.

[22] T.J.R. Hughes, F. Brezzi, A. Masud, and I. Harari. Finite elements with drilling degrees of freedom: Theory and numerical evaluation. In R. Gruber, J. Periaux, and R.P. Shaw, editors, *Proc. of the 5th International Symposium on Numerical Methods in Engineering*, volume 1, pages 3–17. Springer, 1989.

[23] A. Ibrahimbegovic, R.L. Taylor, and E.L. Wilson. A robust quadrilateral membrane finite element with drilling degrees of freedom. *Int. J. Numer. Methods Eng.*, 30:445–457, 1990.

[24] A. Ibrahimbegovic and E.L. Wilson. A unified formulation for triangular and quadrilateral flat shell finite elements with six nodal degrees of freedom. *Commun. Applied Num. Meth.*, 7:1–9, 1991.

[25] A.A Groenwold and N. Stander. An efficient 4-node 24 d.o.f. thick shell finite element with 5-point quadrature. *Eng. Comput.*, 12:723–748, 1995.

[26] T.H.H. Pian. Derivation of element stiffness matrices by assumed stress distributions. *AIAA J.*, 2:1333–1336, 1964.

[27] T.H.H. Pian. State-of-the-art development of the hybrid/mixed finite element method. *Fin. Elem. Anal. Des.*, 21:5–20, 1995.

[28] T.H.H. Pian and K. Sumihara. Rational approach for assumed stress finite elements. *Int. J. Numer. Methods Eng.*, 20:1685–1695, 1984.

[29] T.H.H. Pian and C.-C. Wu. A rational approach for choosing stress terms for hybrid finite element formulations. *Int. J. Numer. Methods Eng.*, 26:2331–2343, 1988.

[30] E.F. Punch and S.N. Atluri. Development and testing of stable, isoparametric curvilinear 2- and 3-D hybrid stress elements. *Comp. Methods Appl. Mech. Eng.*, 47:331–356, 1984.

[31] F. Brezzi. On the existence, uniqueness and approximation of saddle point problems arising from lagrange multipliers. *RAIRO-8*, 000:129–151, 1974.

[32] I. Babuska, J.T. Oden, and J.K. Lee. Mixed-hybrid finite element approximations of second-order elliptic oundary-value problems. *Comp. Methods Appl. Mech. Eng.*, 11:175–206, 1977.

[33] B. Fraeijs du Veubeke. Displacement and equilibrium models in the finite element method. In O.C. Zienkiewicz and G.C. Holister, editors, *Stress analysis*, pages 145–197, Chichester, 1965. John Wiley.

[34] S. Di and E. Ramm. On alternative hybrid stress 2D and 3D elements. *Eng. Comput.*, 11:49–68, 1994.

[35] M.A. Aminpour. An assumed-stress hybrid 4-node shell element with drilling degrees of freedom. *Int. J. Numer. Methods Eng.*, 33:19–38, 1992.

[36] G. Rengarajan, M.A. Aminpour, and N.F. Knight. Improved assumed-stress hybrid shell element with drilling degrees of freedom for linear stress, buckling and free vibration analyses. *Int. J. Numer. Methods Eng.*, 38:1917–1943, 1995.

[37] K-Y Sze and A Ghali. Hybrid plane quadrilateral element with corner rotations. *Journal of Structural Engineering*, 119:2552–2572, 1993.

[38] T.J.R. Hughes. *The finite element method: Linear static and dynamic analysis.* Prentice-Hall, London, 1987.

[39] O.C. Zienkiewicz and R.L. Taylor. *The Finite Element method: Basic formulation and linear problems, Vol. II.* McGraw-Hill, London, 1991.

[40] E.L Wilson. The static condensation algorithm. *Int. J. Numer. Methods Eng.*, 8:199–203, 1974.

[41] R.L. Taylor, J.C. Simo, O.C. Zienkiewicz, and A.C.H. Chan. The patch test - a condition for assesing fem convergence. *Int. J. Numer. Methods Eng.*, 22:39–62, 1986.

[42] K-Y Sze. Efficient formulation of robust mixed element using orthogonal stress/strain interpolants and admissible matrix formulation. *Int. J. Numer. Methods Eng.*, 35:1–20, 1992.

[43] B.M. Irons and A Razzaque. Experience with the patch test for convergence of finite element methods. In A.K. Aziz, editor, *Mathematical Foundations of the Finite Element Method*, pages 557–587, New York, 1972. Academic Press.

[44] O.C. Zienkiewicz, S. Qu, R.L. Taylor, and S. Nakazawa. The patch test for mixed formulations. *Int. J. Numer. Methods Eng.*, 23:1873–1883, 1986.

[45] R.H. Macneal and R.L. Harder. A proposed standard set of problems to test finite element accuracy. *J. Finite Elem. Anal. Des.*, 1:3–20, 1985.

[46] S. Idelsohn. On the use of deep, shallow or flat shell finite elements for the analysis of thin shell structures. *Comp. Meth. Applied Mech. Eng.*, 26:321–330, 1981.

[47] E.N. Dvorkin and K.-J. Bathe. A continuum mechanics based four-node shell element for general non-linear analysis. *Eng. Comput.*, 1:77–88, 1984.

[48] E. Hinton and H.C. Huang. Shear forces and twisting moments in plates using mindlin elements. *Eng. Comput.*, 3:129–142, 1986.

[49] P. Papdopulos and R.L. Taylor. A traingular element based on reissner-mindlin plate theory. *Int. J. Numer. Methods Eng.*, 30:1029–1049, 1990.

[50] K.-J. Bathe. *Finite element procedures in engineering analysis.* Prentice-Hall, London, 1982.

[51] H. Kebari. A one point integrated assumed strain 4-node mindlin plate element. *Eng. Comput.*, 7:284–290, 1990.

[52] A.A. Groenwold. Finite element analysis of composite plates and shells. Master dissertation, University of Pretoria, Department of Mechanical and Aeronautical Engineering, October 1993.

[53] J.A. Robinson. A warped quadrilateral strain membrane element. *Comp. Meth. Applied Mech. Eng.*, 7:359–367, 1976.

[54] A. Ibrahimbegovic. Plate quadrilateral finite element with incompatible modes. *Commun. Applied Num. Meth.*, 8:497–504, 1992.

[55] R.H. Macneal. A simple quadrilateral shell element. *Comp. Struct.*, 8:175–183, 1978.

[56] H. Parisch. An investigation of a finite rotation four node assumed strain shell element. *Int. J. Numer. Methods Eng.*, 31:127–150, 1991.

[57] A.C. Scordelis and K.S. Lo. Computer analysis of cylindrical shells. *J. Amer. Concr. Inst.*, 61:539–561, 1969.

[58] S.P. Timoshenko and S. Woinowsky-Krieger. *Theory of plates and shells.* McGraw-Hill, New-York, 1970.

[59] G.M. Stanley. *Continuum-based shell elements.* Ph.D. dissertation, Stanford University, Department of Mechanical Engineering, 1985.

[60] D.J. Haas and S.W. Lee. A nine-node assumed-strain finite element for composite plates and shells. *Comput. Struct.*, 26:445–452, 1987.

[61] K Moser and A Schmid. Composite structures - modelling, finite element analysis and evaluation. *Composite Structures*, 11:33–56, 1989.

[62] N. Stander and E.L. Wilson. A 4-node quadrilateral membrane element with in-plane vertex rotations and modified reduced quadrature. *Eng. Comput.*, 6:266–271, 1989.

[63] C.H. Edwards, Jr. and D.E. Penny. *Elementary differential equations with boundary value problems.* Prentice Hall, Englewood Cliffs, New Jesey, third edition, 1993.

[64] J.N. Reddy. *An introduction to the finite element method.* McGraw-Hill Book Company, 1984.

[65] K Washizu. *Variational methods in elasticity and plasticity.* Pergamon Press, third edition, 1982.

Appendix A

Element operators

A.1 Membrane element operators

In (2.71), the operators $\boldsymbol{B}_i$ and $\boldsymbol{G}_{\psi i}$ are given as

$$\boldsymbol{B}_i = \begin{bmatrix} N_{i,1} & 0 \\ 0 & N_{i,2} \\ N_{i,2} & N_{i,1} \end{bmatrix} \; ; \; i = 1,2,3,4 \tag{A.1}$$

with N_i, $i = 1,2,3,4$, the Lagrangian interpolation functions. The strain operator associated with the drilling rotation is defined by

$$\boldsymbol{G}_{\psi i} = \frac{1}{8} \begin{bmatrix} (l_{ij}\cos\alpha_{ij}N_{l,1} - l_{ik}\cos\alpha_{ik}N_{m,1}) \\ (l_{ij}\sin\alpha_{ij}N_{l,2} - l_{ik}\sin\alpha_{ik}N_{m,2}) \\ \left\{ \begin{array}{c} l_{ij}\cos\alpha_{ij}N_{l,2} - l_{ik}\cos\alpha_{ik}N_{m,2} \\ + \\ l_{ij}\sin\alpha_{ij}N_{l,1} - l_{ik}\sin\alpha_{ik}N_{m,1} \end{array} \right\} \end{bmatrix} \tag{A.2}$$

where l_{jk} represent the lengths of sides jk and, using a FORTRAN pseudo language,

$$\begin{gathered} i = 1,2,3,4; \; m = i+4; \; l = m - 1 + 4 \text{ int}(1/i); \\ k = \text{mod}(m,4) + 1; \; j = l - 4 \end{gathered} \tag{A.3}$$

The functions N_i, $i = 5,6,7,8$ are serendipity mid-side interpolation functions.
The operators associated with the penalty stiffness $(\gamma/\Omega^e)\boldsymbol{h}^e\boldsymbol{h}^{eT}$ and $\boldsymbol{P}^e_\gamma$ are

$$\boldsymbol{b}_i = < -\frac{1}{2}N_{i,2} \;\; \frac{1}{2}N_{i,1} > \; ; \quad i = 1,2,3,4 \tag{A.4}$$

and

$$\begin{aligned} g_i = & -\frac{1}{16}(l_{ij}\cos\alpha_{ij}N_{l,2} - l_{ik}\cos\alpha_{ik}N_{m,2}) \\ & +\frac{1}{16}(l_{ij}\sin\alpha_{ij}N_{l,1} - l_{ik}\sin\alpha_{ik}N_{m,1}) - N_i \; ; \quad i = 1,2,3,4 \end{aligned} \tag{A.5}$$

with indices j, k, l, m again defined by (A.3). In (2.69), a FORTRAN-like definition of adjacent corner nodes is also employed:

$$j \;=\; i-4\;;\quad k \;=\mathrm{mod}(i,4)+1 \tag{A.6}$$

A.2 Plate element operators

In (4.40) the element curvature-displacement matrix is given by [38]

$$\boldsymbol{B}_{bi} = \begin{bmatrix} 0 & N_{i,1} & 0 \\ 0 & 0 & N_{i,2} \\ 0 & N_{i,2} & N_{i,1} \end{bmatrix} \tag{A.7}$$

and in (4.42) the element shear strain-displacement matrix is given by [38]

$$\boldsymbol{B}_{si} = \begin{bmatrix} N_{i,1} & -N_i & 0 \\ N_{i,2} & 0 & -N_i \end{bmatrix} \tag{A.8}$$

Appendix B

Classification of stress modes

After Feng *et al.*, the following constant and linear stress modes are defined

$$[\{\sigma_1\}\{\sigma_2\}\{\sigma_3\}\{\sigma_4\}\{\sigma_6\}\{\sigma_8\}\{\sigma_5\}\{\sigma_7\}\{\sigma_9\}] = \begin{bmatrix} 1 & 0 & 0 & \xi & 0 & 0 & \eta & 0 & 0 \\ 0 & 1 & 0 & 0 & \xi & 0 & 0 & \eta & 0 \\ 0 & 0 & 1 & 0 & 0 & \xi & 0 & 0 & \eta \end{bmatrix}$$

i.e. $\{\sigma_1\} = \{1\ 0\ 0\}^T$, etc. Four alternative stress modes are defined as

$$[\{\sigma_{10}\}\{\sigma_{11}\}\{\sigma_{12}\}\{\sigma_{13}\}] = \begin{bmatrix} 1 & 1 & 0 & -\xi \\ 1 & -1 & -\eta & 0 \\ 0 & 0 & \xi & \eta \end{bmatrix}$$

while the higher order terms are here defined as

$$[\{\sigma_{14}\}\{\sigma_{15}\}\{\sigma_{16}\}\cdots\{\sigma_{24}\}] = \begin{bmatrix} \xi^2 & 0 & 0 & \eta^2 & 0 & 0 & \xi\eta & 0 & 0 & \eta^2 & \xi^2 \\ 0 & \xi^2 & 0 & 0 & \eta^2 & 0 & 0 & \xi\eta & 0 & -\xi^2 & -\eta^2 \\ 0 & 0 & \xi^2 & 0 & 0 & \eta^2 & 0 & 0 & \xi\eta & 0 & 0 \end{bmatrix}$$

For the 5β family, modes 20 through 24 belong to the zero-energy stress mode. For the 8β(M), 8β(D), 9β(M) and 9β(D) families however, these modes contribute energy.

Appendix C

Constraining the assumed stress field

The transformation operators $\boldsymbol{T}_0$, $\boldsymbol{T}$ and $\boldsymbol{Q}$ are given below:

$$\boldsymbol{T}_0 = \begin{bmatrix} a_1^2 & a_3^2 & 2a_1a_3 \\ b_1^2 & b_3^2 & 2b_1b_3 \\ a_1b_1 & a_3b_3 & a_1b_3 + a_3b_1 \end{bmatrix} \tag{C.1}$$

with the parameters a_i and b_i defined by

$$\begin{bmatrix} a_1 & b_1 \\ a_2 & b_2 \\ a_3 & b_3 \end{bmatrix} = \frac{1}{4}\begin{bmatrix} -1 & 1 & 1 & -1 \\ 1 & -1 & 1 & -1 \\ -1 & -1 & 1 & 1 \end{bmatrix}\begin{bmatrix} x_1 & y_1 \\ x_2 & y_2 \\ x_3 & y_3 \\ x_4 & y_4 \end{bmatrix} \tag{C.2}$$

Also,

$$\boldsymbol{T} = \begin{bmatrix} J_{11}^2 & J_{21}^2 & 2J_{11}J_{21} \\ J_{12}^2 & J_{22}^2 & 2J_{12}J_{22} \\ J_{11}J_{12} & J_{21}J_{22} & J_{11}J_{22} + J_{12}J_{21} \end{bmatrix} \tag{C.3}$$

with

$$J_{ki} = \frac{\partial x^i}{\partial \xi^k} = t^k \quad (i,k = 1,2) \tag{C.4}$$

Finally,

$$\boldsymbol{Q} = \frac{1}{|\boldsymbol{J}|}\begin{bmatrix} \rho & 0 & 0 \\ 0 & 1/\rho & 0 \\ 0 & 0 & 1 \end{bmatrix} \qquad \rho = \sqrt{\frac{J_{21}^2 + J_{22}^2}{J_{11}^2 + J_{12}^2}} \tag{C.5}$$

Appendix D

Reduced integration

D.1 Derivation of numerical integration schemes[1]

Consider the area integral given by

$$I = \int_{-1}^{1} \int_{-1}^{1} F(\xi, \eta) \, \mathrm{d}\xi \mathrm{d}\eta \tag{D.1}$$

where $F(\xi, \eta)$ is any polynomial function of ξ and η. Any polynomial expression of two variables can be expressed in the form

$$F(\xi, \eta) = \sum_{i,j} A_{ij} \xi^i \eta^i \tag{D.2}$$

No limits are placed on the summation indices i and j as any arbitrary polynomial is being considered.

Let any N-point rule be written as

$$I^* = \sum_{n=1}^{N} W_n F(\xi, \eta) \tag{D.3}$$

where I^* represents the numerical approximation to I. Integration point n is given by (ξ_n, η_n) and the associated weight is given as W_n.

Each term of (D.2) may be trivially integrated as follows

$$\int_{-1}^{1} \int_{-1}^{1} A_{ij} \xi^i \eta^i \, \mathrm{d}\xi \mathrm{d}\eta = \begin{cases} \frac{2^2 A_{ij}}{(i+1)(j+1)} & i, j \text{ both even} \\ 0 & \text{otherwise} \end{cases} \tag{D.4}$$

Application of the quadrature rule of (D.3) to the function $F(\xi, \eta)$ in the form of (D.2) gives the following result which is expressed in terms of the coefficients A_{ij} as

$$I^* = A_{00}\sum_{n=1}^{N} W_n + A_{10}\sum_{n=1}^{N} W_n\xi_n + A_{01}\sum_{n=1}^{N} W_n\eta_n + A_{20}\sum_{n=1}^{N} W_n\xi_n^2 + \ldots \tag{D.5}$$

Two points are to be noted:

- Symmetry of the rule in each coordinate implies that the coefficients corresponding to all odd powers will vanish in (D.5). This of course corresponds to the vanishing of the integral of odd powers over this region.
- Symmetry with respect to both coordinates is required to ensure invariance of the rule.

Equating the coefficients of A_{ij} between (D.4) and (D.5) gives a series of equations in the weights W_n and the coordinates ξ_n and η_n. Evidently the number of equations that are satisfied for a particular set of weights and coordinates indicate which polynomial terms are integrated exactly by that particular rule. Also, the degree to which each remaining equation is not satisfied gives the error in that polynomial term. Each equation has the form

$$\sum_{n=1}^{N} W_n\xi_n^i\eta_n^j = \frac{2^2}{(i+1)(j+1)} \tag{D.6}$$

for the coefficient A_{ij}. Clearly all equations containing odd values for either i or j are satisfied identically for symmetric rules.

The maximum number of equations needed for (D.6) is determined by the order of the function $F(\xi,\eta)$ which is to be integrated. If the maximum number of equations possible are satisfied for a particular configuration, then an optimal scheme for that configuration is obtained. However, if less than the maximum number are satisfied a less efficient rule is obtained, but freedom is available for arbitrary selection of some values of weights or coordinates.

D.2 A 5-point integration scheme

The first 5-point integration scheme presented by Dovey [1] is employed to selected problems. (See Figure D.1).

Due to symmetry, the weights W_α are identical. The rule is indicated by

$$I^* = W_0F(0,0) + W_\alpha F(\pm\alpha,\pm\alpha) \tag{D.7}$$

The second term in (D.7) indicates four points when all combinations of positive and negative signs are taken.

Employing (D.6) we obtain the first four equations for the appropriate terms A_{ij} as

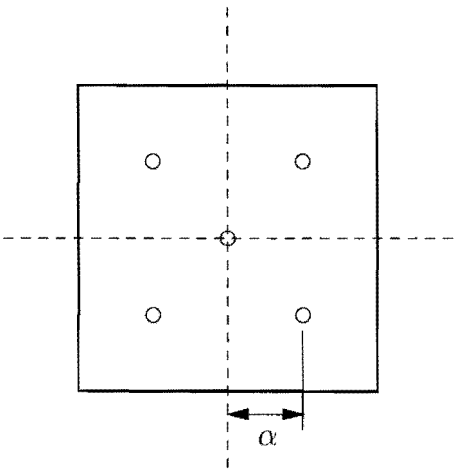

Figure D.1: 5-point integration scheme

$$\begin{array}{lcll} A_{00} & : & W_0 + 4W_\alpha & = & 4 \\ A_{20}, A_{02} & : & 4W_\alpha\alpha^2 & = & \frac{4}{3} \\ A_{22} & : & 4W_\alpha\alpha^4 & = & \frac{4}{9} \\ A_{40}, A_{04} & : & 4W_\alpha\alpha^4 & = & \frac{4}{5} \end{array} \tag{D.8}$$

The last two of these equations are directly inconsistent and so the last is discarded. Also, however, the first three are inconsistent if the center point is retained.

Solving (D.8) leads to

$$\begin{aligned} W_0 &= 0 \\ W_\alpha &= 1 \\ \alpha &= \frac{1}{\sqrt{3}} \end{aligned} \tag{D.9}$$

which is the 2×2 Gaussian product rule. The leading error term is defined by the last of (D.8) and gives the error $(I^* - I)$, corresponding to the fourth power terms ξ^4 and η^4 as

$$E_{40} = \left(4W_\alpha\alpha^4 - \frac{4}{5}\right) A_{40} = E_{04} = \left(4W_\alpha\alpha^4 - \frac{4}{5}\right) A_{04} \tag{D.10}$$

However, the center point may be retained by selecting the value of W_0, computing W_α and α from the first two relationships in (D.8). This implies an error in the A_{22} term. The scheme is now defined by

$$W_\alpha = 1 - \frac{W_0}{4} \tag{D.11}$$

$$\alpha = \left(\frac{1}{3W_\alpha}\right)^{\frac{1}{2}} \tag{D.12}$$

The scheme only has physical meaning while $0 \leq W_0 \leq 4$. The error in the A_{22} term is minimized as $W_0 \to 0$. In practice this implies that the 5-point scheme converges to the 2×2 Gaussian scheme as $W_0 \to 0$.

D.3 An 8-point integration scheme

The 8-point rule is depicted in Figure D.2.

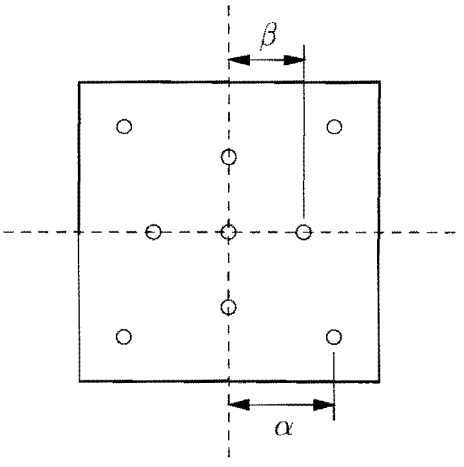

Figure D.2: 8-point integration scheme

This rule was previously employed for membrane elements with in-plane rotational degrees of freedom by Stander and Wilson [62] in the QC9(8) element and also by Ibraimbegovic *et al.* [23] in their drilling degree of freedom membrane element. The rule is described by

$$I^* = W_\alpha F(\pm\alpha, \pm\alpha) + W_\beta[F(\pm\beta, 0) + F(0, \pm\beta)] \tag{D.13}$$

Due to symmetry, the weights W_α are identical as are the weights W_β. The governing equations are given by

$$\begin{array}{lcrcl} A_{00} & : & 4W_\alpha + 4W_\beta & = & 4 \\ A_{20}, A_{02} & : & 4W_\alpha\alpha^2 + 2W_\beta\beta^2 & = & \frac{4}{3} \\ A_{22} & : & 4W_\alpha\alpha^4 & = & \frac{4}{9} \\ A_{40}, A_{04} & : & 4W_\alpha\alpha^4 + 2W_\beta\beta^4 & = & \frac{4}{5} \end{array} \tag{D.14}$$

All four equations may be satisfied and the solution is

$$\begin{aligned} \alpha &= \sqrt{\frac{7}{9}} \\ W_\alpha &= \frac{9}{49} \end{aligned}$$

$$\begin{aligned} \beta &= \sqrt{\frac{7}{15}} \\ W_\beta &= \frac{40}{49} \end{aligned} \tag{D.15}$$

This rule gives the same order of accuracy as the 3×3 Gaussian rule. A scheme of lower accuracy is defined by

$$W_\alpha = 1 - W_\beta \tag{D.16}$$

$$\alpha = \left(\frac{1}{9W_\alpha}\right)^{\frac{1}{4}} \tag{D.17}$$

$$\beta = \left(\frac{\frac{2}{3} - 2W_\alpha\alpha^2}{W_\beta}\right)^{\frac{1}{4}} \tag{D.18}$$

The bounds for W_β are $0 \leq W_\beta \leq 1$. In [23, 62] the typical choice of $W_0 = 0.01$ was employed.

Appendix E

Code

E.1 Subroutines for the isotropic 8β element

```
C=============================================================SHL8
C
C     ELEMENT STIFFNESS MATRIX FOR AN ASSUMED STRESS
C     FOUR NODE MEMBRANE ELEMENT WITH DRILLING DEGREES OF
C     FREEDOM - 8 BETA PARAMETERS
C
C     (K+P)a = f - DISPLACEMENT FORMULATION
C     (K+h)a = f - MIXED FORMULATION
C
C-------------------------------------------------------------------
      SUBROUTINE SHL8(XYZ,ID,MAXN,NSHL8)

      IMPLICIT REAL*8 (A-H,O-Z)
      PARAMETER (NP=8)

      DIMENSION XYZ(4,MAXN),ID(6,MAXN),S(24,24)
      DIMENSION RS(2,16),GWS(2,16),B(3,14),BY(1,14)
      DIMENSION T1(3,14),T4(14,14),T1Y(1,14),T2Y(14,14)
      DIMENSION BTAY(3,4),BTAY2(3,4)
      DIMENSION P(3,NP),P1(3,NP),T2(NP,14),T3(NP,14)
      DIMENSION P2(NP,NP),XDU(NP,NP),CINV(3,3)
      DIMENSION NDOF(6),PPURE(3,NP)
      DIMENSION PTRANSO(3,3),PTRANS(3,3),QTRANS(3,3)
      DIMENSION IPVT(NP),WORK(NP),TEST1(NP,NP)
      DIMENSION NEIG(24),SEIG(24,24)
      DIMENSION BPL(3,12),BS(2,12),T1S(2,12)
      DIMENSION T1PL(6,12),T2PL(12,12)
      DIMENSION DB(3,3),DS(2,2)

      COMMON /CONSTR/ ICONSTR(9)
```

```
      COMMON /VECT  / V(4,3),XYL(3,5)
      COMMON /GENR  / NAM,INE,INI,NIDENT
      COMMON /SIDE  / ALPHA(4),XLENG(4)
      COMMON /TEMP  / IDE,II,JJ,KK,LL,HH,EE,UU
      COMMON /WEIGHI/ WGHTO
      COMMON /IOLIST/ NTM,NTR,NIN,NOT,NSP,NFL,NT7,NT8

      DATA ZERO /0.DO/, ONE /1.DO/, TWO /2.DO/, FOUR /4.DO/
      DATA NEIG /1,2,3,4,5,6,7,8,9,10,11,12,13,14,15,16,17,18,
     &           19,20,21,22,23,24/
      DATA NDOF /1,2,3,4,5,6/
      DATA FF   /1.2DO/

      IAXIS=1

      ND=24
      NUMN=4
      NTOT=0
      NTELE=2           !  DEFAULT - DISPLACEMENT FORMULATION
      INT=9             !  DEFAULT - FULL INTEGRATION
      INTTAY=4
      INT2=4
      NWARP=0           !  DEFAULT - WARP CORRECTION NOT ACTIVE
      NPRINT=0
      NSTAT=1
      NEIGEN=0
      NLOCK=1           !  DEFAULT - LOCKING CORRECTION ACTIVE
      WGHTO=0.01
      GG=-1.            !  DEFAULT - GG=EE/(TWO+TWO*UU)
      IMIXED=5          !  DEFAULT - NT-FORMULATION
      ALPHACORR=ONE
      IPSTATE=2         !  DEFAULT - P-MATRIX CLASSIFICATION

C-----LOOP THROUGH ALL ELEMENTS-----------------------------------
      DO 400 MM=1,NSHL8

C-----READ NODE NUMBERS AND MATERIAL PROPERTIES--------------------
C-------AND ELEMENT PARAMETERS-------------------------------------
      NAM=0
      NIDENT=0
      CALL CFREE
      CALL CFREEPT
      CALL CFREEI(' ',IDE,1)
      CALL CFREEI('N',II,4)
      CALL CFREER('H',HH,1)
      CALL CFREER('E',EE,1)
      CALL CFREER('U',UU,1)
      CALL CFREEI('G',NAM,4)
```

```
      CALL CFREEI('I',INT,1)
      CALL CFREEI('J',INTTAY,1)
      CALL CFREEI('K',INT2,1)
      CALL CFREER('X',GG,1)
      CALL CFREEI('S',NSTAT,1)
      CALL CFREEI('T',NTELE,1)
      CALL CFREEI('B',IPSTATE,1)
      CALL CFREEI('L',NEIGEN,1)
      CALL CFREEI('Z',NLOCK,1)
      CALL CFREER('D',WGHTO,1)
      CALL CFREEI('W',NWARP,1)
      CALL CFREEI('A',IMIXED,1)
      CALL CFREER('Y',ALPHACORR,1)
      CALL CFREEI('F',ICONSTR,9)       !  READ DIFFERENT P-MATRIX

      IF (GG.LT.ZERO) GG=EE/(TWO+TWO*UU)
      IF (GG.EQ.ZERO) NTELE=3
      IF (NAM.EQ.0) NIDENT=0
      NCHCK=NAM

C-----PRINT ELEMENT DATA-----------------------------------------
 10   IF (NPRINT.NE.0) GO TO 15
      CALL TOP
      WRITE (NOT,2003) IMIXED,INT
      WRITE (NOT,2000)
 15   WRITE (NOT,2001) IDE,II,JJ,KK,LL,HH,EE,GG,UU
      NPRINT=NPRINT+1
      IF(NPRINT.GT.50) NPRINT=0

C-----SKIP FOR IDENTICAL ELEMENTS--------------------------------
      IF (NIDENT.LT.0.OR.NIDENT.GT.1) NIDENT=0
      IF (NIDENT.EQ.1.AND.NCHCK.GT.NAM) GOTO 295

C-----LOCAL COORDINATES, SIDE LENGTHS & ANGLES-------------------
      CALL LOCAL(XYZ,MAXN,IAXIS)

      DO 19 I=1,4
      CALL ANGLEN(I,ALPHA(I),XLENG(I))
 19   CONTINUE

C----------------------------------------------------------------
C
C  ELEMENT K MATRIX - MIXED AND DISPL. FORMULATION
C
C----------------------------------------------------------------

C-----CALCULATE COMPLIANCE MATRIX--------------------------------
      CALL MATLWINV(NSTAT,EE,UU,CINV)
```

```
C-----INITIALIZE MATRICES-----------------------------------------
      DO 20 I=1,24
      DO 20 J=1,24
 20   S(I,J)=ZERO

      DO 22 J=1,14
      B(1,J)=ZERO
      B(2,J)=ZERO
      B(3,J)=ZERO
      T1Y(1,J)=ZERO
      BY(1,J)=ZERO
 22   CONTINUE

      DO 23 I=1,NP
      DO 23 J=1,NP
 23   P2(I,J)=ZERO

      DO 24 I=1,14
      DO 24 J=1,14
      T2Y(I,J)=ZERO
 24   CONTINUE

      DO 25 I=1,NP
      DO 25 J=1,14
 25   T2(I,J)=ZERO

      DO 26 J=1,4
      BTAY(1,J)=ZERO
      BTAY(2,J)=ZERO
      BTAY(3,J)=ZERO
 26   CONTINUE

      DO 27 I=1,3
      DO 27 J=1,NP
 27   P(I,J)=ZERO

      CALL FORMTRANSC (PTRANS0)
      CALL MEMXB3 (BY,DETJ0)

C-----CALCULATE ELEMENT AREA--------------------------------------
      CALL ELAREA(AREA)

C-----CALCULATE MEMBRANE LOCKING CORRECTION-----------------------
      IF (NLOCK.EQ.1) THEN
      CALL INTPTS(INTTAY,RS,GWS)
      DO 35 I=1,INTTAY
      CALL MEMLOK(I,RS,BTAY2,DETJ)
```

```
      DO 35 K=1,3
      DO 35 L=1,4
      BTAY(K,L)=BTAY(K,L)+BTAY2(K,L)*GWS(1,I)*GWS(2,I)*DETJ/AREA
 35   CONTINUE
      ENDIF

C-----DEFINE INTEGRATION POINTS----------------------------------
      CALL INTPTS(INT,RS,GWS)

C-----LOOP THROUGH THE INTEGRATION POINTS-------------------------
      DO 80 I=1,INT
      CALL MEMXBTJ  (I,RS,B,DETJ,BTAY,NLOCK,AJM11,AJM12,AJM21,AJM22)
      IF (IPSTATE.EQ.2) THEN
        CALL HQ8P2 (I,RS,PPURE)                 !  DETERMINE P
      ELSEIF (IPSTATE.EQ.1) THEN
        CALL HQ8P1 (I,RS,PPURE)                 !  DETERMINE P
      ELSE
        CALL HQ8PA (I,RS,PPURE)                 !  DETERMINE P
      ENDIF

      CALL FIXP (P,PTRANSO,PTRANS,QTRANS,AJM11,AJM12,AJM21,AJM22,
     &           DETJ,DETJO,PPURE,IMIXED,3,NP)  !  TRANSFORM P

C-----EVALUATE INTEGRAL------------------------------------------
C.....C^-1 x P ...................................................
      DO 50 K=1,3
      DO 50 L=1,NP
      C1=CINV(K,1)*P(1,L)+CINV(K,2)*P(2,L)+CINV(K,3)*P(3,L)
      P1(K,L)=C1*DETJ*HH*GWS(1,I)*GWS(2,I)
 50   CONTINUE

C.....P^t x C^-1 x P..............................................
      DO 54 K=1,NP
      DO 54 L=1,NP
      C1=P(1,K)*P1(1,L)+P(2,K)*P1(2,L)+P(3,K)*P1(3,L)
      P2(K,L)=P2(K,L)+C1
 54   CONTINUE

C.....P^t x B.....................................................
      DO 60 K=1,NP
      DO 60 L=1,12
      C1=P(1,K)*B (1,L)+P(2,K)*B (2,L)+P(3,K)*B (3,L)
      T2(K,L)=T2(K,L)+C1*DETJ*HH*GWS(1,I)*GWS(2,I)
 60   CONTINUE

C-----END OF INTEGRATION LOOP------------------------------------

 80   CONTINUE
```

```
C-----DETERMINE INVERSE OF H ----------------------------------
      CALL XEQY(XDU,P2,NP,NP)
      CALL DGEFA(P2,NP,NP,IPVT,INFO)
      JOB=01
      CALL DGEDI(P2,NP,NP,IPVT,DETX,WORK,JOB)
      CALL TESTINVERSE(XDU,P2,NP,NP,TEST1)

C.....H^-1 * G.....................................................
      DO 90 K=1,NP
      DO 90 L=1,12
      C1=P2(K,1)*T2(1,L)+P2(K,2)*T2(2,L)+P2(K,3)*T2(3,L)
     &  +P2(K,4)*T2(4,L)+P2(K,5)*T2(5,L)+P2(K,6)*T2(6,L)
     &  +P2(K,7)*T2(7,L)+P2(K,8)*T2(8,L)
      T3(K,L)=C1
 90   CONTINUE

C.....K = G^t * H^-1 * G.....................................
      DO 95 K=1,12
      DO 95 L=1,12
      C1=T2(1,K)*T3(1,L)+T2(2,K)*T3(2,L)+T2(3,K)*T3(3,L)
     &  +T2(4,K)*T3(4,L)+T2(5,K)*T3(5,L)+T2(6,K)*T3(6,L)
     &  +T2(7,K)*T3(7,L)+T2(8,K)*T3(8,L)
      T4(K,L)=C1
 95   CONTINUE

C-------------------------------------------------------------------
C
C  ELEMENT P MATRIX - DISPLACEMENT FORMULATION
C
C-------------------------------------------------------------------

      IF (NTELE.EQ.3) GOTO 280
      IF (NTELE.EQ.1) GOTO 200

C-----EVALUATE INTEGRAL AND SUM K AND P MATRICES-------------------
      DO 140 L=1,12
      T1Y(1,L)=BY(1,L)*DETJ0*HH*FOUR
 140  CONTINUE

      DO 141 K=1,12
      DO 141 L=1,12
      T2Y(K,L)=BY(1,K)*T1Y(1,L)
 141  CONTINUE

      DO 150 K=1,12
      DO 150 L=1,12
      T4(K,L)=T4(K,L)+t2y(k,l)*GG
```

```
 150  CONTINUE
      GOTO 280

C-------------------------------------------------------------
C
C  ELEMENT h MATRIX - MIXED FORMULATION
C
C-------------------------------------------------------------

C-----DEFINE INTEGRATION POINTS-------------------------------
 200  CALL INTPTS(INT2,RS,GWS)

C-----LOOP THROUGH THE INTEGRATION POINTS---------------------
      DO 250 I=1,INT2
      CALL MEMXB2 (I,RS,BY,DETJ)

C-----EVALUATE INTEGRAL---------------------------------------
      DO 250 L=1,12
      T1Y(1,L)=T1Y(1,L)+BY(1,L)*DETJ*HH*GWS(1,I)*GWS(2,I)
 250  CONTINUE

C.....h * hT.................................................
      DO 260 I=1,12
      DO 260 J=1,12
      T2Y(I,J)=T1Y(1,I)*T1Y(1,J)
 260  CONTINUE

C.....K + h..................................................

      VOLEL=HH*AREA
      DO 270 I=1,12
      DO 270 J=1,12
      T4(I,J)=T4(I,J)+T2Y(I,J)*GG/VOLEL
 270  CONTINUE

C-----SUM TO FORM MEMBRANE STIFFNESS--------------------------
 280  DO 290 K=1,4
      DO 290 L=1,4
      S(6*K-5,6*L-5)=T4(3*K-2,3*L-2)
      S(6*K-4,6*L-4)=T4(3*K-1,3*L-1)
      S(6*K-5,6*L-4)=T4(3*K-2,3*L-1)
      S(6*K-4,6*L-5)=T4(3*K-1,3*L-2)

C.....DRILLING ROTATIONS.....................................
      S(6*K-0,6*L-0)=T4(3*K-0,3*L-0)
      S(6*K-5,6*L-0)=T4(3*K-2,3*L-0)
      S(6*K-4,6*L-0)=T4(3*K-1,3*L-0)
      S(6*K-0,6*L-5)=T4(3*K-0,3*L-2)
```

```
      S(6*K-0,6*L-4)=T4(3*K-0,3*L-1)
 290  CONTINUE

C-----------------------------------------------------------------
C
C   ELEMENT K MATRIX (BENDING STIFFNESS)
C
C-----------------------------------------------------------------

      INT3=4

C-----DEFINE INTEGRATION POINTS-----------------------------------
      CALL INTPTS(INT3,RS,GWS)

C-----CALCULATE MATERIAL MATRIX-----------------------------------
      CALL MATPL(EE,UU,HH,FF,DB,DS)

C-----INITIALIZE MATRICES-----------------------------------------
      DO 530 I=1,3
      DO 530 J=1,12
 530  BPL(I,J)=ZERO

      DO 531 I=1,2
      DO 531 J=1,12
 531  BS(I,J)=ZERO

      DO 535 I=1,12
      DO 535 J=1,12
      T2PL(I,J)=ZERO
 535  CONTINUE

C-----CALC. JACOBIAN MATRIX AT SAMP. POINTS-----------------------
      CALL JASAPM

C-----LOOP THROUGH THE INTEGRATION POINTS-------------------------
      DO 590 I=1,INT3
      CALL CPT1B (I,RS,BPL,BS,DETJ)

C-----EVALUATE INTEGRAL (MATRIX MULTIPLICATION)-------------------
      DO 550 K=1,3
      DO 550 L=1,12
      C1=DB(K,1)*BPL(1,L)+DB(K,2)*BPL(2,L)+DB(K,3)*BPL(3,L)
      T1PL(K,L)=C1*GWS(1,I)*GWS(2,I)*DETJ
 550  CONTINUE

      DO 555 K=1,2
      DO 555 L=1,12
      C1=DS(K,1)*BS(1,L)+DS(K,2)*BS(2,L)
```

```
      T1S(K,L)=C1*GWS(1,I)*GWS(2,I)*DETJ
 555  CONTINUE

      DO 560 K=1,12
      DO 560 L=1,12
      C1=BPL(1,K)*T1PL(1,L)+BPL(2,K)*T1PL(2,L)+BPL(3,K)*T1PL(3,L)
      C2=BS (1,K)*T1S (1,L)+BS (2,K)*T1S (2,L)
      T2PL(K,L)=T2PL(K,L)+C1+C2
 560  CONTINUE

 590  CONTINUE

C-----END INTEGRATION LOOP-----------------------------------------

C-----SUM TO FORM ELEMENT STIFFNESS MATRIX-------------------------
      DO 580 K=1,4
      DO 580 L=1,4
      S(6*K-3,6*L-3)=T2PL(3*K-2,3*L-2)
      S(6*K-2,6*L-2)=T2PL(3*K-1,3*L-1)
      S(6*K-1,6*L-1)=T2PL(3*K-0,3*L-0)
      S(6*K-3,6*L-2)=T2PL(3*K-2,3*L-1)
      S(6*K-2,6*L-3)=T2PL(3*K-1,3*L-2)
      S(6*K-3,6*L-1)=T2PL(3*K-2,3*L-0)
      S(6*K-1,6*L-3)=T2PL(3*K-0,3*L-2)
      S(6*K-2,6*L-1)=T2PL(3*K-1,3*L-0)
      S(6*K-1,6*L-2)=T2PL(3*K-0,3*L-1)
 580  CONTINUE

C-----CONVERT FROM FLAT TO WARPED----------------------------------
      IF (NWARP.NE.0) CALL TWISTM(S)

C-----ROTATE STIFNESS TO GLOBAL SYSTEM-----------------------------
      CALL ROTATE(S)

C-----IDENTIFY DOF WHICH HAVE STIFFNESS----------------------------
 295  DO 320 K=1,6
      IF (S(K,K).NE.ZERO) ID(K,II)=1
      IF (S(K+6,K+6).NE.ZERO) ID(K,JJ)=1
      IF (S(K+12,K+12).NE.ZERO) ID(K,KK)=1
      IF (S(K+18,K+18).NE.ZERO) ID(K,LL)=1
 320  CONTINUE

C-----SAVE ELEMENT ARRAYS------------------------------------------
      WRITE (NT7) IDE,NUMN,II,JJ,KK,LL,NDOF,ND
      WRITE (NT8) S
      WRITE (NSP) IDE,II,JJ,KK,LL,XYL,T3,IMIXED,PTRANSO,DETJO,
     &            BTAY,NLOCK,ALPHACORR,NWARP
```

```
C-----SAVE STIFFNESS MATRIX TO SOLVE EIGENVALUES-------------------
      IF (NEIGEN.NE.0) THEN
      NPRINT=0
      NEX=24
      DO 350 I=1,NEX
      DO 350 J=1,NEX
 350  SEIG(I,J)=S(NEIG(I),NEIG(J))
      CALL CALJAC(SEIG,NEX,NEIGEN)
      ENDIF

C-----CHECK FOR ELEMENT GENERATION---------------------------------
      IF (NAM.EQ.0) GOTO 400
      NAM=NAM-1
      IDE=IDE+INE
      II=II+INI
      JJ=JJ+INI
      KK=KK+INI
      LL=LL+INI
      NTOT=NTOT+1
      GOTO 10
 400  IF ((MM+NTOT).EQ.NSHL8) RETURN

C-------------------------------------------------------------------
 2000 FORMAT (/,' EL. #    I    J    K    L        H           E'
     *         ,'           G        U ')
 2001 FORMAT (1I6,4I5,1F9.3,2E12.3,1F9.3)
 2002 FORMAT (5E10.3)
 2003 FORMAT (/,' ELEMENT TYPE: SHL8, Version: ',1I1,/,
     *          ' INTEGRATION SCHEME: ',1I2,'-POINT')
      END
C-------------------------------------------------------------------

C=================================================================MEMXBTJ
C
C     SUBROUTINE EVALUATES THE OPERATOR MATRIX
C     [B-MATRIX] FOR THE ELEMENT K MATRIX OF A
C     FOUR NODE 8 DOF MEMBRANE ELEMENT WITH IN-
C     PLANE DRILLING ROTATIONS.
C
C-------------------------------------------------------------------
      SUBROUTINE MEMXBTJ(I,RS,B,DETJ,BTAY,NLOCK,
     &                   AJM11,AJM12,AJM21,AJM22)

      IMPLICIT REAL*8 (A-H,O-Z)

      DIMENSION RS(2,16),QR(9),QS(9),B(3,14),BTAY(3,4)

      COMMON /VECT  / V(4,3),XYL(3,5)
```

```
      COMMON /TEMP  / IDE,II,JJ,KK,LL,HH,EE,UU
      COMMON /SIDE  / ALPHA(4),XLENG(4)
      COMMON /IOLIST/ NTM,NTR,NIN,NOT,NSP,NFL,NT7,NT8

      DATA  ZERO /0.D0/, ONE /1.D0/, TWO /2.D0/,
     &      FOUR /4.D0/, EIGHT /8.D0/

      RCOORD=RS(1,I)
      SCOORD=RS(2,I)

      XYL11=XYL(1,1)
      XYL21=XYL(2,1)
      XYL12=XYL(1,2)
      XYL22=XYL(2,2)
      XYL13=XYL(1,3)
      XYL23=XYL(2,3)
      XYL14=XYL(1,4)
      XYL24=XYL(2,4)

C-----CALCULATE SHAPE FCN. DERIVITIVES AT GIVEN POINT--------------
C.....CALCULATE LINEAR FUNCTIONS.................................
      QR1=-(ONE-SCOORD)/FOUR
      QR2= (ONE-SCOORD)/FOUR
      QR3= (ONE+SCOORD)/FOUR
      QR4=-(ONE+SCOORD)/FOUR
      QR(1)=QR1
      QR(2)=QR2
      QR(3)=QR3
      QR(4)=QR4

C.....CALCULATE QUADRATIC FUNCTIONS..............................
      QR(5)=-RCOORD*(ONE-SCOORD)
      QR(6)= (ONE-SCOORD)*(ONE+SCOORD)/TWO
      QR(7)=-RCOORD*(ONE+SCOORD)
      QR(8)=-(ONE-SCOORD)*(ONE+SCOORD)/TWO
      QR(9)=-TWO*RCOORD*(ONE-SCOORD**TWO)

C.....CALCULATE LINEAR FUNCTIONS.................................
      QS1=-(ONE-RCOORD)/FOUR
      QS2=-(ONE+RCOORD)/FOUR
      QS3= (ONE+RCOORD)/FOUR
      QS4= (ONE-RCOORD)/FOUR
      QS(1)=QS1
      QS(2)=QS2
      QS(3)=QS3
      QS(4)=QS4

C.....CALCULATE QUADRATIC FUNCTIONS..............................
```

```
      QS(5)=-(ONE+RCOORD)*(ONE-RCOORD)/TWO
      QS(6)=-SCOORD*(ONE+RCOORD)
      QS(7)= (ONE+RCOORD)*(ONE-RCOORD)/TWO
      QS(8)=-SCOORD*(ONE-RCOORD)
      QS(9)=-TWO*SCOORD*(ONE-RCOORD**TWO)

C-----CALCULATE JACOBIAN MATRIX-----------------------------------
      AJM11=QR1*XYL11+QR2*XYL12 + QR3*XYL13+QR4*XYL14
      AJM12=QR1*XYL21+QR2*XYL22 + QR3*XYL23+QR4*XYL24
      AJM21=QS1*XYL11+QS2*XYL12 + QS3*XYL13+QS4*XYL14
      AJM22=QS1*XYL21+QS2*XYL22 + QS3*XYL23+QS4*XYL24

C-----INVERT JACOBIAN MATRIX--------------------------------------
      DETJ=AJM11*AJM22-AJM12*AJM21
      IF (DETJ.LE.0.) WRITE(NOT,2000)DETJ
      IF (DETJ.LE.0.) WRITE(NTM,2000)DETJ
      AJI11= AJM22/DETJ
      AJI22= AJM11/DETJ
      AJI12=-AJM12/DETJ
      AJI21=-AJM21/DETJ

C-----CALCULATE SIDE LENGTHS AND ANGLES---------------------------
      DO 40 IC=1,4
      MC=IC+4
      TEMP=ONE/IC
      LC=MC-1+4*INT(TEMP)
      KC=MOD(MC,4)+1
      JC=LC-4
      XLENIJ=XLENG(JC)
      XLENIK=XLENG(IC)
      ALPHIJ=ALPHA(JC)
      ALPHIK=ALPHA(IC)

C-----EVALUATE B-MATRIX-------------------------------------------
      B(1,3*IC-2)=QR(IC)*AJI11+QS(IC)*AJI12
      B(3,3*IC-1)=B(1,3*IC-2)
      B(2,3*IC-1)=QR(IC)*AJI21+QS(IC)*AJI22
      B(3,3*IC-2)=B(2,3*IC-1)
      B(1,3*IC)=XLENIJ*DCOS(ALPHIJ)/EIGHT*
     &          (QR(LC)*AJI11+QS(LC)*AJI12)
     &         -XLENIK*DCOS(ALPHIK)/EIGHT*
     &          (QR(MC)*AJI11+QS(MC)*AJI12)
      B(2,3*IC)=XLENIJ*DSIN(ALPHIJ)/EIGHT*
     &          (QS(LC)*AJI22+QR(LC)*AJI21)
     &         -XLENIK*DSIN(ALPHIK)/EIGHT*
     &          (QS(MC)*AJI22+QR(MC)*AJI21)
      B(3,3*IC)=XLENIJ*DCOS(ALPHIJ)/EIGHT*
     &          (QS(LC)*AJI22+QR(LC)*AJI21)
```

```
     &          -XLENIK*DCOS(ALPHIK)/EIGHT*
     &           (QS(MC)*AJI22+QR(MC)*AJI21)
     &          +XLENIJ*DSIN(ALPHIJ)/EIGHT*
     &           (QR(LC)*AJI11+QS(LC)*AJI12)
     &          -XLENIK*DSIN(ALPHIK)/EIGHT*
     &           (QR(MC)*AJI11+QS(MC)*AJI12)

C-----CORRECT SHAPE FUNCTIONS: MEMBRANE LOCKING--------------------
      IF (NLOCK.EQ.1) THEN
      B(1,3*IC)=B(1,3*IC)-BTAY(1,IC)
      B(2,3*IC)=B(2,3*IC)-BTAY(2,IC)
      B(3,3*IC)=B(3,3*IC)-BTAY(3,IC)
      ENDIF
  40  CONTINUE

C-----ADD BUBBLE---------------------------------------------------
      B(1,13)=QR(9)*AJI11+QS(9)*AJI12
      B(2,14)=QR(9)*AJI21+QS(9)*AJI22
      B(3,13)=B(2,14)
      B(3,14)=B(1,13)
      RETURN

C-------------------------------------------------------------------
 2000 FORMAT(' JACOBIAN=',E15.6,
     *       ' NODE NUMBERS NOT IN ORDER ')
      END
C-------------------------------------------------------------------

C=================================================================HQ8PA
C
C     SUBROUTINE EVALUATES THE P MATRIX OF A HYBRID FOUR NODE
C     MEMBRANE ELEMENT USING 8 BETA PARAMETERS.
C
C-------------------------------------------------------------------
      SUBROUTINE HQ8PA(I,RS,P)

      IMPLICIT REAL*8 (A-H,O-Z)
      PARAMETER (NPOSS=57)

      DIMENSION RS(2,16),P(3,8), SM(3,NPOSS)

      COMMON /IOLIST/ NTM,NTR,NIN,NOT,NSP,NFL,NT7,NT8
      COMMON /CONSTR/ ICONSTR(9)

      DATA  ZERO /0.D0/, ONE /1.D0/, TWO /2.D0/

C-----OBTAIN R & S COORDINATES-------------------------------------
      R=RS(1,I)
```

```
      S=RS(2,I)

C-----INITIALIZE-----------------------------------------------------
      DO 10 K=1,3
      DO 10 L=1,8
 10   P(K,L)=ZERO
      DO 20 K=1,3
      DO 20 L=1,NPOSS
 20   SM(K,L)=ZERO

C-----EVALUATE P-----------------------------------------------------
      SM(1, 1)=ONE
      SM(2, 2)=ONE
      SM(3, 3)=ONE

      SM(1, 4)=R
      SM(1, 5)=S
      SM(2, 6)=R
      SM(2, 7)=S
      SM(3, 8)=R
      SM(3, 9)=S

      SM(1,10)=ONE
      SM(2,10)=ONE
      SM(1,11)=ONE
      SM(2,11)=-ONE

      SM(2,12)=-S
      SM(3,12)=R
      SM(1,13)=-R
      SM(3,13)=S

      SM(1,14)=R*R
      SM(2,15)=R*R
      SM(3,16)=R*R
      SM(1,17)=S*S
      SM(2,18)=S*S
      SM(3,19)=S*S

      SM(1,20)=R*S
      SM(2,21)=R*S
      SM(3,22)=R*S

      SM(1,23)=-R*R
      SM(2,24)=-R*R
      SM(3,25)=-R*R
      SM(1,26)=-S*S
      SM(2,27)=-S*S
```

```
SM(3,28)=-S*S

SM(1,29)=-R*S
SM(2,30)=-R*S
SM(3,31)=-R*S

SM(1,32)=S*S
SM(2,32)=-R*R

SM(1,33)=S
SM(2,33)=-R
SM(1,34)=S
SM(3,34)=-R
SM(1,35)=-R
SM(2,35)=S
SM(2,36)=S
SM(3,36)=-R
SM(1,37)=-R
SM(3,37)=S

SM(2,38)=-R
SM(3,38)=S

SM(1,39)=R
SM(2,39)=-S
SM(1,40)=R
SM(3,40)=-S
SM(1,41)=-S
SM(2,41)=R
SM(2,42)=R
SM(3,42)=-S

SM(1,43)=-S
SM(3,43)=R

SM(2,44)=-S
SM(3,44)=R

SM(1,45)=S*S
SM(3,45)=-R*R
SM(1,46)=-R*R
SM(2,46)=S*S
SM(2,47)=S*S
SM(3,47)=-R*R
SM(1,48)=-R*R
SM(3,48)=S*S
SM(2,49)=-R*R
SM(3,49)=S*S
```

```
      SM(1,50)=R*R
      SM(2,50)=-S*S
      SM(1,51)=R*R
      SM(3,51)=-S*S
      SM(1,52)=-S*S
      SM(2,52)=R*R
      SM(2,53)=R*R
      SM(3,53)=-S*S
      SM(1,54)=-S*S
      SM(3,54)=R*R
      SM(2,55)=-S*S
      SM(3,55)=R*R

      SM(1,56)=S*S
      SM(3,56)=-R*S
      SM(2,57)=-R*R
      SM(3,57)=R*S

      DO 50 K=1,8
      DO 40 L=1,3
      P(L,K)=SM(L,ICONSTR(K))
 40   CONTINUE
 50   CONTINUE
      RETURN

      END
C-----------------------------------------------------------------

C=================================================================FIXP
C
C     A-MATRIX FOR AN ASSUMED STRESS FOUR NODE MEMBRANE ELEMENT
C     WITH DRILLING DEGREES OF FREEDOM - 8 BETA PARAMETERS
C
C-----------------------------------------------------------------
      SUBROUTINE FIXP (P,PTRANSO,PTRANS,QTRANS,AJM11,AJM12,
     &                 AJM21,AJM22,DETJ,DETJO,PPURE,IMIXED,I,J)

      IMPLICIT REAL*8 (A-H,O-Z)

      DIMENSION P(I,J), PTRANSO(3,3), PTRANS(3,3), QTRANS(3,3)
      DIMENSION PPURE(I,J)

      DATA  ZERO /0.DO/, ONE /1.DO/, TWO /2.DO/

      GOTO (10,20,30,40,50,60) IMIXED
      STOP 'ILLEGAL MIXED ELEMENT FORMULATION SPECIFIED'

C-----NC (OR I) NOT CONSTRAINED-----------------------------------
```

```
 10   DO 15 K=1,I
      DO 15 L=4,J
      P(K,L)=PPURE(K,L)
 15   CONTINUE
      GOTO 500

C-----EP EQUILIBRIUM CONSTRAINED-----------------------------------
 20   DO 25 K=1,I
      DO 25 L=4,J
      C1=PTRANS0(K,1)*PPURE(1,L)+PTRANS0(K,2)*PPURE(2,L)+
     &   PTRANS0(K,3)*PPURE(3,L)
      P(K,L)=C1
 25   CONTINUE
      GOTO 500

C-----OC ORTHOGONAL CONSTRAINED------------------------------------
 30   DO 35 K=1,I
      DO 35 L=4,J
      C1=PTRANS0(K,1)*PPURE(1,L)+PTRANS0(K,2)*PPURE(2,L)+
     &   PTRANS0(K,3)*PPURE(3,L)
      P(K,L)=C1/(DETJ)
 35   CONTINUE
      GOTO 500

C-----EC ELEMENT OPTIMALLY CONSTRAINED-----------------------------
 40   STOP ' 4: NOT IMPLEMENTED'
      GOTO 500

C-----NT NORMALIZED TRANSFORMATION OF STRESS FIELD-----------------
 50   DO 55 K=1,I
      DO 55 L=4,J
      CALL FORMTRANSJ  (PTRANS,AJM11,AJM12,AJM21,AJM22)
      C2=PTRANS (K,1)*PPURE(1,L)+PTRANS (K,2)*PPURE(2,L)+
     &   PTRANS (K,3)*PPURE(3,L)
      P(K,L)=C2/(DETJ**2)
 55   CONTINUE
      GOTO 500

C-----PH PHYSICAL COMPONENTS IN ISOPARAMETRIC SPACE----------------
 60   DO 65 K=1,I
      DO 65 L=4,J
      CALL FORMTRANSJQ (QTRANS,AJM11,AJM12,AJM21,AJM22,DETJ)
      C3=QTRANS (K,1)*PPURE(1,L)+QTRANS (K,2)*PPURE(2,L)+
     &   QTRANS (K,3)*PPURE(3,L)
      P(K,L)=C3
 65   CONTINUE
      GOTO 500
```

```
C-----ASSIGN LOWER ORDER STRESS-----------------------------------
 500  DO 550 K=1,3
      DO 550 L=1,3
      P(K,L) = PPURE(K,L)
 550  CONTINUE
      RETURN

      END
C-----------------------------------------------------------------

C=================================================================MATLWINV
C
C     INVERSE MATERIAL LAW FOR MEMBRANE ELEMENTS
C     COMPLIANCE MATRIX
C
C-----------------------------------------------------------------
      SUBROUTINE MATLWINV(NSTAT,EE,UU,C)

      IMPLICIT REAL*8 (A-H,O-Z)

      DIMENSION C(3,3)

      DATA ZERO /0.D0/, ONE /1.D0/, TWO /2.D0/, HALF /0.50D0/

C-----MEMBRANE PLANE STRESS---------------------------------------
      IF (NSTAT.EQ.2) GO TO 20
      ENTRY=ONE/EE
      C(1,1)=ENTRY
      C(2,2)=ENTRY
      C(1,2)=-UU/EE
      C(2,1)=-UU/EE
      C(3,3)=TWO*(ONE+UU)/EE
      GO TO 40

C-----MEMBRANE PLANE STRAIN---------------------------------------
 20   ENTRY=( (ONE+UU)*(ONE-TWO*UU) ) / ( TWO * EE * (UU-HALF) )
      C(1,1)=-ENTRY*(ONE-UU)
      C(2,2)=-ENTRY*(ONE-UU)
      C(1,2)= ENTRY*UU
      C(2,1)= ENTRY*UU
      C(3,3)=-ENTRY*TWO

 40   C(1,3)=ZERO
      C(2,3)=ZERO
      C(3,1)=ZERO
      C(3,2)=ZERO
      RETURN
```

```
      END
C-----------------------------------------------------------------------
```

Appendix F

List of definitions

Advanced elements

Finite elements with both drilling degrees of freedom and an assumed stress interpolation field.

Composite materials

Generally a composite material is a material with two or more constituents, combined by physical process on the macroscopic scale.

Dirichlet problem [63]

Boundary value problem:

$$\begin{aligned} \frac{\partial^2 u}{\partial x_1^2} + \frac{\partial^2 u}{\partial x_2^2} &= 0 && \in R \\ u(x_1, x_2) &= f(x_1, x_2) && \forall (x_1, x_2) \in C \end{aligned} \tag{F.1}$$

Finding a solution of Laplace's equation in a region R with given boundary values, is called a Dirichlet problem. It is known that, if the boundary curve C and the boundary value function are reasonably well behaved, then there exists a unique solution to the Dirichlet problem in (F.1).

Drilling degrees of freedom

In-plane rotational degrees of freedom of membrane elements.

Finite elements [64]

A geometrically complex domain of a problem is represented as a collection of geometrically simple subdomains, called finite elements.

Interpolation functions [64]

Over each finite element the approximation functions are derived using the basic idea that any continuous function can be represented by a linear combination of algebraic polynomials. The approximation functions are derived using concepts from interpolation theory, and are therefore called interpolation functions.

Low order elements

Finite elements with the least possible number of nodes per element. For example a quadrilateral element with only four nodes.

Orthotropic materials

Materials that posses different stiffnesses along three perpendicular axes.

Strain-displacement relations [65]

In small displacement theory the strain-displacement relations are given as follows:

$$\begin{aligned}
\epsilon_{11} &= \frac{\partial u_1}{\partial x_1} \\
\epsilon_{22} &= \frac{\partial u_2}{\partial x_2} \\
\epsilon_{33} &= \frac{\partial u_3}{\partial x_3} \\
\gamma_{12} &= \frac{\partial u_2}{\partial x_1} + \frac{\partial u_1}{\partial x_2} \\
\gamma_{13} &= \frac{\partial u_3}{\partial x_1} + \frac{\partial u_1}{\partial x_3} \\
\gamma_{23} &= \frac{\partial u_3}{\partial x_2} + \frac{\partial u_2}{\partial x_3}
\end{aligned} \tag{F.2}$$

Stress [65]

The state of internal force at a point of the body is defined by nine components of stress:

$$\begin{matrix}
\sigma_{11} & \tau_{12} & \tau_{13} \\
\tau_{21} & \sigma_{22} & \tau_{23} \\
\tau_{31} & \tau_{32} & \sigma_{33}
\end{matrix} \tag{F.3}$$

which should satisfy the equations of equilibrium:

$$\begin{aligned}
\frac{\partial \sigma_{11}}{\partial x_1} + \frac{\partial \tau_{12}}{\partial x_2} + \frac{\partial \tau_{13}}{\partial x_3} + U_1 &= 0 \\
\frac{\partial \tau_{21}}{\partial x_1} + \frac{\partial \sigma_{22}}{\partial x_2} + \frac{\partial \tau_{23}}{\partial x_3} + U_2 &= 0 \\
\frac{\partial \tau_{31}}{\partial x_1} + \frac{\partial \tau_{32}}{\partial x_2} + \frac{\partial \sigma_{33}}{\partial x_3} + U_3 &= 0
\end{aligned} \tag{F.4}$$

and

$$\begin{aligned}
\tau_{12} &= \tau_{21} \\
\tau_{13} &= \tau_{31} \\
\tau_{23} &= \tau_{32}
\end{aligned} \tag{F.5}$$

where U_1, U_2 and U_3 are components of the body forces per unit volume. By eliminating τ_{21}, τ_{31} and τ_{32} by the use of (F.5), then (F.4) becomes:

$$\begin{aligned}
\frac{\partial \sigma_{11}}{\partial x_1} + \frac{\partial \tau_{12}}{\partial x_2} + \frac{\partial \tau_{13}}{\partial x_3} + U_1 &= 0 \\
\frac{\partial \tau_{12}}{\partial x_1} + \frac{\partial \sigma_{22}}{\partial x_2} + \frac{\partial \tau_{23}}{\partial x_3} + U_2 &= 0 \\
\frac{\partial \tau_{13}}{\partial x_1} + \frac{\partial \tau_{23}}{\partial x_2} + \frac{\partial \sigma_{33}}{\partial x_3} + U_3 &= 0
\end{aligned} \tag{F.6}$$

Strain [65]

The state of strain at a point of the body is defined by six components of strain, namely:

$$\epsilon_{11},\ \epsilon_{22},\ \epsilon_{33},\ \gamma_{12},\ \gamma_{13} \text{ and } \gamma_{23}. \tag{F.7}$$

Sobolev spaces of functions [38]

Sobolev spaces of functions are defined as follows:

$$H^k = H^k(\Omega) = \{w | w \in L_2; w_{,x} \in L_2; ...; w_{,x...x} \in L_2\} \tag{F.8}$$

where

$$L_2 = L_2(\Omega) = \{w | \int_0^1 w^2 \, \mathrm{d}x < \infty\} \tag{F.9}$$

In words, the Sobolev space of degree k, denoted H^k, consists of functions that possess square-integrable generalized derivatives through order k. A square-integrable function is called an L_2-function, by virtue of (F.9). From (F.8), it can be seen that:

$$H^0 = L_2 \tag{F.10}$$

and that

$$H^{k+1} \subset H^k \tag{F.11}$$

Variational form [64]

In the variational solution of differential equations, the differential equation is put into an equivalent variational form, and then the approximate solution is assumed to be a combination, $\sum c_j \phi_j$, of given approximation functions ϕ_j. The parameters c_j are determined from the variational form. The variational methods suffer from the disadvantage that the approximation functions for problems with arbitrary domains are difficult to construct.